0554
31735
729452

IDO-17019
January 1965

R
cy. 41
c2

SNAPTRAN 2/10A-3 DESTRUCTIVE TEST RESULTS

W. E. Kessler, O. L. Cordes, G. A. Dinneen,
R. D. Fletcher, and G. F. Brockett

Declassified 9-18-80
J.C. Case 2-26-85
H K Peterson 12/20/

PHILLIPS PETROLEUM COMPANY

PHILLIPS 66

ATOMIC ENERGY DIVISION

REPOSITORY INEL
COLLECTION Public Reading Room
US DOE Public Reading Room
BOX No. IDO, University Place
FOLDER IDO-17019

NATIONAL REACTOR TESTING STATION

U.S. ATOMIC ENERGY COMMISSION

PRINTED IN USA. PRICE $4.00. AVAILABLE FROM THE CLEARINGHOUSE FOR FEDERAL SCIENTIFIC AND TECHNICAL INFORMATION, NATIONAL BUREAU OF STANDARDS, U. S. DEPARTMENT OF COMMERCE, SPRINGFIELD, VIRGINIA

LEGAL NOTICE

This report was prepared as an account of Government sponsored work. Neither the United States, nor the Commission, nor any person acting on behalf of the Commission:

A. Makes any warranty or representation, express or implied, with respect to the accuracy, completeness, or usefulness of the information contained in this report, or that the use of any information, apparatus, method, or process disclosed in this report may not infringe privately owned rights; or

B. Assumes any liabilities with respect to the use of, or for damages resulting from the use of any information, apparatus, method, or process disclosed in this report.

As used in the above, "person acting on behalf of the Commission" includes any employee or contractor of the Commission, or employee of such contractor, to the extent that such employee or contractor of the Commission, or employee of such contractor prepares, disseminates, or provides access to, any information pursuant to his employment or contract with the Commission, or his employment with such contractor.

1256063

DISTRIBUTION RECORD FOR IDO-17019

External Distribution - Standard

In accordance with TID-4500, Edition 36, under the category Aerospace Safety.

Internal Distribution

P. M. Arnold, Bartlesville
J. P. Lyon
M. H. Bartz
D. R. deBoisblanc
W. E. Nyer
L. J. Weber
B. F. Boardman
F. H. Tingey
J. F. Kaufmann, ID (3)
J. F. Kaufmann, ID (30)
W. L. Ginkel
R. L. Detterman, AI (4)
R. K. Stitt, AI (2)
F. Schroeder
J. C. Haire
G. O. Bright (2)
V. A. Walker
T. R. Wilson
F. L. Bentzen
E. C. Newman
R. W. Decker (2)
D. G. Reid
J. H. Ronsick
O. L. Cordes
W. B. Lewis
S. O. Johnson
G. F. Brockett
O. M. Hauge
W. J. Neal
R. P. Rose
J. M. Waage
G. B. Matheney
G. B. Homer
G. L. Smith
W. E. Kessler
G. E. Bingham
Technical Library (10)

Number of Copies

External Distribution - Standard	404
Internal Distribution	53
Sale (by CFSTI)	75
Total	532

1256064

REACTOR SAFETY

STEP PROJECT

IDO-17019
AEC Research and Development Report
Aerospace Safety
TID-4500 (36th Ed.)
Issued: January 1965

SNAPTRAN 2/10A-3 DESTRUCTIVE TEST RESULTS

by

W. E. Kessler
O. L. Cordes
G. A. Dinneen
R. D. Fletcher
G. F. Brockett

PHILLIPS
PETROLEUM
COMPANY

Atomic Energy Division
Contract AT(10-1)-205
Idaho Operations Office
U. S. ATOMIC ENERGY COMMISSION

1256065

ACKNOWLEDGEMENT

Valuable assistance in the preparation of this report was given by F. L. Bentzen, R. P. Rose, R. E. Prael, K. A. Dietz, B. J. Norman, B. M. Reed, R. J. Norris, J. R. McGeachin, D. N. Tillitt, H. D. Curet, members of the STEP staff, STEP Design Engineering, USAEC-ID Health and Safety, and the U. S. Weather Bureau.

1256055

THE SNAPTRAN 2/10A-3 DESTRUCTIVE TEST

CONTENTS

I. SUMMARY 1

A. Scope 1

B. Test Package Description 1

C. Conduct of Test 2

D. Analysis of Results 2

E. Conclusions 3

II. INTRODUCTION 4

A. Background 4

B. Objectives of Test 4

III. TEST ARRANGEMENT 5

A. Description 5

B. Conceptual Considerations 12

C. Measurement Considerations 13

D. Photographic Coverage 14

IV. TEST RESULTS 17

A. Sequence of Events 17

B. Photographic Results 20

C. Nuclear Measurement Results 22

D. Non-Nuclear Measurement Results 30

E. Radiological Measurement Results 45

F. Post-Test Material Analysis 53

V. ANALYSIS OF RESULTS 63

A. Phenomenological Time Sequence 63

B. Feedback Analysis 65

1256067

C. Energy Probe Behavior 69

D. Energy Determination 72

VI. CONCLUSIONS 80

REFERENCES 82

APPENDIX A - Experimental Measurements 83

APPENDIX B - Details Concerning the Conduct of Test 117

TABLES

I. SNAPTRAN 2/10A-3 Reactor Characteristics 6

II. SNAPTRAN 2/10A-3 Destructive Test Cameras 14

III. Relative Time of Significant Events During the Test 19

IV. EG&G Dynafax Photographic Results 20

V. Summary of Nuclear Data 27

VI. Pressures at the Vessel Surface 41

VII. Integrated Doses from the Radioactive Cloud 49

VIII. Air Sampler Filter Data 51

IX. Sample Wafer Identification and Location 58

X. Hydrogen Analysis 60

XI. Fission Product Distribution 61

XII. Destructive Test Energy Determination by Various Methods . . 75

A-I. Summary of SNAPTRAN 2/10A-3 Recording Channel Requirements . 102

B-I. Measured Critical Configurations 118

B-II. Power Calibration Results 122

1256068

FIGURES

Fig. 1 SNAPTRAN 2/10A-3 Core Cross Section 7

Fig. 2 SNAPTRAN 2/10A-3 Reactor With Calorimeter 8

Fig. 3 SNAPTRAN 2/10A-3 Reactor and Flatcar Assembly 9

Fig. 4 Pyrotechnic Poison Sleeve Ejection System 11

Fig. 5 Camera Station Layout and Summary 16

Fig. 6 Destructive Test Sequence-of-Events Data Summary 18

Fig. 7 EG&G High Speed Photographs of Reactor Disassembly 21

Fig. 8 Elevation View (1 through 6) of Destructive Test Sequence . 23

Fig. 9 Elevation View (1 through 12) of Destructive Test Sequence. 24

Fig. 10 Overhead View (A through D) of Destructive Test Sequence . 25

Fig. 11 Burst Shape Comparison of Linear Nuclear Detector Signals . 28

Fig. 12 Comparison of Log and Linear Detector Signals 29

Fig. 13 10 wt% Energy Probe Results 31

Fig. 14 5 wt% Energy Probe Results 32

Fig. 15 Indicated Strain on Reactor Vessel and Pedestal 34

Fig. 16 Indicated Pressure in Water Environment Around Reactor . . 38

Fig. 17 Pressure Transducer Locations in Environmental Tank 40

Fig. 18 Summary of Mechanical Effects Data 43

Fig. 19 Test Cell Radiological Dose Measurements 47

Fig. 20 Dose Measurements from Radiological Tower Locations 48

Fig. 21 Transient Dose Rate Measurements at Downwind Locations . . 52

Fig. 22 Post-Test Remains of Reactor After Removal of Superstructure 54

Fig. 23 SNAPTRAN 2/10A-3 Core Layout 55

Fig. 24 Fuel Rod Remains Arranged According to Core Layout 56

Fig. 25 Views (A through D) of Miscellaneous Pieces of Fuel Remains 57

1256069

Fig. 26 Overall Data Summary Encompassing Power Excursion 64

Fig. 27 Compensated Reactivity vs Time During Destructive Test . 68

Fig. 28 Compensated Reactivity vs Average Core Temperature During Destructive Test 68

Fig. 29 Nuclear Energy per Unit Temperature Rise of 5 wt% Energy Probe vs Temperature Rise of 5 wt% Energy Probe 70

Fig. 30 Nuclear Energy per Unit Temperature Rise of 10 wt% Energy 70

Fig. 31 Radial Fission Source Distribution as Defined by Energy Probes 72

Fig. 32 Axial Fission Source Distribution as Defined by Energy Probes 72

Fig. 33 Time Variation in Radial Temperature Distribution 73

Fig. 34 Time Variation in Axial Temperature Distribution 74

Fig. A-1a SNAPTRAN 2/10A-3 Nuclear Detector Layout 88

Fig. A-1b SNAPTRAN 2/10A-3 Nuclear Detector Summary 89

Fig. A-2 SNAPTRAN 2/10A-3 Nuclear Detector Range Coverage . . . 90

Fig. A-3 SNAPTRAN 2/10A-3 Flight Tube Arrangement 91

Fig. A-4 SNAPTRAN 2/10A-3 In-Core Energy Probe Locations 93

Fig. A-5a SNAPTRAN 2/10A-3 Pressure Transducer Locations 94

Fig. A-5b SNAPTRAN 2/10A-3 Pressure Transducer Summary 95

Fig. A-6 SNAPTRAN 2/10A-3 Strain and Nuclear Detector Locations Proximate to Core 96

Fig. A-7 SNAPTRAN 2/10A-3 Signal Conditioning and Recording Equipment Block Diagram 99

Fig. A-8 IET - Radiological Grid to a Radius of 300 Meters . . . 104

Fig. A-9 IET - Radiological Grid Beyond a Radius of 300 Meters . 105

Fig. A-10 SNAPTRAN 2/10A-3 Compartmental Catch Trays for Destructive Test Debris 107

Fig. A-11 SNAPTRAN 2/10A-3 Catch Cans for Destructive Test Debris 108

1256070

Fig. A-12 Radiological Sequential Air and Particle Sampler . . . 111

Fig. A-13 Telemetering Radiological Monitoring Station 113

Fig. A-14 Radiological Fallout Plate 115

Fig. B-1 Time History of Typical Energy Probe and Nuclear Detector During Power Calibration 119

Fig. B-2 Time History of 10 wt% Energy Probes During Power Calibration 123

1256071

I. SUMMARY

A. Scope

As part of the Atomic Energy Commission's Reactor Safety Program, a SNAP 10A/2 reactor core was subjected to rapid water immersion such as might result from an aborted space mission. The resulting reactivity excursion was designed to represent the upper limit attainable from such an accident and was destructive in nature. The test was conducted in Idaho at the National Reactor Testing Station by Phillips Petroleum Company with the assistance of Atomics International.

The objectives of the test were to provide information concerning: (1) the radiological results of the test, and (2) those aspects of the reactor behavior which influenced the radiological results. More specifically, the radiological results dealt with the release and migration of radioactive fission products while the particular aspects of the reactor behavior which affect the radiological results were related to the energy release and to the mechanical mode of disassembly during the destructive excursion.

B. Test Package Description

Tests had shown that all components external to the reactor vessel (including the beryllium reflector) become disengaged upon rapid entry of a SNAP 10A/2 reactor into water[1]. A reactor configuration for this test was therefore chosen in which a SNAP 10A/2 reactor vessel with enclosed core was mounted in the center of a large environmental water tank. The core consisted of 37 SNAP fuel elements (4.75 kg of U-235) and six beryllium inserts used to retain the hexagonal fuel element array within the cylindrical vessel. A sleeve, fabricated from a thermal neutron absorbing material (Binal), was positioned around the reactor vessel to maintain subcriticality and was rapidly withdrawn from around the vessel to initiate the destructive transient. The reactor system, including the environmental tank, was mounted on a railroad flatcar which was used to transport the reactor remains to the TAN hot shop for post-test examination.

1256072

C. Conduct of Test

Preliminary to the SNAPTRAN 2/10A-3 destructive test program, static physics measurements were performed to determine basic physics parameters expected to affect the reactor behavior during the destructive excursion. In addition, several dry runs were performed to establish that a high degree of reliability of the experimental equipment could be expected. Weather requirements were imposed to insure that the fission product release would be directed toward the heavily instrumented sector of the radiological grid.

The destructive test was conducted on April 1, 1964 and a summary of the data is presented below:

Asymptotic Period of the Power Rise	640 ± 30 μsec
Peak Power	18,000 ± 2000 Mw
Total Nuclear Energy Release	45 ± 4 Mw-sec
Maximum Core Averaged Fuel Temperature	1900 ± 200°F
Excess Reactivity	3.75 ± 0.25 dollars
Maximum Disassembly Pressure	1000 ± 300 psi
Radiation Level at the Rim of the Environmental Tank (2 hrs after test)	< 25 r/hr
(24 hrs after test)	≈ 3 r/hr
Peak Dose Rate 100 meters downwind	≈ 2 r/hr
Noble Gas Release	< 5%

D. Analysis of Results

The power-time history associated with any nuclear excursion depends primarily on the reactivity driving function and any feedback mechanisms which come into play. An excess reactivity of 3.75 dollars was calculated from the asymptotic power rise (τ = 640 μsec) using a value of 1.75 msec for ℓ/β_{eff}. Up to the time of peak power, the reactivity feedback appears to have been linear with fuel temperature and was determined to be -0.19¢/°F. Since no appreciable core vessel expansion occurred until at or immediately after the time of peak power, it was concluded that nearly all reactivity compensation to that time was due to the intrinsically neutronic behavior of the fuel material.

1256073

After peak power was reached, a more rapid power decline occurred coincidental with the explosive expansion of the core vessel. Once disassembly started, the reactivity compensation no longer depended on energy or temperature level but rather on the deranged condition of the core.

The most probable value of the energy release resulting from the destructive power excursion was determined from a number of different measurements to be 45 ± 4 Mw-seconds.

Moderate radiological effects resulted from the test. A direct dose of only 150 rem was recorded at a point eight feet above the reactor. This measurement encompassed the direct radiation from the burst and the decay, during a one hour period following the burst. The halogens that escaped from the fuel were retained in the water, and as a result, no airborne iodine was detected. The radioactive cloud resulting from the destructive excursion consisted primarily of noble gases and their daughters. It was estimated that less than 5% of noble gas present in the core were released. The radiation from this cloud decreased to background about 12 miles downwind. Sensitive air monitors revealed no airborne beryllium contamination.

E. Conclusions

As a result of this test, it can be concluded that minimal radiological hazards result from the rapid water immersion of a SNAP 10A/2 reactor. In addition, the information gained concerning the reactor behavior provided a basis for predicting the consequences of similarly fueled reactors under accident conditions.

1256074

II. INTRODUCTION

A. Background

Consistent with the Atomic Energy Commission's goal of achieving a high degree of safety in the nuclear industry, an experimental program has been initiated to assess the safety of aerospace nuclear systems. A portion of this safety program is directed toward determining the consequences of nuclear incidents under actual accident conditions and providing physics and engineering information of importance to understanding the kinetic behavior, assessing the nuclear safety, and improving the design of aerospace nuclear systems with respect to safety.

A test designated "SNAPTRAN 2/10A-3" was performed to provide this kind of information as it pertains to SNAP 10A/2 reactors under transient conditions. Phillips Petroleum Company, Atomics International, and Edgerton, Germeshausen and Grier were the major participants in the SNAPTRAN 2/10A-3 program.

SNAP 10A/2 reactor systems are subject to large reactivity insertions upon accidental water immersions. Very rapid reactor water immersion, as could be experienced from a launch abort, has been shown to result in the separation of the external beryllium reflector from the reactor vessel. The resulting supercritical configuration is that of a standard SNAP 10A/2 reactor core and vessel surrounded by water as a reflector. The SNAPTRAN 2/10A-3 destructive test was performed to simulate this accident.

B. Objectives of Test

The objectives of the SNAPTRAN 2/10A-3 destructive test were: (1) to assess the radiological hazards resulting from rapid water immersion of a SNAP 10A/2 type reactor, and (2) to gain information on those aspects of reactor behavior which contributed to the spread of fission products.

1256075

III. TEST ARRANGEMENT

A. Description

The SNAPTRAN 2/10A-3 reactor was a modification of the small, zirconium-hydride-uranium fueled, beryllium-reflected SNAP 10A/2 reactor. The core was a cylinder approximately 9 inches in diameter by 13 inches long. The fuel rods were fabricated of an alloy of zirconium-hydride and fully enriched uranium and were clad with Hastelloy-N. The core was composed of 37 fuel rods arranged in a close-packed hexagonal array and contained 4.75 kg of U-235 and 464 gm-moles of hydrogen. These rods were contained in a stainless steel vessel having a wall thickness of 0.032 inches. Allowance was made in the reactor vessel for containment of NaK in the core and for installation of in-core instrumentation. Table I summarizes the reactor characteristics and Figure 1 shows a cross section of the core and beryllium inserts.

The reactor was controlled by a 1/4 inch-thick cylindrical neutron absorbing Binal sleeve which surrounded the vessel. Two sleeve drive mechanisms were used to remove the sleeve from around the reactor vessel and raise the reactivity state of the reactor. A slow drive with an electrical motor drive and a gear train mechanism was used for non-destructive operations. The destructive reactor excursion was initiated by means of the pyrotechnic actuator which was directly coupled to the Binal sleeve and allowed free vertical movement of the sleeve by raising and lowering the piston located inside the actuator cylinder.

The reactor vessel was surrounded by a lucite calorimeter during power calibration runs. The calorimeter was removed for the destructive test. Figure 2 is a diagram of the core, vessel, calorimeter, and support pedestal.

The reactor vessel containing the core was located on a pedestal centered in an environmental tank having an internal diameter of 14 feet and a height of 10 feet as shown in Figure 3. The tank walls were fabricated from 0.75 inch-thick carbon steel and the base was fabricated from 1.5 inch-thick carbon steel. The size and construction of the environmental tank was selected to simulate a large body of water, to facilitate

1256076

TABLE I

SNAPTRAN 2/10A-3 REACTOR CHARACTERISTICS

Reactor Design	
Fuel Elements	
Number	37
Fuel diameter (inches)	1.212
Cladding material	Hastelloy-N
Cladding diameter, OD (inches)	1.25
Cladding thickness (inches)	0.015
Fuel alloy (wt% U in Zr)	10
Degree of hydriding, N_H (10^{22} a/cm^3)	6.5
Active fuel length (inches)	12.25
U-235 enrichment (percent)	93
U-235 loading/fuel element (gm)	127.16 ± 1.16
U-235 total core loading (kg)	4.75
Internal Reflectors	
Composition	Beryllium
Lower Grid Plate	
Material	Hastelloy-C
Thickness (inches)	0.500
Upper Grid Plate	
Material of standard grid plate	Hastelloy-C
Thickness (inches)	0.125
Core Vessel	
Material	316 ss
Internal diameter (inches)	8.875
Thickness (inches)	0.032
Neutron Absorbing Sleeve	
Material	B_4C dispersed in Al
Natural boron content (wt%)	10.5
Diameter ID (inches)	9.5
Length (inches)	30
Thickness (inches)	0.25

pressure measurements, and to permit evaluation of the effect of possible metal-water reactions and secondary criticality. In order to maintain integrity during the high pressure surges which were expected during the destructive disassembly of the reactor, the tank was backed on the sides by concrete which was 1 foot thick at the top and 2 feet thick at the base. The entire system was mounted on a flatcar to facilitate transport to the hot shop for examination following the test. The test package was

1256077

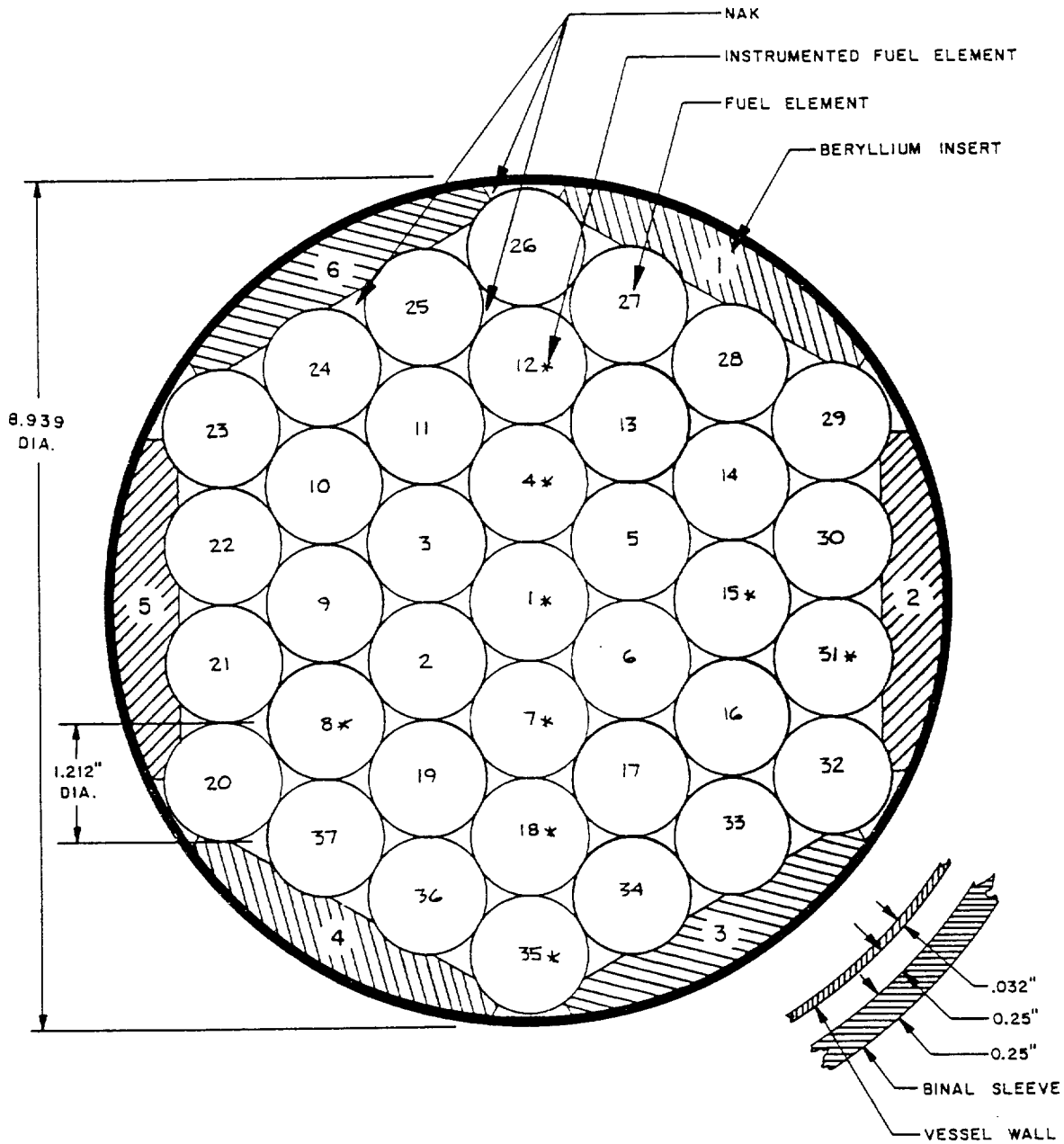

Fig. 1 SNAPTRAN 2/10A-3 Core Cross Section

1256078

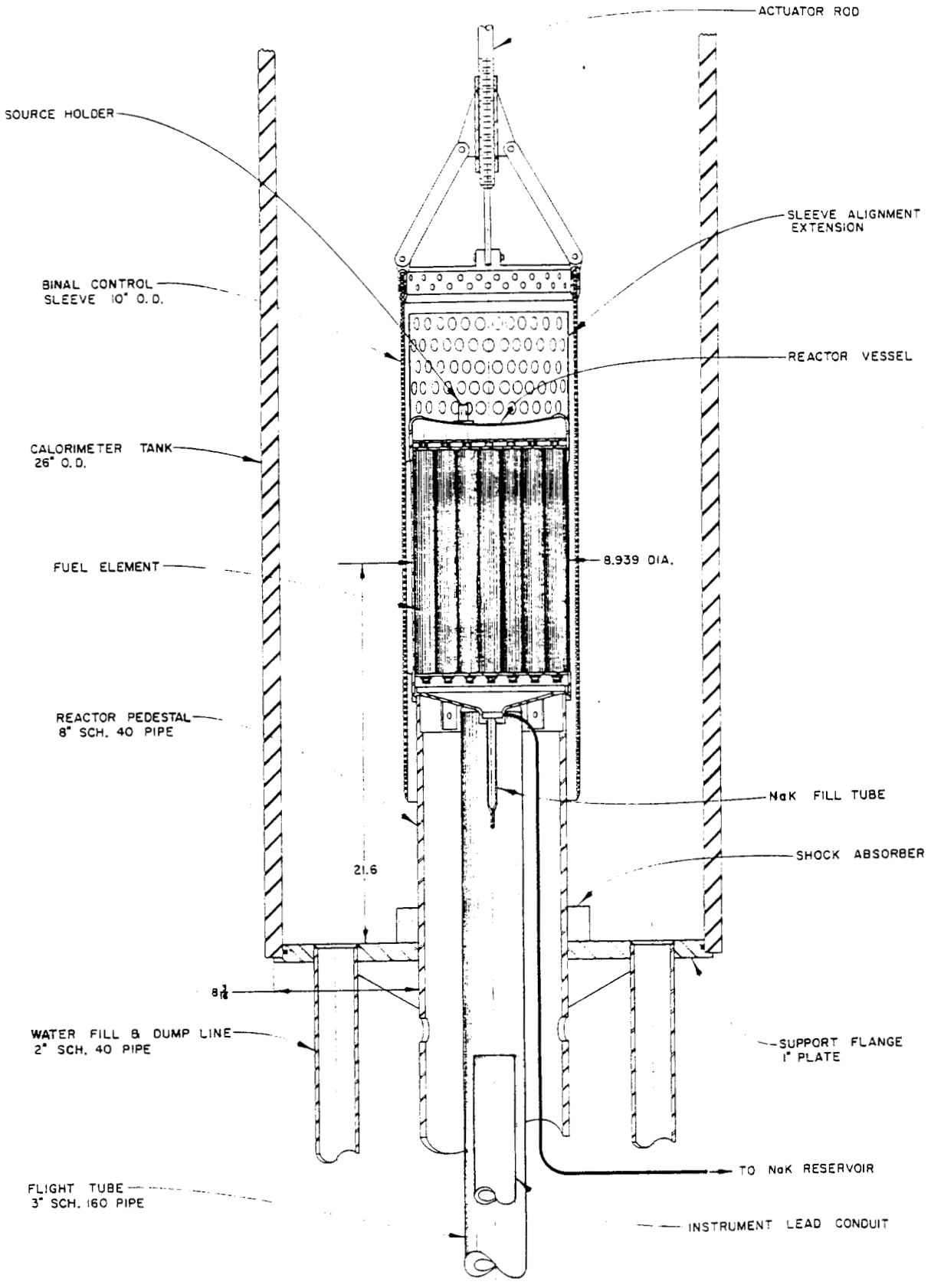

Fig. 2 SNAPTRAN 2/10A-3 Reactor with Calorimeter

1256019

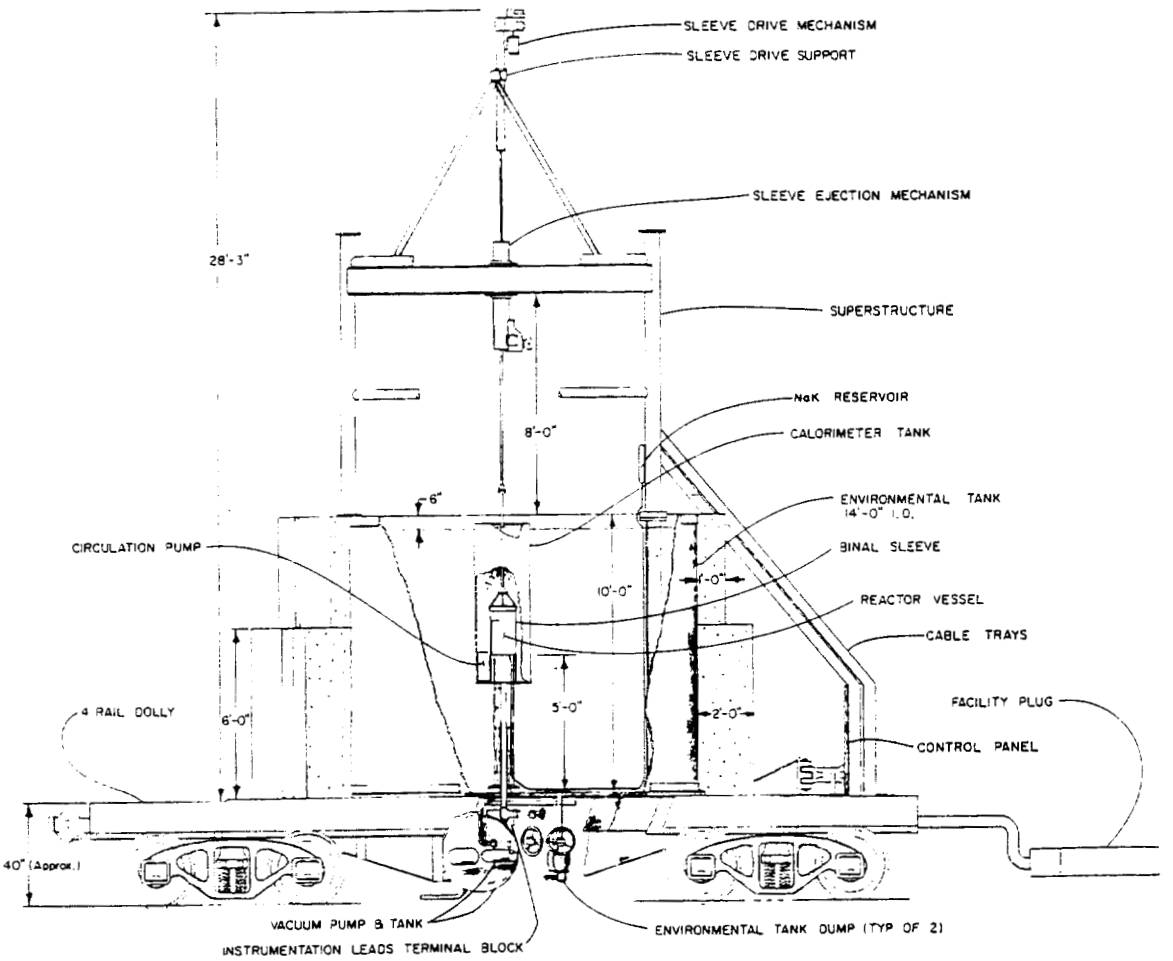

Fig. 3 SNAPTRAN 2/10A-3 Reactor and Flatcar Assembly

1256080

housed in a mobile test building which was removed before initiation of the destructive excursion.

The reactor control console was located in the Initial Engineering Test Facility (IET) control room. The console panels were equipped with reactor controls, startup instrumentation, power level recording instrumentation, period and power level safety instrumentation, television monitors, and a program sequence timer. Recorders indicating water level and temperature in the environmental tank were located in the control room in the process control panel.

Scram shutdown of the reactor during normal operation could be accomplished by dropping the poison sleeve from the raised position or by rapidly draining water from the calorimeter to an evacuated tank. Dropping the sleeve was accomplished by de-energizing the electromagnet which coupled the poison sleeve to its raising mechanism. Draining of the water from the calorimeter could be accomplished by de-energizing the solenoids which held the calorimeter dump valves closed. Filling and draining the environmental tank was accomplished by a 350 gpm centrifugal pump which was controlled from the control console.

An electrically driven mechanism was used to vertically position the poison sleeve with respect to the reactor core. Cam operated switches were provided to give indication at the limiting drive positions: (1) mechanical lower limit, (2) mechanical upper limit, and (3) the position at which the bottom of the raised sleeve was one inch below the top of the reactor vessel (upper limit).

A pictorial representation of the sleeve ejection mechanism showing the powder chamber and detonating squibs in the safe position is presented in Figure 4. A key switch on the console activated the powder chamber rotating circuit. Arming for the destructive test consisted of running the electromagnetic drive to its upper limit, rotating the powder chamber into the actuator cylinder, and activating the squib detonating circuits.

Additional information concerning the test package can be found in IDO-16929, "Safety Analysis Report - SNAPTRAN 2/10A-3 Water Immersion Tests".

1256081

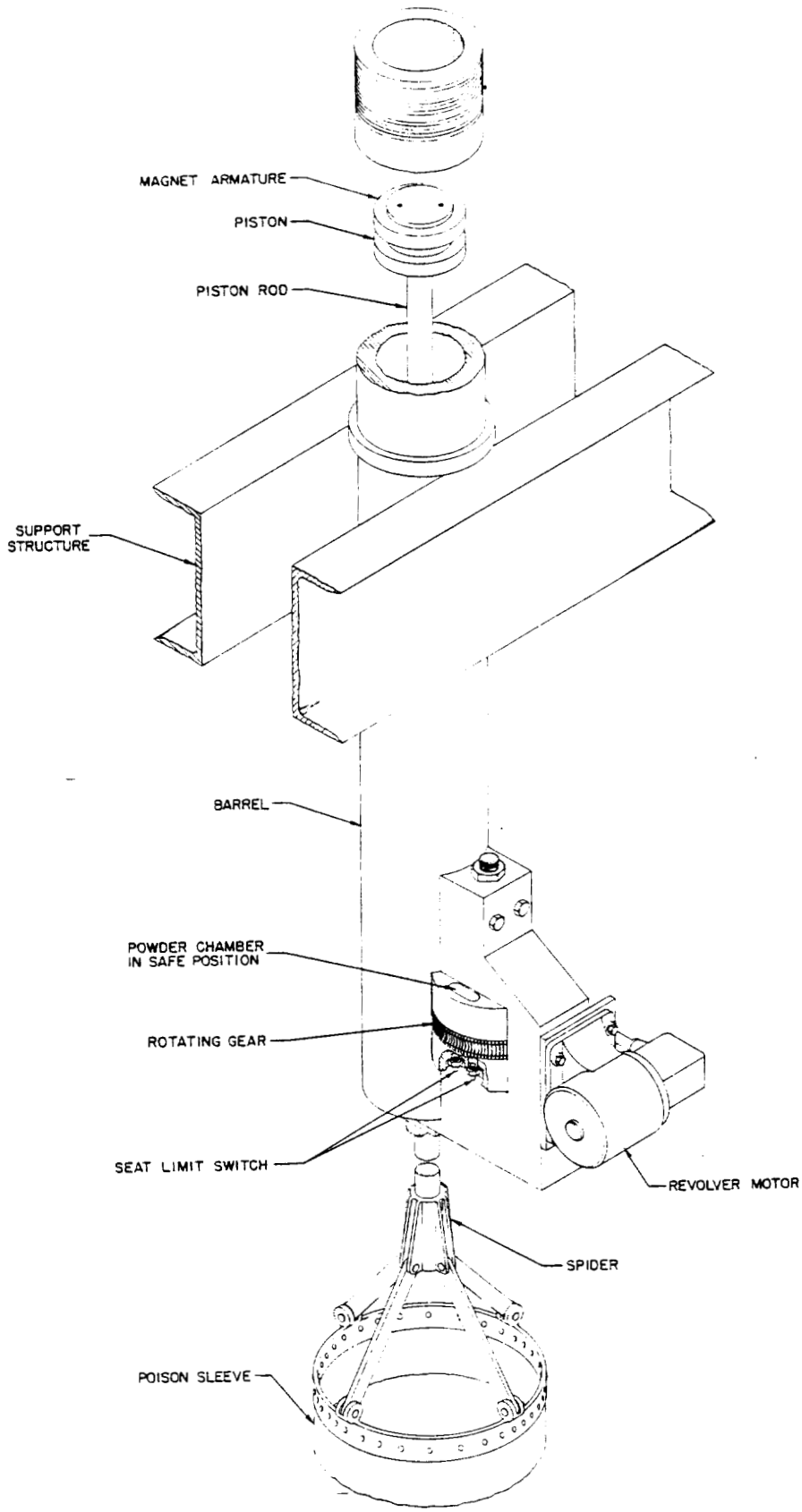

Fig. 4 Pyrotechnic Poison Sleeve Ejection System

1256082

B. Conceptual Considerations

Several experimental techniques of reactor water immersion were investigated with respect to ease of instrumenting, reliability, reactivity insertion rate, and typification of the actual accident. Dropping the reactor into a body of water would most typically simulate the actual accident, but the need for internal and surface-mounted instrumentation presented a nearly insurmountable design problem. Instead, the reactor was permanently mounted in a fixed position and provision made to rapidly introduce the effect of full water immersion as test initiation. In addition to facilitating adequate reactor instrumentation, complete water immersion without spurious void pockets was considered desirable in simulating the maximum reactivity accident. Complete water immersion was considered important since it would have been very difficult to predict and/or simulate the voids developed in the actual case and also since any void formation would reduce the reactivity state, thereby reducing the severity of the excursion. A bubble collapse technique proved to be too slow to insert all available reactivity before feedback effects could cause distortion of the asymptotic reactor power rise. Since the excess reactivity was to be determined by the asymptotic period of the power rise, a faster mode of reactivity insertion (or effective water immersion) was sought to insure that adequate asymptotic period data without feedback would be available.

Experiments performed by Atomics International [2] indicated that a 1/4 inch-thick Binal sleeve placed around the periphery of the water immersed reactor vessel was capable of maintaining the shutdown state of the reactor. A cylinder and piston arrangement using black gun powder as the driving force was chosen as the means for rapidly removing the sleeve to initiate the destructive excursion. Subsequent tests proved the feasibility and reliability of attaining adequate reactivity insertion rates by means of the cannon arrangement. The reactor was fixed on a pedestal through which instrumentation leads were routed from the reactor vessel to the terminal strips below the flatcar.

1256083

C. Measurement Considerations

The measurements required to define the phenomena of interest can be placed in three categories: (1) measurements concerning the radiological effects resulting from the test, (2) measurements of the nuclear and physical phenomena which define the reactor behavior and resulting consequences to the environment; and (3) the photographic coverage which, while mainly for documentary purposes, has definite value as experimental data. The location and types of measurement devices and a description of the signal conditioning and recording equipment for the first two categories is discussed in detail in Appendix A.

A brief discussion is given here to provide some insight into the considerations attendant to the various kinds of measurements made during the test. Initially, consideration was given to the expected range, rise time, accuracy, and redundancy required of the analog detector signals describing a given phenomenon during the test. The selection of detectors and signal conditioning equipment was based on these considerations and the specific locations of detectors were based on range and the capability of describing spatial and time-of-event information. The magnetic tape recording equipment used during the test to record the analog detector signals had provisions for rapidly transferring the recorded analog signal to a digital tape for use in computer data treatment. Strip chart recorders were used as backup and for less rapidly occurring phenomenological event recording.

Measurement of the radiological consequences as a result of the destructive test include fission product release, direct gamma and neutron doses, spread of airborne contamination and the release of beryllium. The measurements were accomplished by use of a radiological monitoring grid which was set up as a series of concentric arcs with the reactor test pad as the center.

The heavily instrumented sector of the grid was oriented about a centerline on 30° east of true north which is in line with the direction of the prevailing winds. Weather conditions required for performance of the destructive test were established by the AEC and U. S. Weather Bureau in order that the fission product release would be directed toward the heavily instrumented sector of the grid.

1256084

In addition to the grid sampling equipment, radiological sampling equipment was placed on a 150 foot tower and on the existing IET stack. Water catch cans and trays were located on the reactor dolly. Film-badge-drop devices were located on an approximate 10 meter arc and special high range dosimeters and activation foil boxes were employed in the immediate reactor area. Clothesline-type sample stations were located east of the reactor and an aircraft was provided to follow the radioactive cloud.

D. Photographic Coverage

Photographic data and documentary coverage were provided for the destructive test through the use of 21 cameras. Camera types included 2-1/4 x 2-1/4 inch (70 mm) rapid-sequence cameras and 16 mm standard-speed framing cameras. Table II summarizes the camera types used for direct viewing of the destructive test.

TABLE II

SNAPTRAN 2/10A-3 DESTRUCTIVE TEST CAMERAS

Camera Type	Framing Rate	Film Size	Film Capacity	Number Used
Photosonics 16-1B	300 to 1000 f/sec	16 mm	100 and 400 feet	9
Waddell 16-1	2000 to 10,000 f/sec*	16 mm	100 and 400 feet	3
Bell and Howell	16 to 48 f/sec	16 mm	100 and 400 feet	2
Arriflex	16 to 48	16 mm	100 and 400 feet	1
Hulcher Press	single framing to 20 f/sec	70 mm	100 feet $2\frac{1}{4}$x$2\frac{1}{4}$ in.	2
Dynafax (EG&G)	17,680 f/sec and 8,840 f/sec	16 mm fr on 35 mm	224 16 mm frames	2
EO-600 (EG&G)	1 fr every 20 μsec	4 x 5 in.	6 frames	2

* Limited lighting restricted these cameras to a framing rate of 3000 f/second.

1250085

Selection and Positioning of Cameras

Four camera positions were selected to obtain photographs of the disassembly (Stations 1, 2, 3, and 10 in Figure 5). A combination of camera type and positioning was chosen which was expected to result in comprehensive and interpretable films. Each station contained at least two high speed cameras (300 - 10,000 f/sec). These high speed cameras were fitted with lenses which afforded an optimum compromise between field-of-view and closeup detail capabilities. Slower cameras (one 24 f/sec and one 48 f/sec) were placed 600 and 180 feet from the reactor. Seventy millimeter rapid sequence cameras were placed at 600 and 180 feet. These slower cameras and rapid sequence cameras were fitted with lenses which afforded a large field-of-view.

Camera Stations 1 and 2 were positioned 180 feet from the reactor at ground level. Camera Station 3 was positioned at the top of a 150 foot tower. Camera Station 10 was positioned 650 feet from the reactor and elevated about 20 feet. Weather and temperature protection was provided by these stations.

Specialized Ultra High Speed Cameras

Ultra high speed framing cameras were employed by Edgerton, Germeshausen and Grier (EG&G) to obtain silhouette photographs of the reactor vessel during disassembly. Water filled periscopes attached to the inside of the environmental tank were used in obtaining these photographs.

The two EO-600 cameras were triggered by breakbands set to start at the time radial vessel expansion began. These cameras were adjusted to operate at framing intervals of 20 microseconds. The purpose of these cameras was to record the occurrence of very rapidly changing phenomena. Two Dynafax motion picture cameras operated at rates of 17,680 and 8,840 f/sec respectively. These cameras provided broader coverage of less rapidly occurring phenomena than those covered by the EO-600 cameras. The Dynafax cameras were triggered by a gamma chamber at about 200 kw of reactor power.

1256086

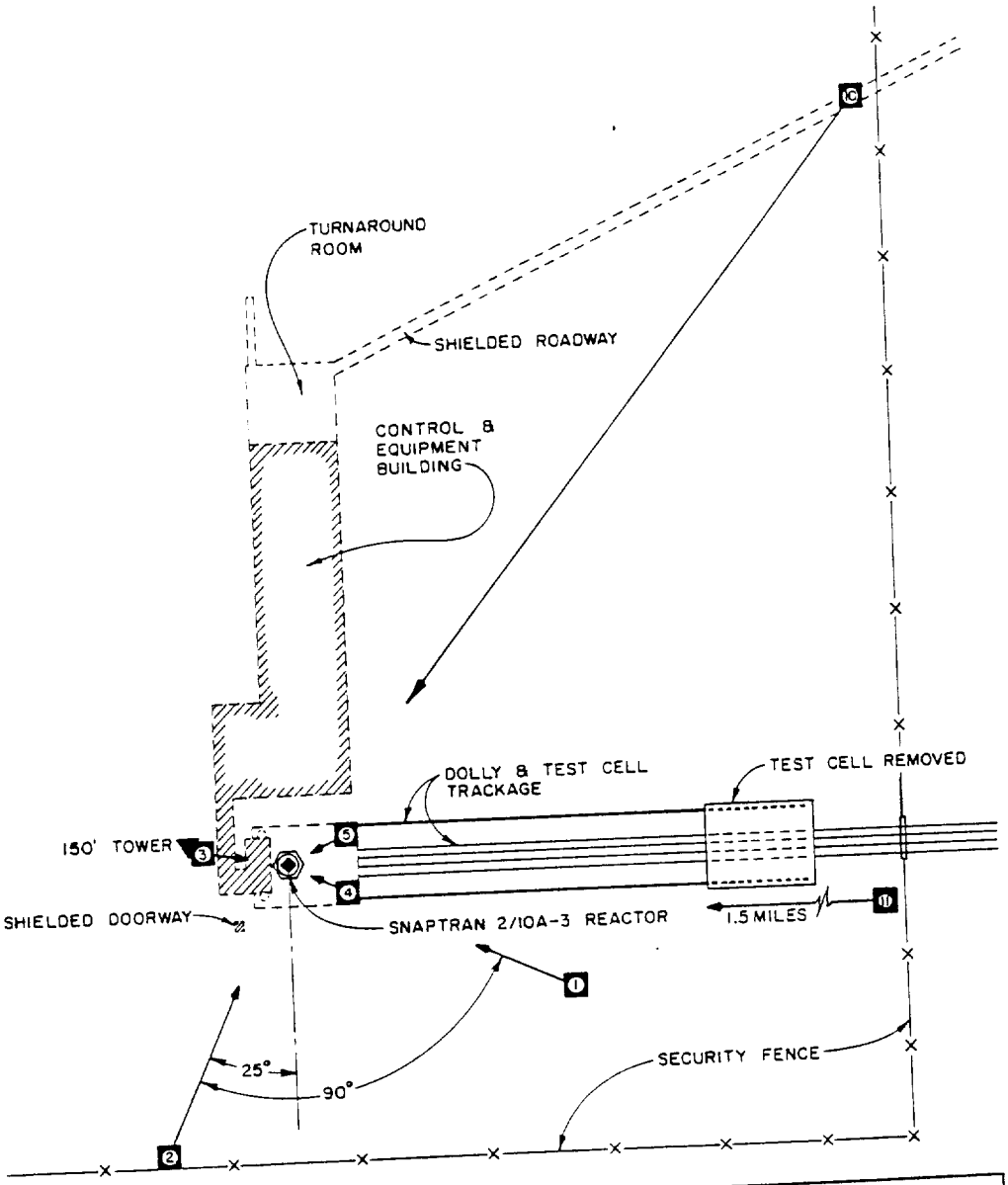

SNAPTRAN 2/10A-3 PHOTOGRAPHIC COVERAGE							
CAMERA STATION NUMBER	DISTANCE	CAMERA SPEED	NUMBER OF CAMERAS	CAMERA RUNNING TIME	TYPE OF FILM	PRIMARY PURPOSE	REMARKS
1	180 FT.	3000 F/s	1	2.8 SEC.	16MM/B&W	HI SPEED DATA	POSITION 1 & 2 ARE ON SHIELDED SLEDS, 1000 F/s CAMERA AS BACK-UPS FOR 3000 F/s CAMERAS
1	180 FT.	1000 F/s	1	14 SEC.	16MM/B&W	HI SPEED DATA	
1	180 FT.	450 F/s	1	40 SEC.	16MM/COLOR	HI SPEED DOCUMENTARY	
1	180 FT.	450 F/s	1	40 SEC.	16MM/B&W	HI SPEED DATA	
2	180 FT.	48 F/s	1	8 MIN.	16MM/COLOR	MED. SPEED DOCUMENTARY	
2	180 FT.	3000 F/s	1	2.8 SEC.	16MM/B&W	HI SPEED DATA	
2	180 FT.	1000 F/s	1	14 SEC.	16MM/B&W	HI SPEED DATA	
2	180 FT.	450 F/s	1	40 SEC.	16MM/B&W	HI SPEED DOCUMENTARY	
2	180 FT.	RAPID SEQUENCE	1	40 SEC.	70MM/COLOR	HI RESOL DOCUMENTARY	
3	175 FT.	3000 F/s	1	2.8 SEC.	16MM/B&W	HI SPEED DATA	VIEW FROM 150' TOWER
3	175 FT.	1000 F/s	1	14 SEC.	16MM/B&W	HI SPEED DATA	
3	175 FT.	450 F/s	1	40 SEC.	16MM/COLOR	HI SPEED DOCUMENTARY	
4	20 FT.	50,000 F/s	2	120 µs	4" x 5"	HI SPEED DATA	PROVIDES SILHOUETTE VIEW OF CORE EXPANSION
5	20 FT.	17,680 F/s	2	12.7 MS	35MM/B&W	HI SPEED DATA	
10	650 FT.	450 F/s	1	40 SEC.	16MM/COLOR	HI SPEED DOCUMENTARY	OVERALL DOCUMENTATION
10	650 FT.	450 F/s	1	40 SEC.	16MM/B&W	HI SPEED DATA	
10	650 FT.	RAPID SEQUENCE	1	40 SEC.	70MM/COLOR	HI RESOL DOCUMENTARY	
10	650 FT.	24 F/s	1	12 MIN.	16MM/COLOR	STD. SPEED DOCUMENTARY	
11	1½ MILES	24 F/s	1	12 MIN.	16MM/COLOR	STD. SPEED DOCUMENTARY	

Fig. 5 Camera Station Layout and Summary

1256081

IV. TEST RESULTS

A. Sequence of Events

Before discussing the detailed features of particular categories of experimental data, it is appropriate to consider the gross correlations of many of the nuclear and physical phenomena occurring during the test. Table III lists the relative times of the significant events during the test referenced to peak power. The symbols used in the "Source of Information" column designate by code the type and identification number of the detector and recorder channel used. For example, N-13 T-6 - 10 designate a nuclear detector on tape transport 6 channel number 10.

Figure 6 presents the long term time dependent behavior of the more significant events. Trace SW-1 indicates the motion of the poison sleeve being ejected from around the reactor. The trace indicates the cessation of sleeve withdrawal at about 20 msec prior to peak power. An analysis of the data has shown that the sleeve was off the reactor ~ 40 msec prior to the onset of any observable feedback mechanisms, thus providing 60 e-folds of unperturbed asymptotic rise. The power trace N-13 appears as a spike and is included for completeness in presenting the long term behavior of other effects. Trace P-9 represents the pressure generation in the environmental tank as a result of reactor disassembly. This pressure, seen to last in the order of 30 msec, initiates water expulsion shown by the point plot from the motion picture analysis. The water is shown to rise to a height of about 25 feet at about 1000 msec after peak power. At this time, the temperature as determined by a fast response thermocouple (TC-2) placed above the environmental tank for sensing of the potential hydrogen-oxygen and other chemical reactions, shows a rise of about 20°F which persists for the duration of the water plume. Data from temperature traces and the air pressure data reveal no evidence of severe disturbance from chemical reaction. The severe spikes shown on the figure are the result of electromagnetic noise.

Trace P-28 indicates a plot of the air pressure generation resulting from the water expulsion. The spikes have been correlated with the time of (1) squib firing, (2) gas release from pyrotechnic actuator, and (3)

1256080

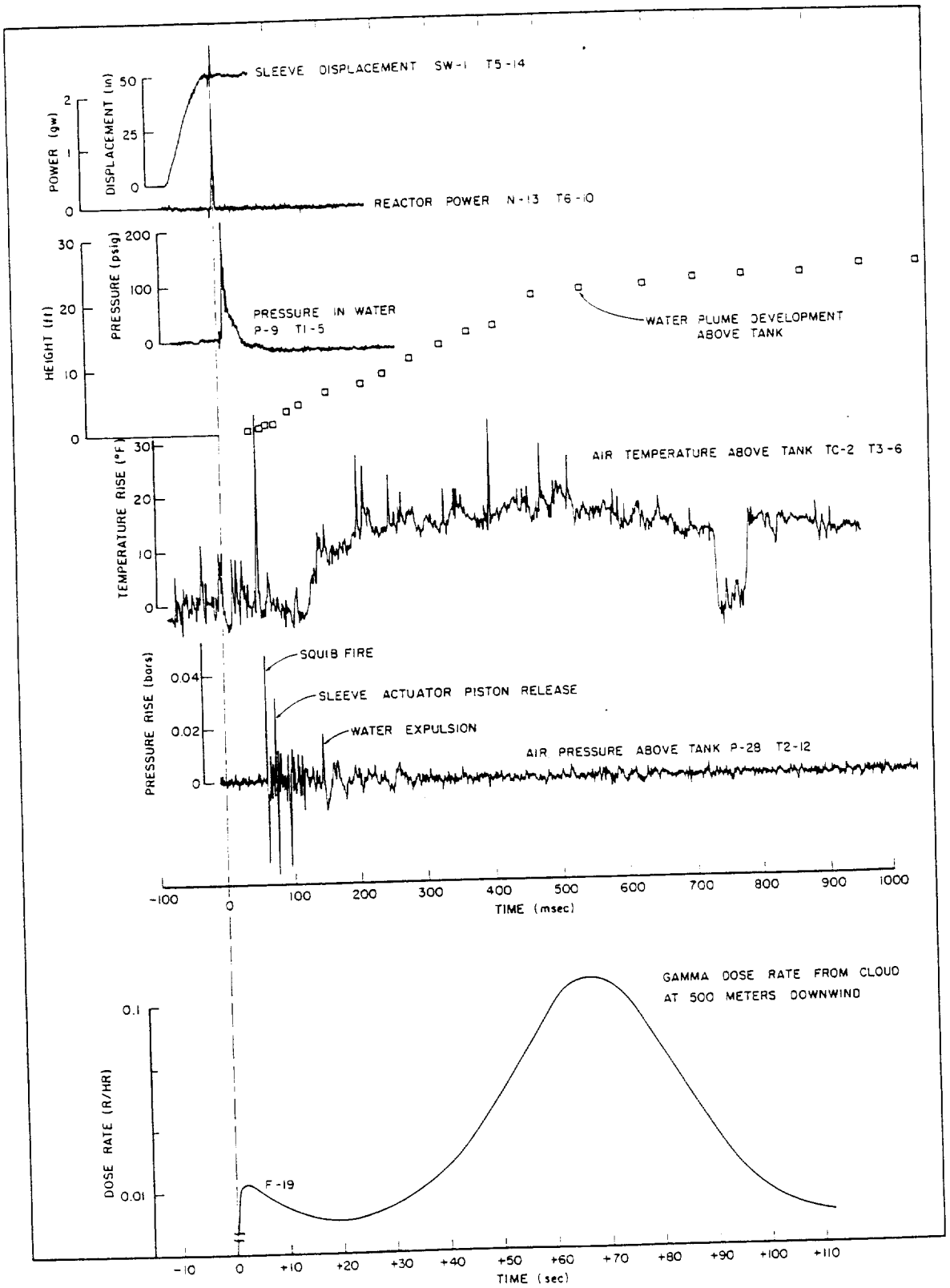

Fig. 6 Destructive Test Sequence-of-Events Data Summary

1256089

TABLE III

RELATIVE TIME OF SIGNIFICANT EVENTS DURING THE TEST

Event	Time Referenced to N-13 Peak Power (msec)	Source of Information
Timer contact closure	-119.0	N-13 T6 -10
Squib flash	- 71.0	L-3 Camera
Sleeve initial motion	- 68.6	SW-1 T11-14
Criticality position of poison sleeve and lower breakwire signal	- 52.7	BW-1, SW-1 T11-9
Sleeve clearing top of vessel	- 44.5	BW-1, SW-1 T11-9
Upper breakwire signal	- 42.0	BW-1, SW-1 T11-9
Smoke from pyrotechnic actuator cylinder	- 38.2	L-3 Camera
EG&G chemical flash trigger	- 11.8	EG-1 T11-4
Cavitation in water above vessel becomes evident	- 9.7	L-3 Camera
Cerenkov becomes evident	- 5.6	L-3 Camera
First EG&G Dynafax frame	- 1.03	EG-1 T11-4
Peak power N-13, N-17	0.0	T6-10, T6-12
Peak power N-10	+ 0.18	T3-11
Xenon flash	+ 0.81	Dynafax Camera
Cerenkov obscured, NaK reaction begins	+ 2.0	L-3 Camera
NaK reaction flow ends	+ 18.0	L-3 Camera
Explosive flash on lip of tank Number 1	+ 58.0	L-3 Camera
Red glow, Number 2	+263-285	L-3 Camera
Water plume peak	+1100	L-3 Camera
Peak gamma dose rate passing 500 meter point downwind	+65,000	F-19

1256090

onset of water expulsion. The lower plot shows the gamma dose rate which was measured at 500 meters downwind from the reactor. A detailed discussion of photographic, nuclear, non-nuclear, radiological, and post-test results follow.

B. Photographic Results

The photographic documentation to record the reactor disassembly and resulting effects was accomplished by employing a variety of fast and standard speed, color and black-and-white cameras around and above the test area. Figure 7 shows a series of photographs taken by EG&G depicting a two-dimensional profile of the reactor during disassembly. These photographs were taken through a periscope arrangement by a Dynafax camera at a speed of 17,680 f/second. The salient features of these photographs are described in the following table.

TABLE IV

EG&G DYNAFAX PHOTOGRAPHIC RESULTS

Picture Number	Frame Number	Time from peak power (msec)	Event
1	12	-0.41	Binal sleeve removed - Cerenkov glow masks reactor
2	30	+0.61	Vessel begins to expand - Cerenkov glow still observable
3	34	+0.83	Xenon lights flash illuminating "break bands"
4	39	+1.12	Expansion continues - dome begins to bulge
5	45	+1.46	Displacement of water environment begins
6	51	+1.79	Outline effect caused by a fractured internal Be reflector seen on left
7	55	+1.96	Venting begins
8	59	+2.25	Vessel has expanded to an approximate spherical shape - venting is profuse

1256091

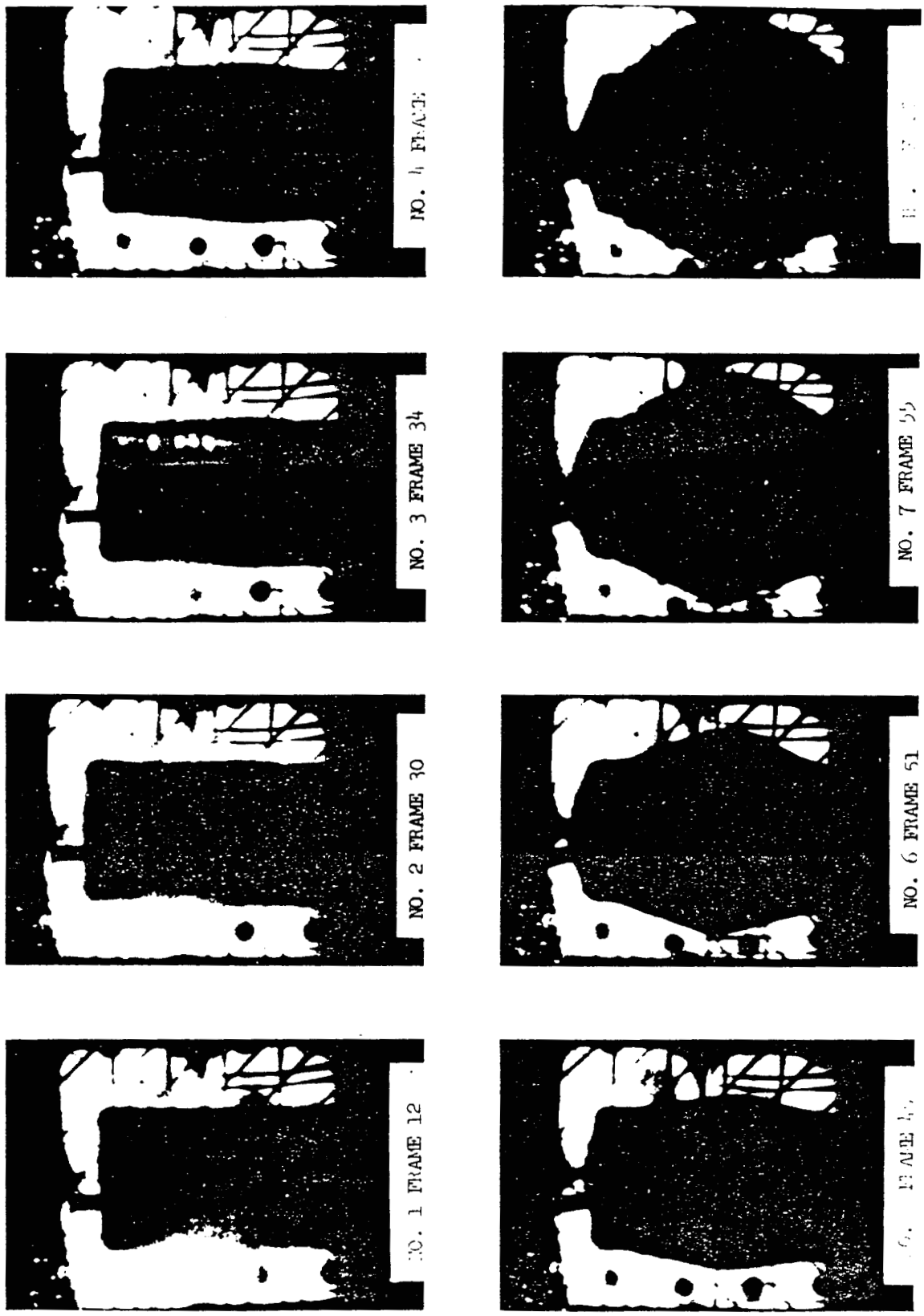

Fig. 7 EG&G High Speed Photographs of Reactor Disassembly

1256092

Figures 8 and 9 show a series of "rapid sequence" photographs taken from ground level (camera Station 2). The events depicted, with time referenced to peak power, are as follows:

1. The pyrotechnic actuator has been fired, the shock absorber (A) is compressed indicating sleeve removal, the drive mechanism (B) is in place.

2. The shock absorber is still compressed, the drive mechanism cap has been thrown off, water expulsion has begun.

3. Water expulsion continues.

4. A bright spot (D) presumed to be NaK-water reaction, about 9 inches in diameter is seen above the environmental tank.

5. The bright spot diminishes in size and intensity.

6-7. The water spout reaches maximum height.

8-9. The upper grid plate (C) is seen falling back onto the test pad.

10-11-12. Expelled water falls onto the test pad and forms secondary "clouds" which begin drifting with the wind, the environmental tank is seen still intact.

Figure 10 shows a sequence of pictures taken from a camera located 150 feet above the test area (camera Station 3). Picture A shows the pyrotechnic actuator squibs firing; B shows the beginning of the Cerenkov glow; C shows the Cerenkov glow at maximum intensity and the EG&G lights illuminating the entire tank interior; and D shows the water plume as it engulfs the superstructure. A red glow, which occurred about 300 msec after peak power and which is believed to be caused by a NaK-water reaction, was photographed from the tower camera station on color film. The intensity of this glow however, was not sufficient to be seen through the water plume on black and white film.

C. Nuclear Measurement Results

The nuclear data to be presented are the result of digital processing and computor treatment of analog data originally recorded on magnetic tape. The digitally processed data are accurate to within ± 3%.

1256093

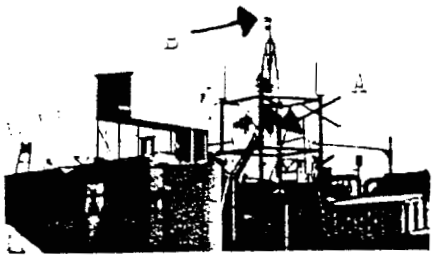

No.1 (T_o - 22msec)

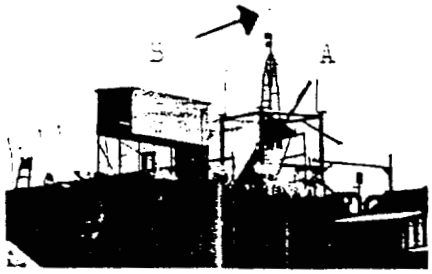

No. 2 (T_o + 127msec)

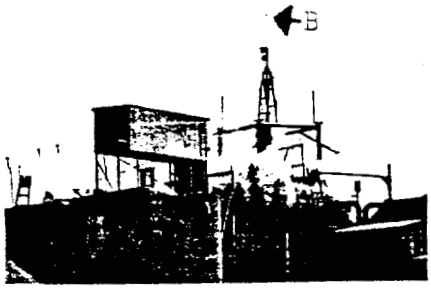

No. 3 (T_o + 149msec)

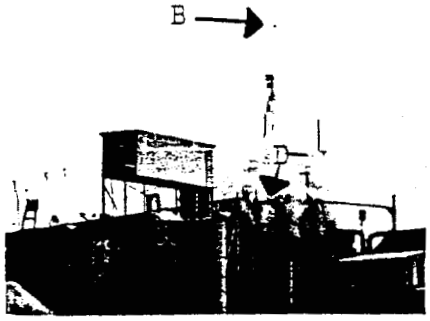

No. 4 (T_o + 275msec)

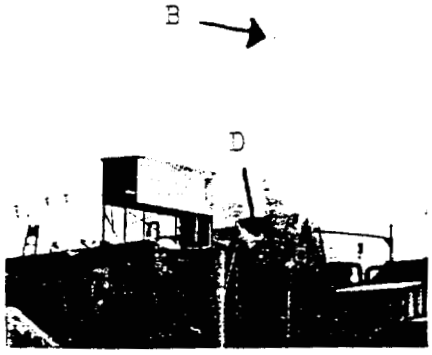

No. 5 (T_o + 380msec)

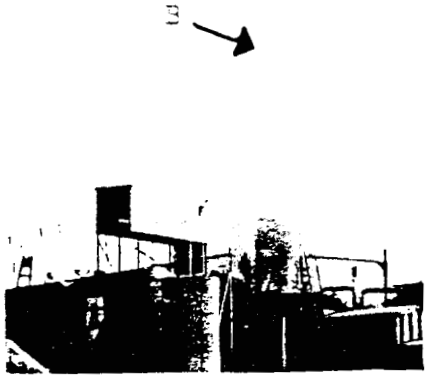

No. 6 (T_o + 410msec

Fig. 8 Elevation View (1 through 6) of Destructive Test Sequence

1256094

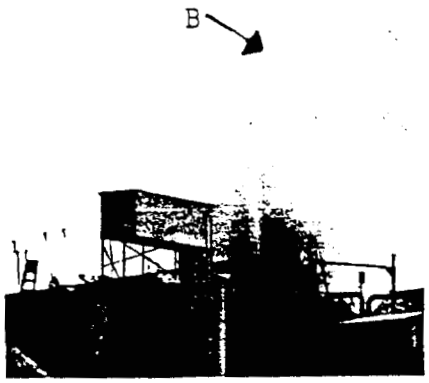

No. 7 (T_o + 550msec)

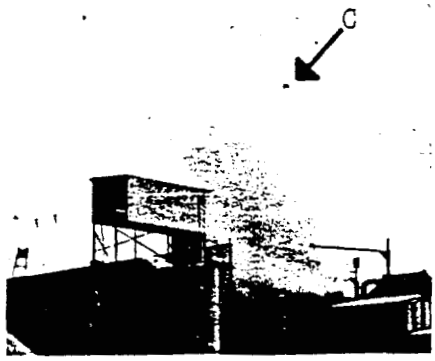

No. 8 (T_o + 1.31sec)

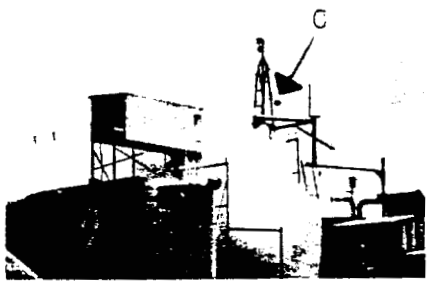

No. 9 (T_o + 1.96sec)

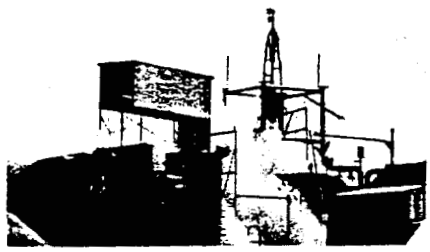

No. 10 (T_o + 2.6sec)

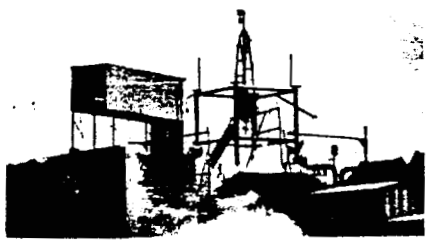

No. 11 (T_o + 3.1sec)

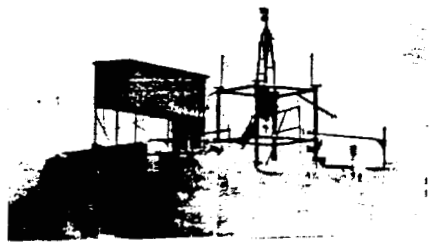

No. 12 (T_o + 3.3sec)

Fig. 9 Elevation View (7 through 12) of Destructive Test Sequence

1256095

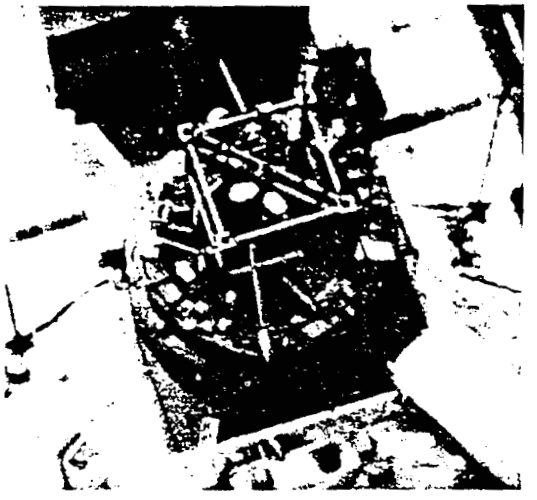

A

PK PWR - 69.5 msec

B

PK PWR - 1.5 msec

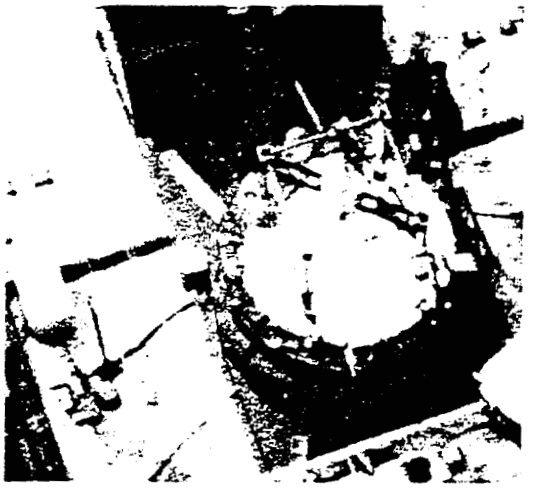

C

PK PWR - 0.0 msec

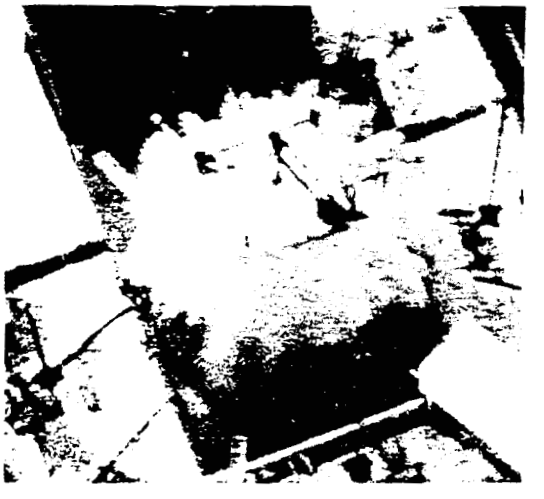

D

PK PWR + 200 msec

Fig. 10 Overhead View (A through D) of Destructive Test Sequence

1256096

In addition to the error present in the digitally processed data, uncertainties due to intercalibration of detectors, detector linearity, and field effects were included in the interpretation of the data shown in Table V.

Table V is a summary comparison of the salient nuclear information indicated by the various nuclear detectors. Two gamma detectors (N-9 and N-11) were used for the intercalibration of detectors between the power calibration and the destructive test. This intercalibration was required to encompass the range of 10^{10} nv occurring during power calibration to 10^{17} nv occurring at peak power of the destructive test. The gamma detectors provide a straight forward correlation of the power calibration power level to the destructive test power level.

During the power calibration both delayed and prompt gammas contributed to the observed signal, however, the bulk of the delayed gammas (90% or more) lag the prompt gammas by greater than 10 milliseconds.

Thus for short period transients such as the destructive test, the gamma signal seen by gamma detectors is, at any given time, reduced by the amount of the delayed gamma contribution. The delayed gamma contribution amounts to about 42% of the total gamma signal. Because of the short period and duration of the destructive power burst, the delayed gamma distortion of neutron detector output is insignificant.

Figure 11 shows linear power versus time for detectors N-10, N-13, and N-17. Detectors N-10 and N-17 have been normalized to the N-13 peak power and N-10 has been normalized in time to coincide with the time of peak power as seen by N-13 and N-17. From this figure it is apparent that the detectors N-13 and N-17 give essentially the same value for the total nuclear energy release, while N-10 gives a slightly larger value.

From Figure 12, showing log power versus time for detectors N-2, N-9, N-10, N-13, N-17, and N-19 it can be seen that, with the exception of N-10, all detectors within the range capability of each detector channel follow the burst shape of N-13. Detector N-10 was shown to have non-linear gamma sensitivity over a large portion of its dynamic range. This non-linearity results in distortion of the burst shape.

TABLE V

SUMMARY OF NUCLEAR DATA

Make & S.N.	Type	Location	Record Mode	Front Side τ (msec)	Time of Peak Power (msec)	Peak Power (Gigawatts)	E_{total} (Mw-sec) ± 95% Confidence Interval
N-2 GE Mini #545641	Thermal Neutron Detector	In-core Z = + 2" (1)(4)(5)	Linear F.M.	630	Saturated @ Peak Power		
N-9 GE Gamma #4131132	Gamma Detector	In-water tank 45" from core	Log F.M.	630	Saturated @ Peak Power		
N-10 Reuterstokes Semi Rad #E-531	Thermal Neutron Detector	In-water tank 26" from core	Linear F.M.	780	0.18	19	45 ± 13
N-13 ITT Photo Tube Scintillator #1462	Fast Neutron Detector	Flight Tube	Linear F.M.	640	0	18	43 ± 8
N-17 Reuterstokes Gamma #E-498	Gamma Detector	Under Flat Car	Linear F.M.	660	0	22	53 ± 9
N-19 ITT Photo Tube Scintillator #1478	Fast Neutron Detector	Flight Tube	Log F.M.	695	0	18	43 ± 9

1251098

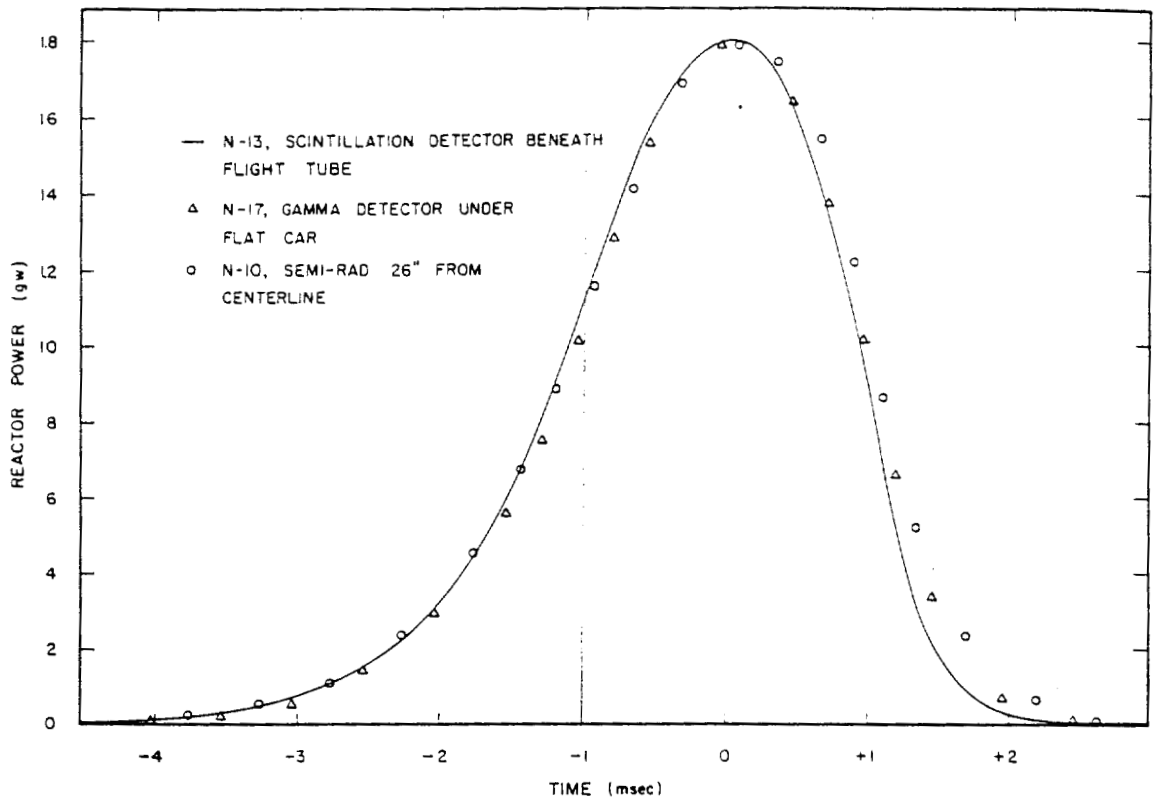

Fig. 11 Burst Shape Comparison of Linear Nuclear Detector Signals

Figure 12 also indicates that the logarithmic output of detectors N-9 and N-19 can follow a short period burst with reasonable accuracy after the log converter overcomes the response lag.

Table V indicates that the time of peak power for detector N-10 occurs 0.18 milliseconds after that indicated by detectors N-13, N-17, and N-19. This delay can be attributed to neutron residence time in water. Detectors N-13 and N-19 are fast neutron detectors located below the flight tube and have essentially no delay time. Detector N-17, a gamma detector, likewise has no delay in response.

Since detector N-13 most accurately represents the power-time history throughout the reactor excursion, the output of this detector was used for all computational treatment involving transient power.

1256099

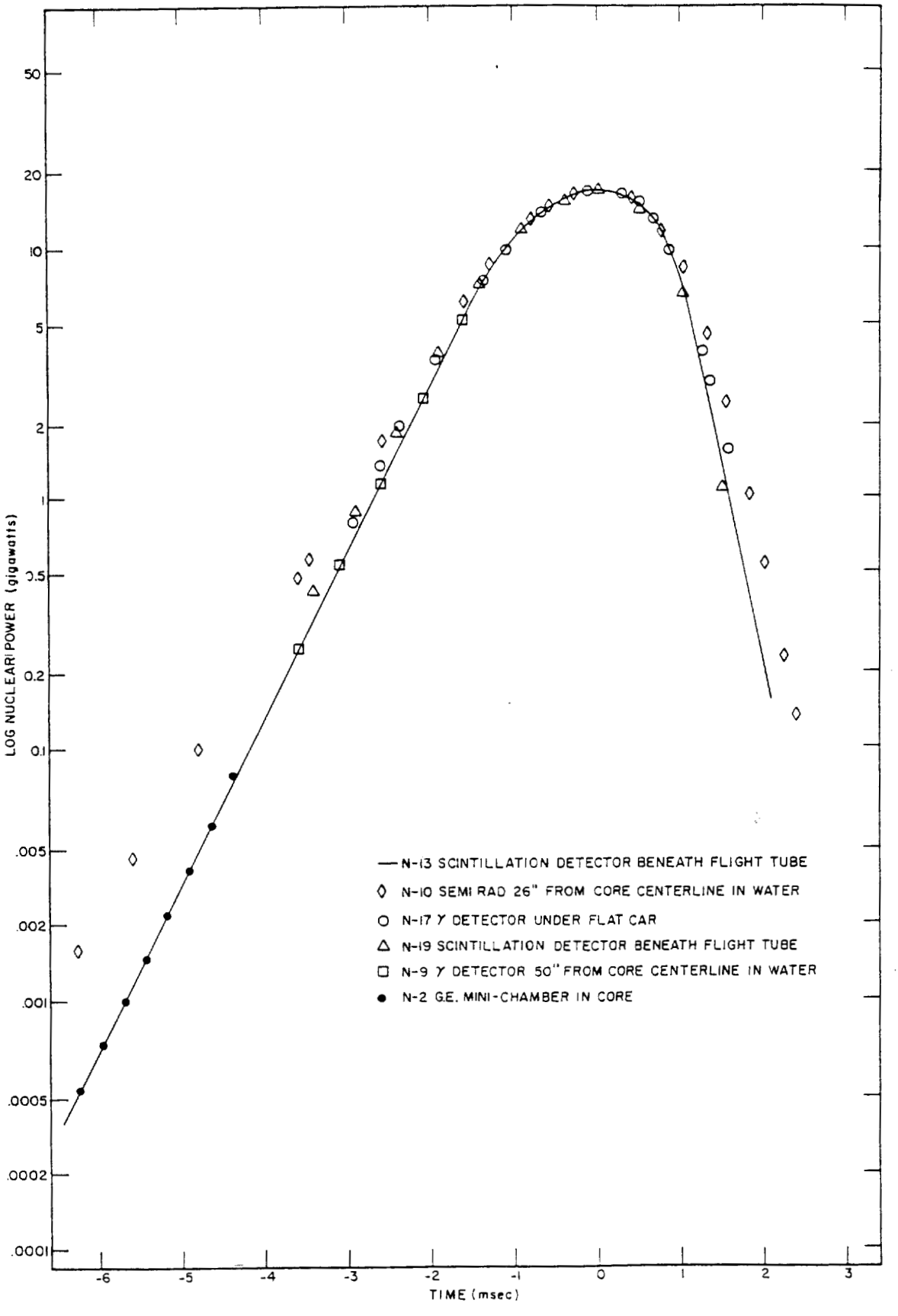

Fig. 12 Comparison of Log and Linear Detector Signals

1256100

D. Non-Nuclear Measurement Results

The non-nuclear information is considered to include reactor temperature, reactor diassembly behavior, environmental pressure generation in the water, and other environmental effects such as water expulsion, flatcar displacement, air pressure generation and air temperature rise above the tank. The data presented were reduced from the original analog tape recordings by means of a time-base-expansion process using the recording techniques. The time-base-expanded data retain the raw signal information to a real-time bandwidth of about 10 kc. These data are accurate to within ± 6%.

Core Temperature

The reactor fuel temperature generated during these tests was not measured directly but has been implied from measurements derived from the energy probes placed in interstices throughout the core, and from information concerning nuclear power, flux distribution, and heat capacity.

Data from the energy probes are presented in logarithmic form in Figure 13 for 10 wt% energy probes (typical of reactor fuel loading) and in Figure 14 for the 5 wt% loading. For comparative purposes, a trace of energy deposition as determined from the scintillation detector N-13 is also shown. The energy probe traces in both these figures are seen to rise at an asymptotic rate similar to the energy trace. The deviation of the energy probe trace from the energy trace is the result of the heat capacity change attendent to the temperature rise of the fuel. These figures are arranged to show the top trace as the outermost energy probe in the reflector while the 7th trace from the top shows the energy probe located closest to the center of the core.

The 10 wt% reflector energy probes shown in Figure 13, display erratic behavior and ultimate failure at a temperature of about 1800°F a millisecond prior to peak power. The flux peak in the reflector causes early failure of these probes. Trace EP-6, located about 0.06 inch inside the core boundary, shows that the fuel near the outer ring of the reactor is at a considerably lower flux level than that in

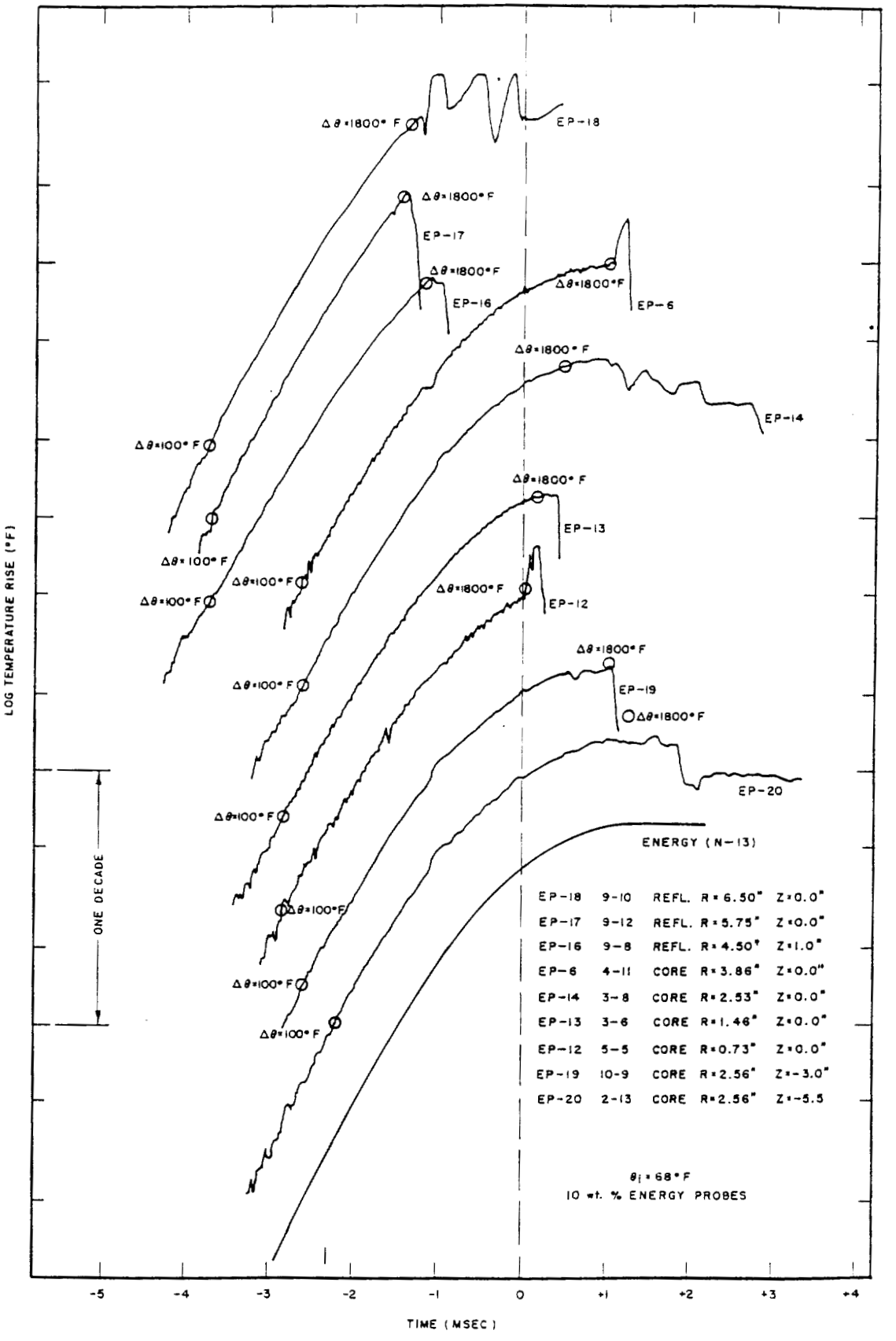

Fig. 13 10 wt% Energy Probe Results

1255102

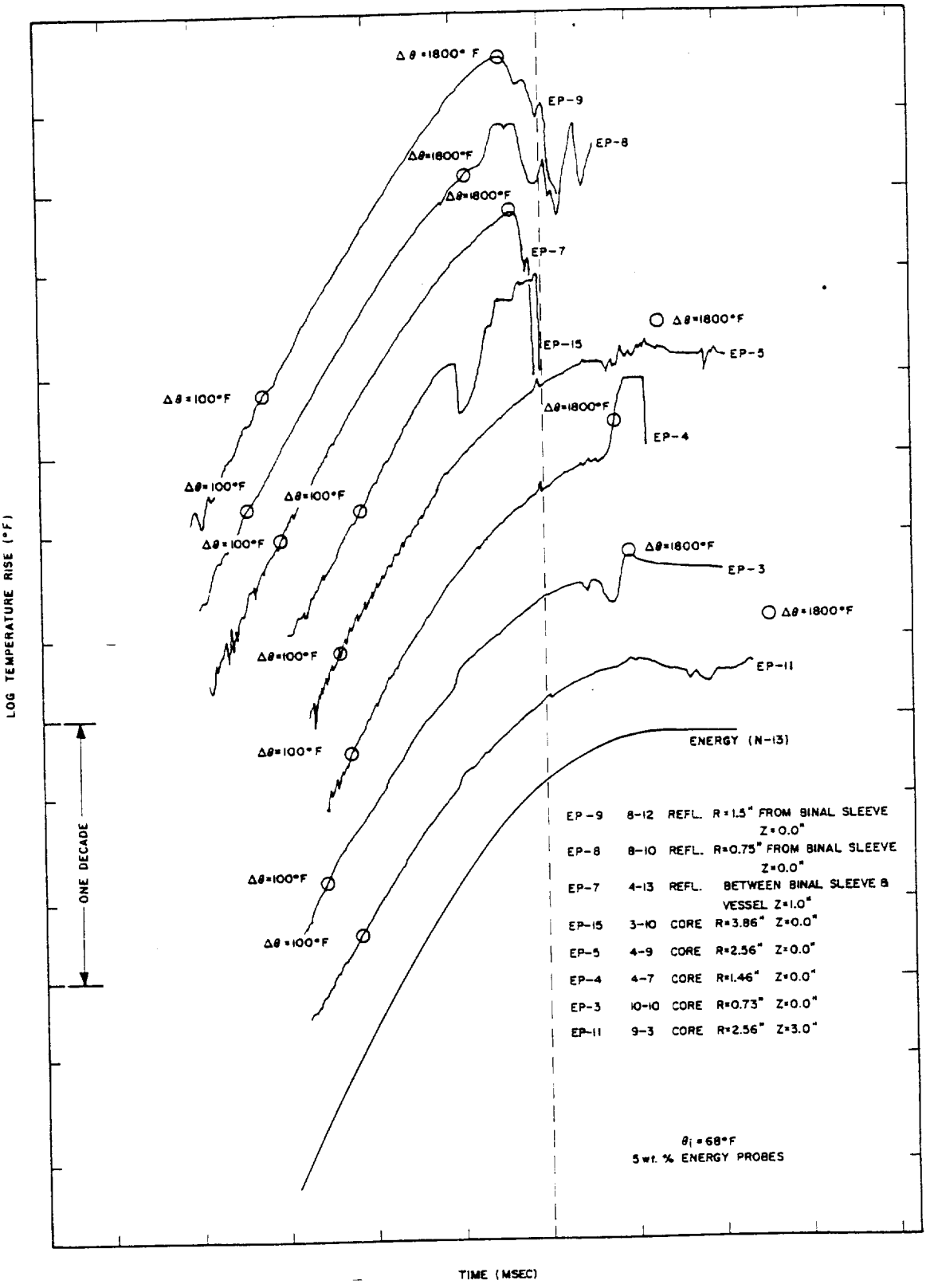

Fig. 14 5 wt% Energy Probe Results

1256103

either the reflector or the center of the reactor. The region in which EP-6 is located does not reach the 1800°F point until about a millisecond after peak power. Probe EP-14 which is near to the center of the core reaches 1800°F about 600 microseconds after peak power. Probe EP-20, located 5-1/2 inches below the core centerline, reaches only 1300°F and does not fail until about 2 milliseconds after peak power. Failure of these energy probes appears to result at higher temperatures than 1800°F or at a time characteristic of gross core disassembly.

The 5 wt% energy probes, as seen in Figure 14, reveal much the same general characteristics as the 10 wt% energy probes. The top three traces in this figure represent the reflector thermal neutron density and show failure prior to peak power but at a later time than that shown by the corresponding 10 wt% probes. The remainder of the 5 wt% in-core probes reveal temperatures not exceeding 1500°F. A detailed analysis of these probes in providing both fuel temperature indication, flux distribution, and total energy release information is given in Section V-C.

Reactor Disassembly

The time history of the reactor vessel disassembly is indicated by (1) vessel strain measurements, (2) the signal from an EG&G breakband, (3) the rapid sequence photographs taken by EG&G, and (4) the onset of pressure generation in the water created by vessel expansion.

Strain Measurements - Data from the strain gauges attached to the reactor vessel are shown in Figure 15. The top trace represents a dummy gauge attached to the vessel wall and is useful for its time of failure and for revealing any environmental temperature or radiation sensitivities.

Traces SG-4, SG-5, and SG-6 represent strain as indicated from gauges placed at 90° intervals around the vessel. The bottom two traces represent strains occurring on the reactor vessel bottom which, because of the inverted orientation of the vessel for this test, was on top. With the exception of the dummy gauge, all other gauges are indicated on a scale of 2000 microinches/inch/division. This represents an elongation at the point of measurement of 0.2% which is considered to be the beginning of yield.

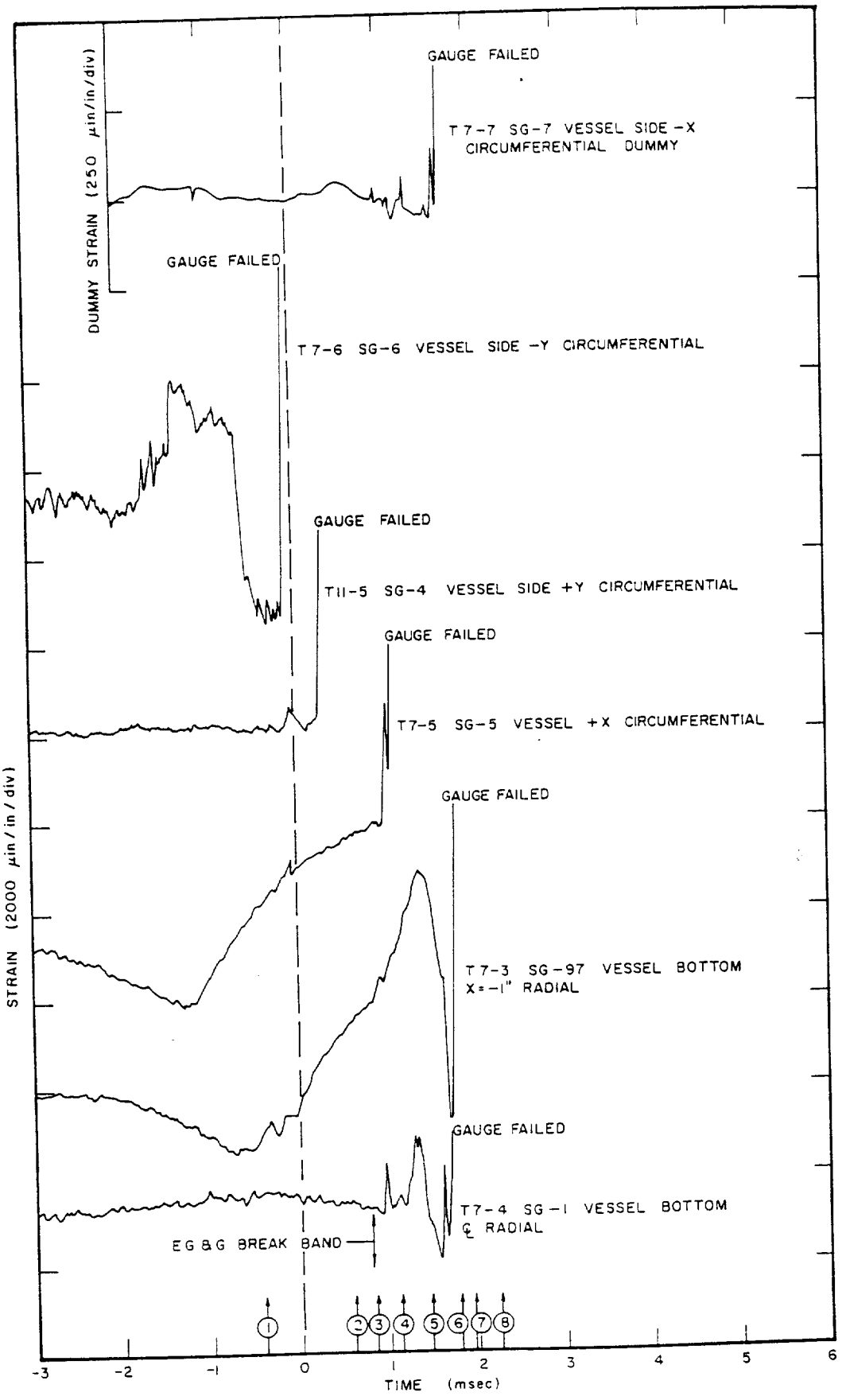

Fig. 15. Indicated Strain on Reactor Vessel and Pedestal

1250105

Trace T7-6, reveals a disturbance beginning about 2 msec prior to peak power. This disturbance shows a slight tendency toward vessel expansion followed by a relaxation and ultimately a very rapid strain increase to gauge failure at 100 microseconds prior to peak power.

Trace T11-5 from the gauge located diametrically opposite the gauge just discussed shows a lack of any significant phenomena prior to peak power except for the spike seen at the time of severe vessel expansion, as shown by trace T7-6. The rupture occurring on the minus Y region of the reactor permits a momentary relaxation in the plus Y region for 200-300 microseconds after which severe strain is indicated in the plus Y region. The characteristics of trace T7-5 appear to indicate radiation sensitivity although the dummy gauge (SG-7) shows none. In this particular case, the results are sufficiently close to the behavior of a differentiated power burst that little significance should be attached to the data. However, at about 1 millisecond following peak power the abrupt deviation from this trend indicates a severe strain increase at that location.

Gauge SG-97, located on the vessel bottom, indicates much the same behavior regarding radiation sensitivity as gauge SG-5. However, at 1 msec after peak power, an increase of strain appears at a time commensurate with the gauge failure of SG-5. Gauge SG-1, similar to SG-97, was located at the very center of the bottom head, and indicated the existance of a spike at the time the plus X gauge appeared to fail. Beyond the time of this spike, the behavior of both bottom gauges is very similar in character and both show failure at about 1.8 msec following peak power. It should be noted here that the gauges represented by traces T7-6 and T11-5 are mounted on the outer vessel surface adjacent to the beryllium filler pieces. These gauges would not be expected to experience a great deal of vessel expansion until such time as the beryllium filler pieces were broken, after which a severe strain at a rapid rate could be expected. This effect can be seen in the figure.

<u>EG&G Photographs</u> - Additional information regarding the disassembly behavior in the region of 1-2 msec following peak power is presented by the EG&G photography and associated timing signals.

1256106

Specifically, the reactor vessel was encircled by breakbands used to trigger the Xenon flash lamps. These breakbands, designed to cause electrical circuit discontinuity at about 1/2% elongation, represented a gross measurement of the change in vessel circumference. The breakbands were determined to have broken at about 800 microseconds following peak power. The EG&G photographs presented in Figure 7 show evidence of vessel expansion as a function of time following peak power. From these photographs it can be seen that pictures 1 through 3 show very little vessel enlargement. However, beginning with frame 4 at 1.1 msec after peak power, vessel expansion becomes apparent and continues to total disassembly.

Onset of Pressure - It can generally be concluded from the above information that water was not significantly displaced from its original position until sometime between peak power and 1 msec after peak power. This same interval of time also marks the onset of severe reactor disassembly as revealed by the pressure information to be discussed next.

Pressure Generation

Information on the pressure generation and propagation within the water environment around an expanding source or vessel can be useful in determining the pressure at the source and the mechanical energy generated by the expanding source. The mechanical energy is manifested by work done on the environment, viz., causing disarray within the tank, expelling water, displacing the environmental tank, etc.

For this particular test, a detailed understanding of the pressure-time history can also provide information on the partition of expansion forces between hydrogen pressure buildup and the combination of steam generation and NaK-water reaction. Although it is beyond the scope of this document to attempt a complete analysis of the pressure information, some discussion of the data will be made to indicate its interpretability.

In order to interpret the various pressure-time histories, consideration must first be given to certain acoustical aspects of the test

1256107

configuration, e.g., size of expanding source, propagation velocity in the medium surrounding the source, distance to relief and reflecting boundaries, effective wave length characteristics, volume rate-of-change or the rise time represented by the expanding source, location of pressure measuring detectors with respect to source and boundaries, etc.

An examination of the pressure-time history data presented in Figure 16 reveal the general features of a 1 millisecond rise time, certain high frequency modulations near the beginning of a relatively long pulse decay, and a duration of about 25-30 milliseconds. It can be shown that a 1 millisecond rise time is equivalent to a characteristic frequency of 300-400 cycles per second which represents a wave length in water of about 15 feet. Since the diameter of the reactor at the time the first pressure peak occurs is approximately 13 inches as seen in the bottom trace of the EG&G photographs, Figure 7, the source size is therefore considerably less than the wave length represented by the rise time. The source can thus be considered spherical and the propagation from that source treated as a spherical wave. As most other portions of the pressure pulse represent longer wave lengths than the initial rise, the entire pulse can be treated as a spherically propagating disturbance, implying a 1/R pressure dependence with no severe directionality effects.

It is of interest that the rise time is several orders of magnitude longer than that considered to represent a shock wave generation. Also, the peak pressure is two orders of magnitude lower than that required for "shocking up" of a simple acoustic disturbance. Therefore, standard "small amplitude" techniques are adequate for analyzing the water pressure disturbances resulting from the destructive test.

The 1 millisecond rise time represents an effective wave length, until time of rupture, of greater than 50 feet implying that the pressure environment within the vessel can be considered to be isotropic.

Since the propagation velocity for a disturbance traveling in water is about 5 feet per millisecond, the initial pressure rise and first peak will be unaffected by the physical boundaries represented by the water surface or tank walls. This permits treatment of the early portion of the pressure

1256108

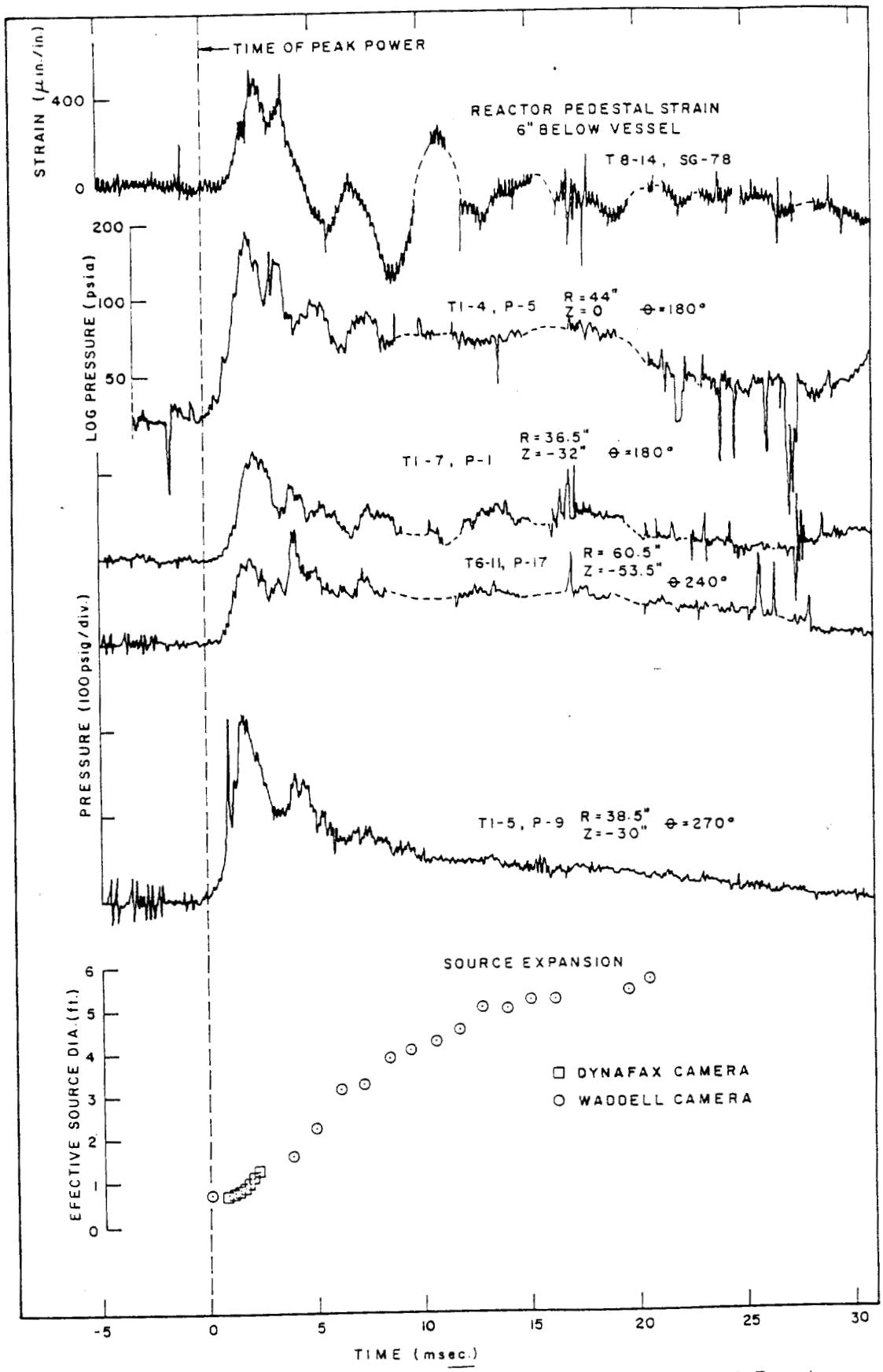

Fig. 16 Indicated Pressure in Water Environment Around Reactor

1253109

rise according to compressible flow theory. The significance of this result is that the volume expansion created by the growing vessel is acting on the bulk modulus of the water resulting in a pressure which is equal to that within the reactor vessel.

The pressure pulse following the first peak persists for many complete transit times from source to boundary and boundary to boundary. The fundamental mode represented by the pressure pulse can therefore be treated according to a combination of incompressible and compressible flow theory.

The significance of the detailed long-term portion of the pulse is of lower interest here since it is characteristic of the effect of the experiment geometry on NaK water reaction and steam generation and not indicative of the reactor diassembly. Emphasis has therefore been placed on the initial rise and the fine structure associated with the first few peaks in the pressure pulse.

Pressure Data

Before discussing the detailed features of these pressure traces certain aspects of pressure measurements will be considered. The pressure measurements indicated were made at several positions within the environmental tank as shown in Figure 17. These measurements taken at the various radii have been corrected for the propagation distance compared to the source size at a particular time in order to accurately predict the pressure being generated at the source. The delay time represented by the various detector locations was also accounted for in correlating time history features from one detector to another, and in correlating the events generated at the source referenced to the time of events at the source.

All pressure transducers for which traces are presented were capable of DC to 20 kc or greater response. Three of the pressure transducers, P-1, P-9, and P-17 are scaled to 100 psi per division. P-5 is shown on a logarithmic scale. The traces on the figure have been arranged according to those locations which are similar in direction away from the reactor such that comparison of detailed features can be readily made.

1256110

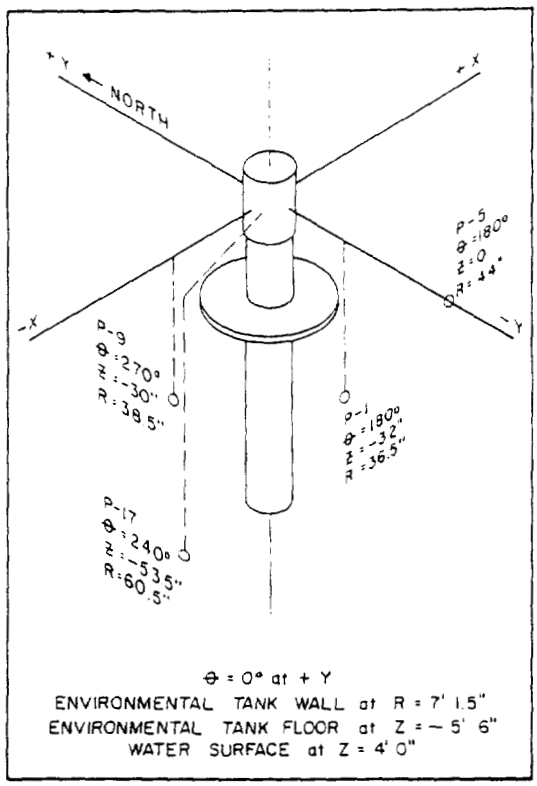

Fig. 17 Pressure Transducer Locations in Environmental Tank

The general features presented by these traces reveal a reasonable similarity between transducers, thereby verifying the existance of a simple spherical source. The detailed modulations, however, show an apparent lack of similarity. If, however, the difference in distance between the transducers and the source is accounted for as the source size grows, the magnitude of the difference of the modulations on these traces can be easily accounted for.

In the near-field region of a spherical source, a close approximation of the pressure at the surface may be obtained by extrapolation on a 1/R basis to one source-radius from the source center. Therefore, the magnitude of the first pressure peak indicates a pressure at the surface of the vessel of 1320 psi for P-9 and 850 psi for P-17. The difference between these two values is thought to result from the different geometry between the detector and the center of the source caused by preferential disassembly. The existence of preferential disassembly is supported by the difference in pressure indicated by these two transducers and also by the motion pictures from the tower station (camera station 3). The preferential venting was in the northwest direction ($\theta \approx 315^{\circ}$). Since the reactor vessel had ruptured at the time of peak pressure, the pressure within the vessel should be very near that at the surface. The trace showing reactor pedestal strain indicated the onset of significant downward thrust at this time, giving further evidence that the vessel had ruptured.

Table VI lists the calculated pressures at the vessel surface using the extrapolation process described previously and the appropriate source diameters indicated in the bottom trace in Figure 16.

1256111

TABLE VI

PRESSURES AT THE VESSEL SURFACE

Pressure Transducer	Radius From Source Center	Assumed Source Radius	Time After Peak Power*	Pressure Measured at Transducer	Calculated Pressure at Source Surface
	(in.)	(in.)	(msec)	(psi)	(psi).
P-9	38.5	4.8	1	60	480
	38.5	6.4	2	220	1320
	38.5	9.5	4	135	550
P-17	60.5	4.8	1	40	500
	60.5	6.4	2	90	850
	60.5	9.5	4	110	700
P-1	36.5	4.8	1	30	230
	36.5	6.4	2	120	680
	36.5	9.5	4	70	270
P-5	44	4.8	1	55	500
	44	6.4	2	160	1100
	44	9.5	4	86	400

* Pressure information corrected for propagation time.

These figures indicate that at about 1 millisecond after peak power the vessel surface pressure was about 500 psi. This value was obtained assuming the source to be an expanding sphere. The spherical approximation in this case yields pressures slightly lower than actually existed at the moving portion of the vessel. The vessel as it expanded acted on the bulk modulus of the water. Since the water represented a considerably stiffer impedance to motion than did the vessel retention strength which was about 500 psi static at 50% elongation, the pressure magnitude within the reactor was only slightly more than that indicated at the surface.

The source surface pressures calculated at a time of +4 milliseconds show a shift in the source center toward the -X direction indicating venting is profuse at this time. The pedestal strain trace shows a complete unloading of the pedestal at 4 milliseconds substantiating that the vessel must be completely ruptured. The remainder of the pressure pulse is presumed to be due to steam generation and NaK-water reaction. Not included in the above table are the effective

1256112

source surface pressures represented by certain fine structures modulating the gross fundamental of the pressure trace. One example is the spike most evident on P-9 at 900 microseconds (more clearly seen in Figure 27 of the next section). This spike when conservatively treated as a 10 inch diameter piston radiating into "free space" extrapolates to a pressure at the vessel surface of about 2000 psi.

In summary, the information from vessel strain gauges, Xenon flash break band, onset of pressure generation, and the vessel expansion photographs give conclusive evidence that reactor disassembly was initiated at about 500 microseconds following peak power. The pressure information during the next 15 milliseconds indicates that the pressure magnitude at the reactor surface and within the reactor was about 1000 psi with local regions reaching two or three times this value. The forces resulting from hydrogen release persist to about 5 milliseconds after peak power - at which time the steam generation and NaK-water reactions persist for an additional 20 milliseconds.

Miscellaneous Effects Following Pressure Generation

Since the pressure generation and propagation is primarily a manifestation of mechanical energy development, it is appropriate to consider the manner in which the pressure affected the environment following the excursion. Figure 18 shows several physical phenomena resulting from the pressure generation. Trace T1-5 reveals a typical pressure. One consequence of the pressure generation was water expulsion from the tank. Traces T6-7, T9-9, and T9-11, indicate the water surface displacement as derived from a float-slidewire arrangement located at positions near the edge of the tank, halfway between the edge and the center, and near the center of the tank. This information is primarily useful in determining the energy imparted to the water expelled from the tank and in determining transport characteristics of fission products.

A second consequence of the pressure generation in this particular experimental configuration is the flatcar displacement. This is shown

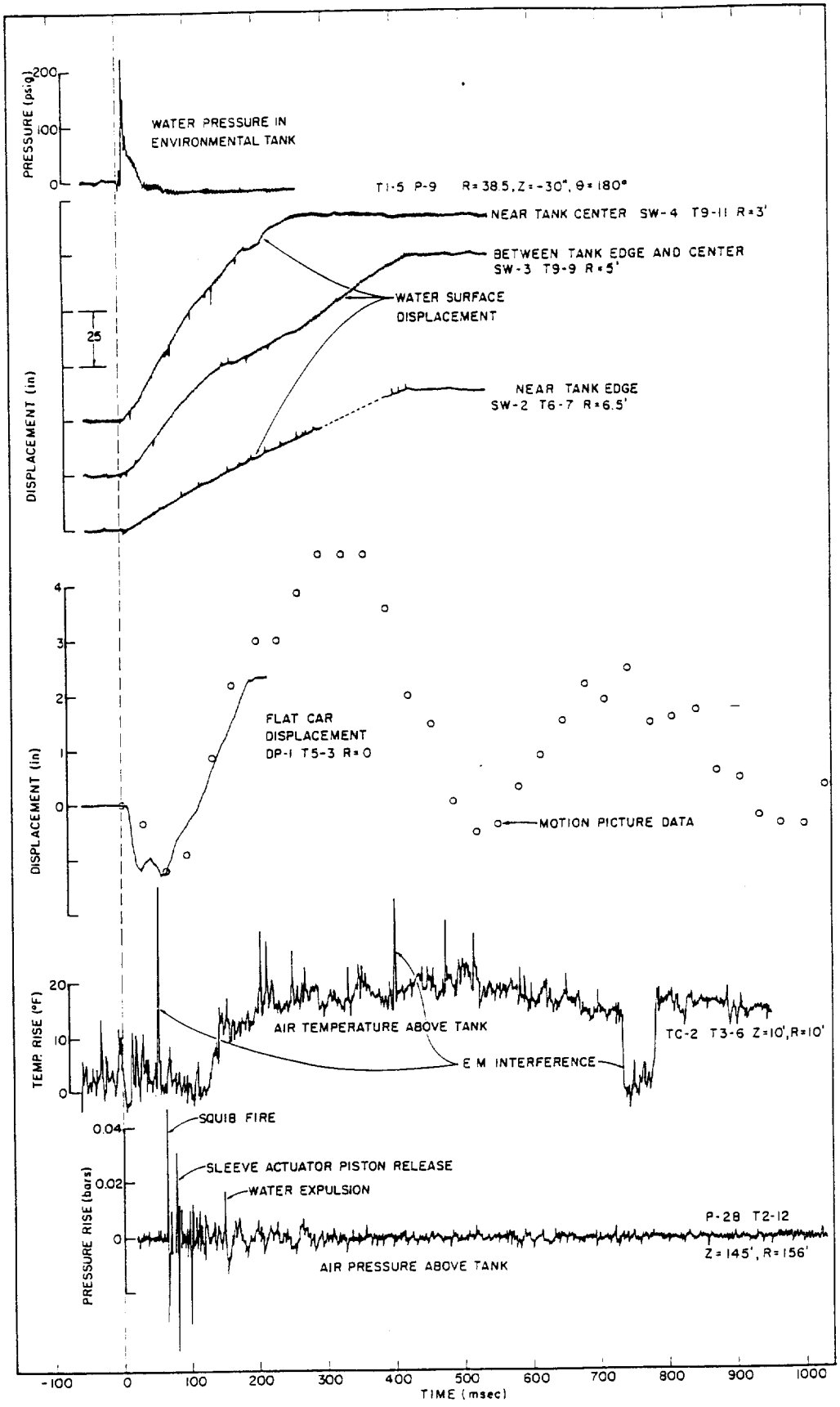

Fig. 18 Summary of Mechanical Effects Data

1256114

in trace T5-3. The excursion of the flatcar was beyond the range of the analog detector and data from the motion pictures are shown to supplement the information covering this time period. The flatcar is shown to be accelerated in a downward direction for the duration of the pressure pulse. Higher frequency modes superimposed on the natural ringing frequency of the flatcar are evident in trace T5-3. The residual position of the flatcar was measured to be lower than the original position, indicating permanent deformation of the flatcar frame.

Trace T3-6 indicates the environmental temperature existing above the tank as measured by one of the fast response thermocouples. These data were intended to show evidence of hydrogen-oxygen explosions or NaK-steam reactions existing above the tank. The trace reveals a gradual rise in temperature consistent with the water surface expulsion giving no evidence of hydrogen-oxygen explosion or Nak-steam reaction.

Trace T2-12 represents the air pressure as seen 150 feet above the tank. This information has been studied in detail on a much more expanded time scale and the various spikes have been identified as shown on the plot. Air pressure information at ground level and at various distances from the reactor tank show similar behavior at considerably lower levels of pressure. The interpretation of the air pressure measurements has revealed that the mechanical energy generation in the air environment above the tank was considerably less than the 200 kw-sec used to remove the poison sleeve with the pyrotechnic actuator.

The discussion presented in the foregoing represent a limited analysis of the data available. Further examination should reveal considerably more detail on rate of effects, on intercorrelation between the various phenomena, and on accuracy by statistically treating the outputs from several detectors. In addition, several types of detectors reveal evidence of severe electromagnetic interference taking place during the excursion. This interference is presumed due to NaK-water, hydrogen-oxygen, or other exothermic reactions. There is evidence that these interferences correlate with observations of flashes seen in the motion pictures. In no way, however does the electromagnetic interference seriously obscure information to be gained from the experimental data.

1256115

E. Radiological Measurement Results

Introduction

Monitoring of the radiological effects of the destructive test include measurements of the fission product release, direct gamma and neutron doses, and spread of airborne contamination. Measurements concerning the release of beryllium are also included in this section. A radiological monitoring grid was set up as described in Appendix A. The grid, with the reactor test pad as the focal point, was arranged as a series of concentric arcs with a heavily instrumented 60° sector centered on 30° east of true north.

Weather criteria for performance of the destructive test were established as follows:

(1) Wind direction variance: 180° to 240°

(2) Minimum wind speed: 10 mph

(3) Lapse conditions

(4) No precipitation.

Phillips Petroleum Company Health and Safety personnel were responsible for radiological measurements to approximately 2500 meters and measurements beyond this arc were the responsibility of the AEC-ID Health and Safety Division.

In addition to the sampling equipment in the grid, radiological sampling equipment was placed on a specially constructed 150 foot tower and on the existing IET stack. Water catch cans and trays were located on the reactor dolly, film-badge-drop devices were located on an approximate 10 meter arc, air support to follow the radioactive cloud was provided, "clothesline-type" sample stations were located east of the reactor, and special high range dosimeters and activation foil boxes were employed in the immediate reactor area.

Radiological monitoring results from the grid and reactor area during and after the test are summarized in this section. A detailed analysis of the radiological results will be published in IDO-17038, "Radiological Aspects of the SNAPTRAN 2/10A-3 Destructive Test".

1256116

Direct Radiation Measurements

The direct radiation resulting from the excursion and the residual fission products was monitored by both remote radiation monitors and film badge dosimeters. A remote radiation monitor with a 1,000 r/hr detector was located on the edge of the environmental tank. The reading from this monitor went off scale at the instant of the power burst and then failed as it was deluged by water and debris from the environmental tank. A remote radiation monitor 20 feet directly west of the reactor which was shielded by the environmental tank gave a peak reading of 30 r/hr. This radiation field decayed to 0.055 r/hr 120 minutes after the test. Twenty four hours later the field was 2 mr/hr at this point.

The readings from the film badge dosimeters that were on or near the environmental tank are shown in Figure 19. The film badges situated around the top of the environmental tank recorded an average gamma dose of approximately 25 rem resulting from the power burst and 24 hours exposure to the residual fission product decay radiation.

The highest reading of the three film badges attached to the clothesline was 150 rem. This high reading resulted from the badge dosimeter being positioned in the most direct line of sight with the reactor core. The "clothesline" film badge dosimeters were retrieved approximately one hour after the test.

Doses measured by the film badge dosimeters on the radiological tower are shown in Figure 20. The indicated beta readings up to and including the 40 foot level were due to the radioactive cloud. The low readings in some of the areas can be explained by the presence of various amounts of shielding between the film dosimeter and the reactor and its remains.

Radioactive Cloud

Within milliseconds following the initiation of the reactor excursion, a cloud of steam and water was ejected. The cloud maintained its symetrical shape for a short time until the majority of the water fell back into the environmental tank. At this point, a visible vapor-filled cloud arose and was blown down over the instrumented

1256117

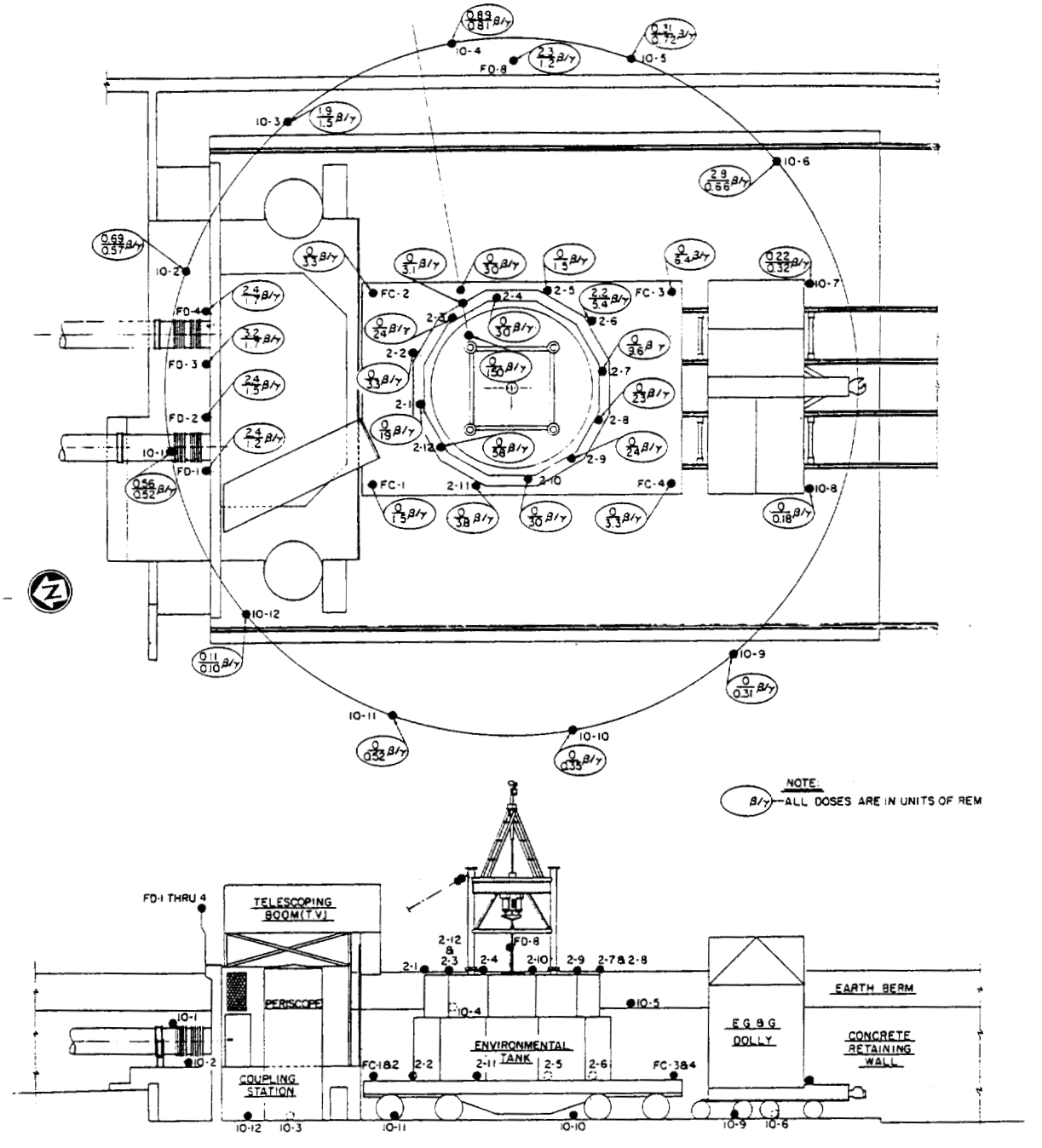

Fig. 19 Test Cell Radiological Dose Measurements

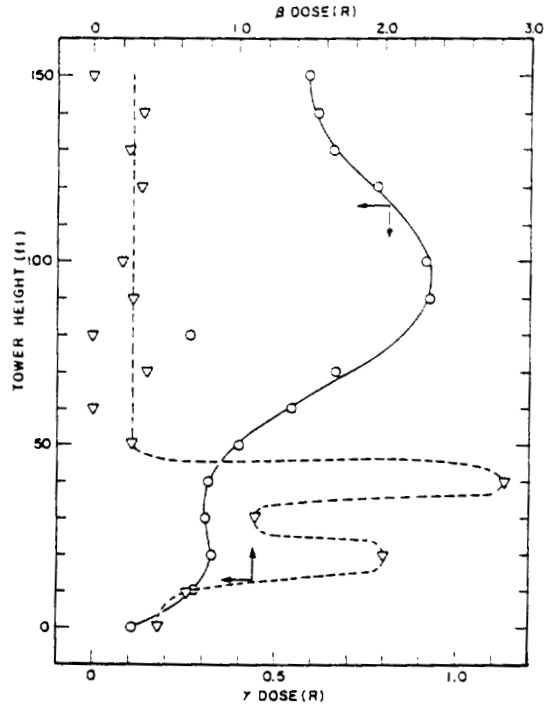

Fig. 20 Dose Measurements from Radiological Tower Locations

60° section of the radiological grid. Movies indicate that there may have been three distinct airborne releases of fission products from the test, one during the initial burst which did not collapse with the cloud, a second that rose up with the vapor filled cloud, and a third that came from the environmental tank following the collapse of the cloud. The third release appeared to merge with the cloud by the time it reached the radiological tower.

The airplane intercepted the main cloud at one mile from the test site and followed it for 21 miles before cloud dispersion and radioactive decay reduced the radiation levels to background. Eleven miles from the test site the airplane, employing a scintillation type detector, measured a peak reading of 0.1 mrem/hr while flying at 1200 feet above the terrain.

Radioactive Noble Gas Release

Two independent methods were used to calculate the quantity of fission gases released from the reactor during the destruct test. The first method utilized data from the balloon type fission gas detector (described in Appendix A). Using an estimated upper limit for the cloud size of 1.46×10^6 cu. ft. at the detector position, calculations indicate that 13.8 curies of Xe-138 (roughly 2% of the amount available) was released.

The second method compares the amount of Cs-137 remaining in the fuel to the amount ideally available from the total chain yield of Cs-137 for the integrated energy release from the fuel. The difference between the calculated value of available Cs-137 and the measured value remaining gives the number of parent atoms (I-137 and Xe-137) that

1256119

were released. The second technique indicates that the maximum release of Xe-137 from the reactor was less than 5%.

Based on these two measurements and the assumption that all noble fission gases behave essentially the same as Xenon, it appears that only a few percent of the noble gases were released under the imposed test conditions.

Radiation Exposures From the Radioactive Cloud

The radiation from the small quantity of fission products released to the cloud was insufficient to give positive readings on the film badge dosimeters at most positions on the grid. Those dosimeters which did show significant readings from the cloud are listed in Table VII. This table indicates that the maximum cloud dose beyond 25 meters from the reactor was less than 1 rem.

TABLE VII

DOWNWIND INTEGRATED RADIATION DOSE

Film Dosimeter Location	Gamma Reading (mrem)	Beta Reading (mrem)
A-1	130	100
A-2	130	0
A-3	115	450
A-4	170	850
A-5	195	800
A-6	180	270
A-7	90	220
A-8	115	150
A-9	60	0
A-10	65	150
A-11	80	120
A-12	95	0
B-1	15	60
B-2	10	60
B-3	30	70
B-4	140	500
B-5	15	0
B-6	25	0
B-7	20	0
B-8	50	30
B-9	35	0

1256120

TABLE VII (cont'd.)

INTEGRATED DOSES FROM THE RADIOACTIVE CLOUD

Film Dosimeter Location	Gamma Reading (mrem)	Beta Reading (mrem)
B-10	50	30
B-11	25	60
B-12	50	50
C-8	30	250
D-8	45	0
E-18	25	0
F-18	40	0
A-3 Well	50	190
A-5 Well	30	260
B-4 Well	75	0
B-5 Well	0	0
C-7 Well	0	0
C-8 Well	35	0
C-9 Well	0	0

Fallout Plates

Only trace amounts of radioactive material were indicated by the fallout plates.

Iodine Release

Although many samplers on the grid were specifically set up to collect iodine, iodine isotopes were not detected except in the environmental tank water. Since these instruments are sufficiently sensitive to have detected trace amounts of any iodine released, the apparent conclusion is that very little if any was released. Recent work at BNL[3] offers a possible explanation for this minimal iodine release. The BNL work indicates that iodine reacts with hydrogen to form hydriodic acid (HI) if there is sufficient free hydrogen available as is thought to have been the case with SNAPTRAN fuel where high energy densities existed. Since HI is nearly infinitely soluable in water, all of the direct yield iodine (iodine available for reaction while the hydrogen was available) could have been trapped and retained in the environmental tank water as hydriodic acid. Tellurium-produced

1256121

iodines I-131, I-132 and I-133 were detected with a grid type sampler (highvolume air sampler with a carbon trap) two days later as they evolved from both the environmental tank and from the vent of the liquid hot-waste tank. At this time free hydrogen was no longer available to combine with the iodine as it evolved from the water surfaces upon which the tellurium parent had plated. These iodine concentrations were below the values contained in the Recommended Concentration Guides for continuous breathing.

Fission Products Released to the Environment

All data from the grid measurements indicate that the quantity of fission products released from the reactor and the environmental tank was much lower than expected. Table VIII summarizes the post-test fission product activity detected on the grid, normalized to 2.28 hours following the test (i.e., the time when the first sample was counted).

TABLE VIII

AIR SAMPLER FILTER DATA

Sample Location	9.7 hr Sr^{91} d/s	2.7 hr Sr^{92} d/s	55 min Y^{91m} d/s	3.6 hr Y^{92} d/s	85 min Ba^{139} d/s
A-3	1.30×10^4	1.20×10^4	1.10×10^4	5.64×10^3	8.40×10^3
A-4	2.7×10^4	2.58×10^4	2.29×10^4	1.21×10^4	3.52×10^4
B-3	1.09×10^4	1.11×10^4	9.26×10^3	5.22×10^3	1.60×10^4
B-4	2.90×10^4	2.94×10^4	2.47×10^4	1.38×10^4	4.22×10^4
C-8	1.86×10^4	7.07×10^3	1.58×10^4	3.32×10^3	4.75×10^4
D-8	7.63×10^3	6.08×10^3	6.48×10^3	2.85×10^3	8.92×10^3
E-16	1.27×10^3	1.05×10^3	1.08×10^3	4.93×10^2	1.82×10^3
F-18	7.99×10^2	3.82×10^2	6.79×10^2	1.79×10^2	5.75×10^2
F-20	1.06×10^3	8.85×10^2	9.01×10^2	4.16×10^2	1.60×10^3
G-15	5.1×10^2	3.56×10^2	4.33×10^2	1.67×10^2	7.00×10^2
H-11	4.6×10^2	3.61×10^2	3.91×10^2	1.69×10^2	8.48×10^2
H-12	6.1×10^2	4.84×10^2	5.18×10^2	2.27×10^2	1.03×10^3
Tower (15' high)	5.04×10^4	5.36×10^4	4.28×10^4	2.52×10^4	1.64×10^4
Tower (30' high)	1.91×10^4	1.92×10^4	1.62×10^4	9.02×10^3	7.20×10^3

1256122

The fact that the detected fission products are all daughters of short lived (half life < 50 sec) radioactive noble gases demonstrates that only noble gases were released. The balloon type fission-gas-detector with its built in delay system showed that 17 minute Xe-138 was also released although its daughter Cs-138 was not detected by the grid air samplers.

Remote Radiation Monitors

Five remote radiation monitors located on the radiological grid detected the gamma dose rates from the cloud and also measured the dose rates from the fission product decay following the test. These measured dose rates are shown as a function of time in Figure 21. The recorder connected to the D-8 station failed to ink until the cloud reached the D arc therefore a broken line is used to extrapolate results prior to that time.

Water Samplers

Water ejected from the environmental tank at the time of the

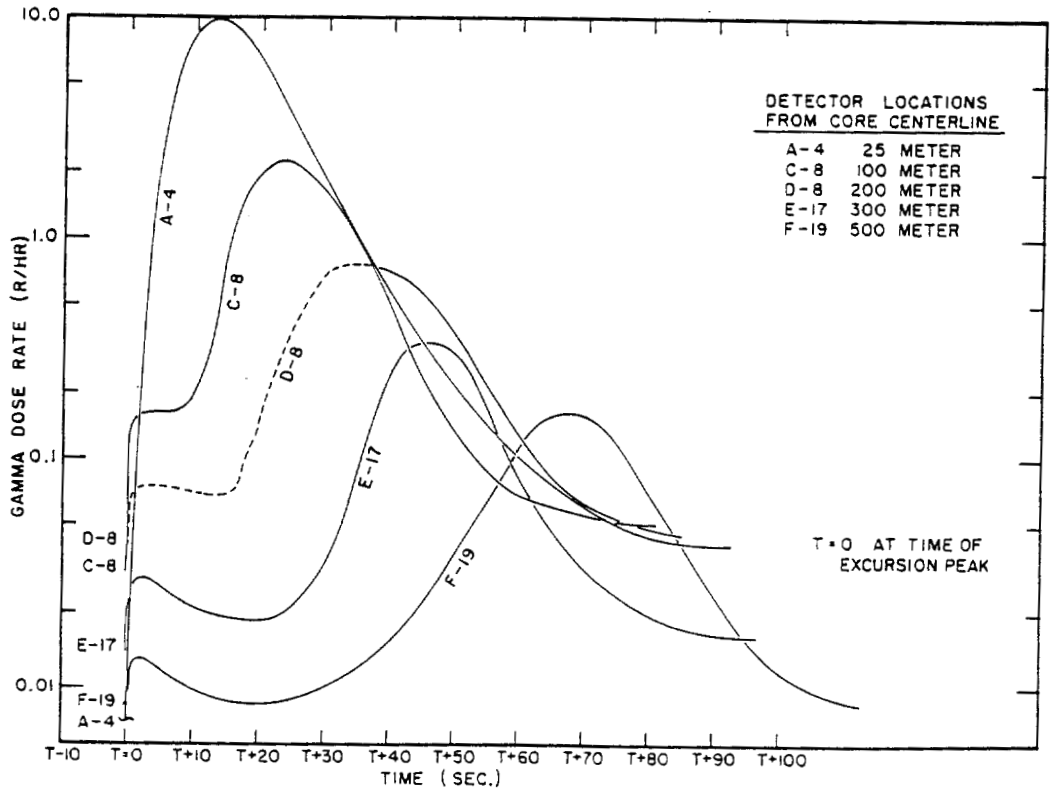

Fig. 21 Transient Dose Rate Measurements at Downwind Locations

1256123

excursion was trapped in each of the four water trays and in several catch cans positioned on the lip of the environmental tank. This water, as well as the water samples taken from the environmental tank, was analyzed. The analysis showed that the water outside the tank and that remaining in the tank had essentially the same concentration of radioactive isotopes.

Because NaK coolant was present in the vessel during the destructive excursion, the analysis of the reactor water shortly following the test showed only 15 hour Na-24. After 120 hour decay time, trace amounts of the following isotopes were found: Ce-141, Ce-143, Np-239, Na-24, Te-132, I-131, I-132, I-133, Ba-146, La-140, and Sr-89-90. After 30 days, Zr-95 and Nb-95 were also found to be present.

Beryllium Data

All data from the airborne beryllium samplers, including the particle size detectors, showed that no beryllium was released during the test.

F. Post-Test Material Analysis

The destructive excursion resulted in the complete dispersal of the reactor fuel within the environmental tank and the rupture of all fuel elements in the core. Figure 22 shows the fuel and reactor components scattered over the bottom of the environmental tank after the tank water had been drained and the superstructure removed following the test. Approximately 98% of the fuel and cladding was recovered from the environmental tank by remote manipulation in the TAN hot shop and examined for identifying marks. The original core layout is shown in Figure 23. Figure 24 is a composite picture of the identifiable fuel and cladding pieces in their relative locations in the original core. The core location number is shown above and the fuel element number is shown below (i.e., E-66). Examples of the extent of the fuel element damage are shown in the four pictures of Figure 25. The pictures are identified as follows: A - Cross section 4-1/2 inches from the bottom of fuel element E-65; B - Broken end of E-9 three inches from the bottom; C - Fuel element E-80; and D - Small pieces of unidentified fuel.

1256124

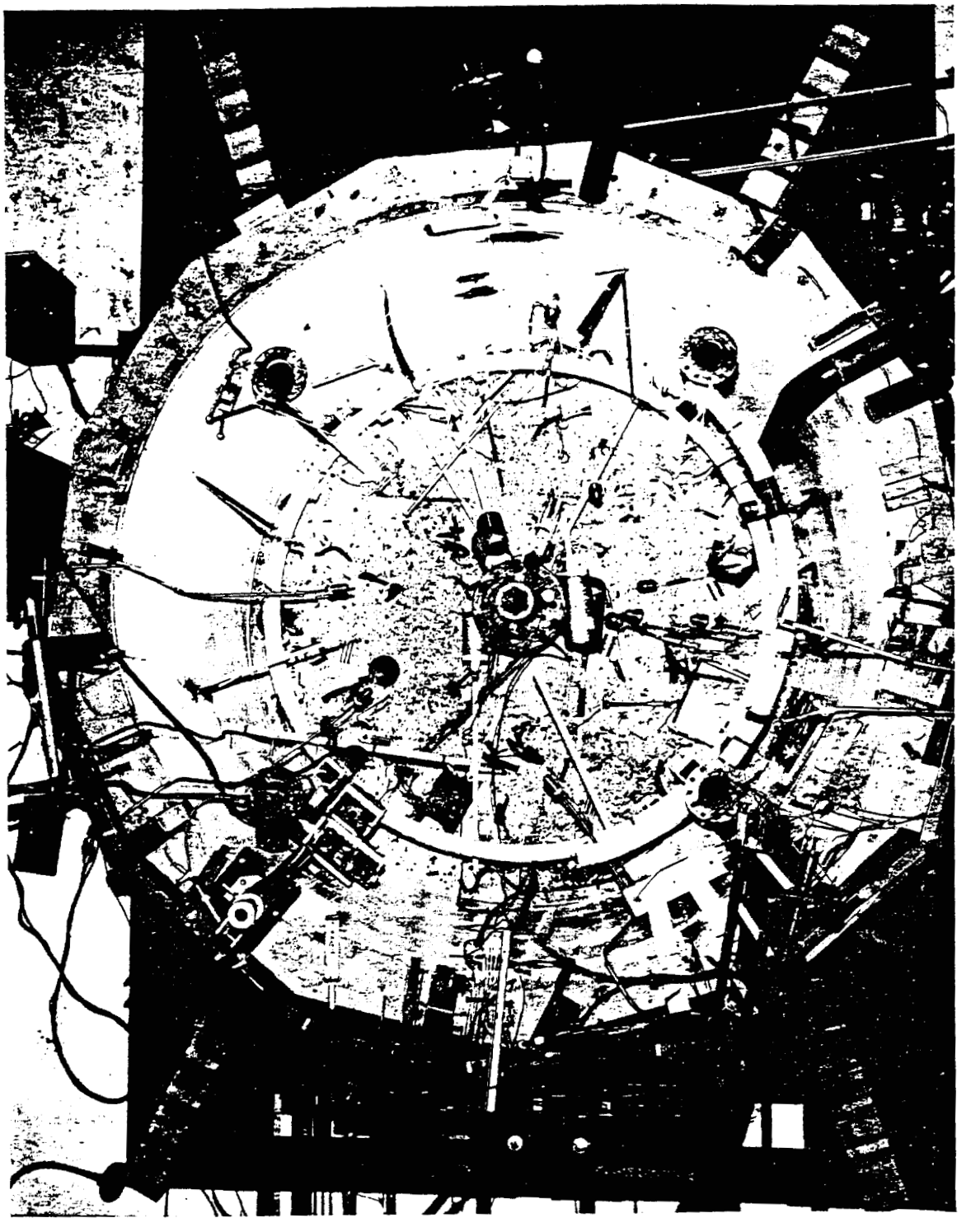

Fig. 22 Post-Test Remains of Reactor after Removal of Superstructure

1256125

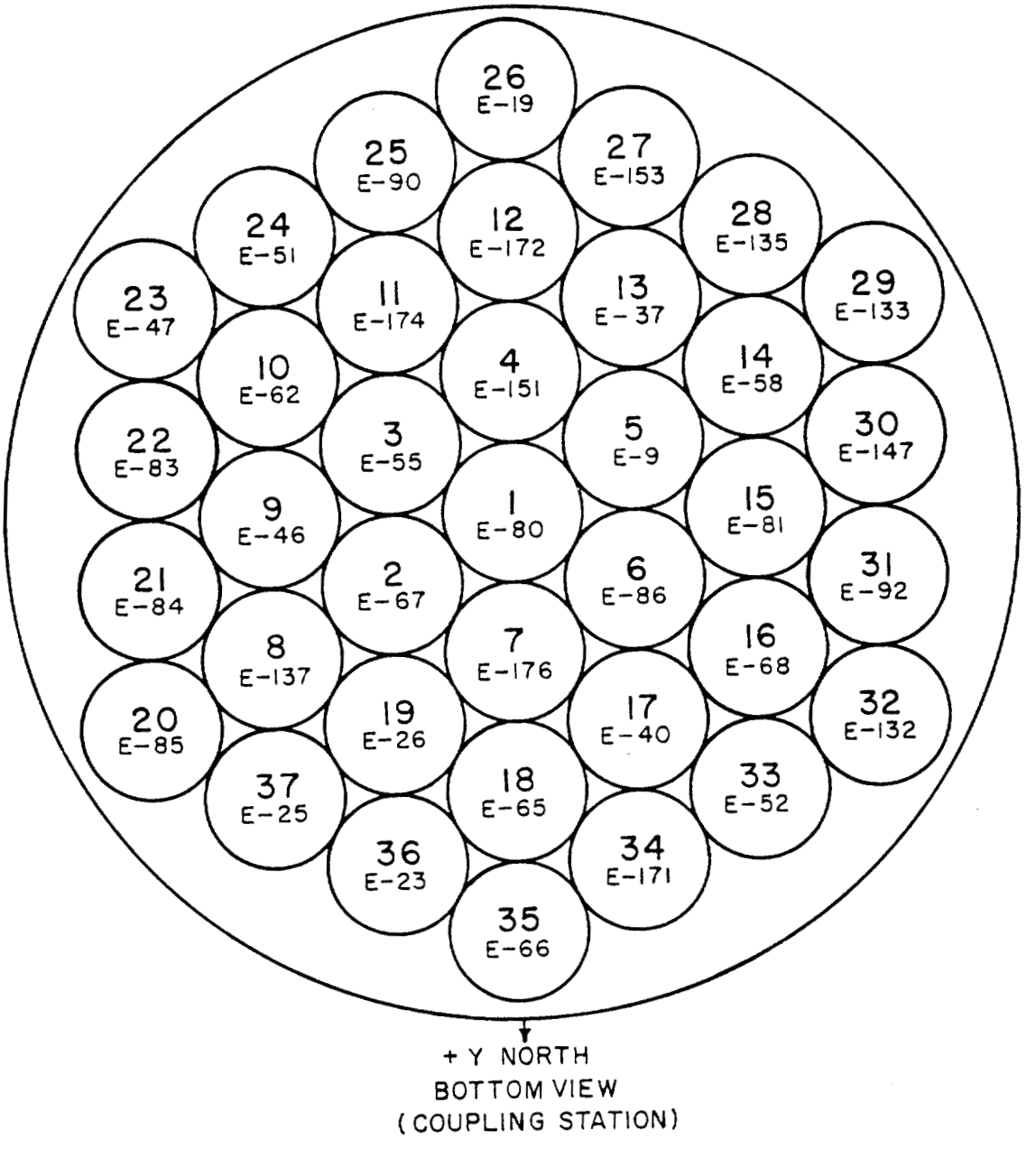

Fig. 23 SNAPTRAN 2/10A-3 Core Layout

1256126

Fig. 24 Fuel Rod Remains Arranged According to Core Layout

1256127

A

B

C

D

Fig. 25 Views (A through D) of Miscellaneous Pieces of Fuel Remains

1256128

Sample wafers have been cut from several of the fuel elements for both chemical and metallurgical analysis. The elements sampled were E-65, E-151, E-153, and the bottom of element E-84. The sample wafers from E-65, E-151, and E-153, for chemical analysis, were cut from each end of each fuel element as well as from either side of the missing center section resulting in four wafers from each fuel element. The wafers were numbered 1 through 4 starting at the bottom of each element and are identified as 65-1, 65-2, 65-3, etc. Their location on the original fuel element and approximate thicknesses are given in Table IX. The analyses completed to date include hydrogen distribution, fission product distribution, Cr-51 in the Hastelloy-N cladding by activation and total chromium, and U-Zr in the cladding to determine if a eutectic was formed at ~ 1700°F. Included in the metallurgical analysis of wafers from E-65, E-151, and E-153, and longitudinal slices of E-84 is the examination for phase changes, temperature gradients, melted zones, etc.

TABLE IX

SAMPLE WAFER IDENTIFICATION AND LOCATION

Sample Identification	Original Location	Approximate Thickness
65-1	12-1/4" to 12-1/2" from top shoulder	1/4"
65-2	8" to 8-1/2" from top shoulder	1/2"
65-3	3-1/2" to 4" from top shoulder	1/4"
65-4	0" to 1/4" from top shoulder	1/4"
151-1	12-1/8" to 12-1/2" from top shoulder	3/8"
151-2	10-3/8" to 10-3/4" from top shoulder	3/8"
151-3	2-1/8" to 2-1/2" from top shoulder	3/8"
151-4	0" to 3/8" from top shoulder	3/8"
153-1	12-3/8" to 12-1/2" from top shoulder	1/8"
153-2	9-1/4" to 9-5/8" from top shoulder	3/8"
153-3	2" to 2-3/8" from top shoulder	3/8"
153-4	0" to 1/8" from top shoulder	1/8"

NOTE: The cladding was removed from all the sample wafers immediately following cutting except 65-3 and 151-3. These two cladding rings were used for Cr-51 activation analysis and U-Zr eutectic investigation which are discussed elsewhere in this section. Also, the sections of the original fuel elements between the -2 and -3 wafers were missing following the destruct test.

1259129

The hydrogen distribution was determined for each of the three elements both radially and longitudinally. Five radial samples from the center outward were taken from each wafer listed in Table IX. These samples are identified by H-1 at the center to H-5 at the edge. Small unidentifiable fuel pieces recovered from the environmental tank were analyzed and found to contain only 22% of the original hydrogen content. The results of the hydrogen analyses are listed in Table X with the original hydrogen content of each fuel element also given. The listed values have a 95% confidence interval of ± 0.02 wt%. The results indicate that there was essentially no hydrogen loss from the extreme ends of the fuel elements and only a 10-15% loss at the broken ends of elements E-65 and E-151 near the center of the reactor core. Element E-153 located at the outside edge of the core apparently had a negligible hydrogen loss even at the broken ends. A close examination of the hydrogen content of the five samples from each of the -2 and -3 wafers indicates that the surface appearance (cracks and fissures) probably explains the wide range of results reported. In several cases the edges of the cracks were a much darker color than the remainder of the wafer indicating an oxide formation or a change in structure. Figure 25-A is an example of crack formation in E-65-3. The results reported in the table are an average of duplicate analyses having a difference no greater than 0.02 wt%. However, the range for individual wafers is from 0.06 wt% in 153-3 to 0.35 wt% in 65-2.

The remaining portion of each fuel wafer was analyzed for the following fission products: I-131, Ba-La-140, Ce-141, Zr-Nb-95, Cs-137 and are presented in Table XI. The results give a longitudinal but not a radial distribution of the fission products for three fuel elements and indicate that the flux was higher near the center of each fuel element than at the ends. The variations in the I-131 results may be attributed to sublimation and/or migration of the iodine. Although the strontium analysis was made for both the Sr-89 and Sr-90 isotopes, the disintegrations from the Sr-89 represents > 99% of the total strontium activity at that time. Consequently, the Sr-90 was not detectable.

1256130

TABLE X

HYDROGEN ANALYSIS

E-65 Original H_2 1.80 wt%	Sample Appearance	E-151 Original H_2 1.81 wt%	Sample Appearance	E-153 Original H_2 1.78 wt%	Sample Appearance
65-1 H-1 1.79 wt% H-2 1.78 H-3 1.84 H-4 1.77 H-5 1.84 avg 1.80	No cracks in fuel	151-1 H-1 1.73 wt% H-2 1.75 H-3 1.74 H-4 1.73 H-5 1.76 avg 1.74	No cracks	153-1 H-1 1.69 wt% H-2 1.72 H-3 1.73 H-4 1.73 H-5 1.71 avg 1.72	No visible cracks
65-2 H-1 1.43 wt% H-2 1.52 H-3 1.39 H-4 1.53 H-5 1.74 avg 1.52	Large cracks many fissures	151-2 H-1 1.67 wt% H-2 1.55 H-3 1.50 H-4 1.72 H-5 1.73 avg 1.63	Pitted, numerous cracks	153-2 H-1 1.71 wt% H-2 1.71 H-3 1.63 H-4 1.72 H-5 1.70 avg 1.69	Cracks and fissures darkened at edge
65-3 H-1 1.55 wt% H-2 1.38 H-3 1.50 H-4 1.47 H-5 1.69 avg 1.52	Numerous cracks and fissures	151-3 H-1 1.44 wt% H-2 1.43 H-3 1.58 H-4 1.56 H-5 1.57 avg 1.52	Pitted, numerous cracks	153-3 H-1 1.72 wt% H-2 1.72 H-3 1.73 H-4 1.72 H-5 1.67 avg 1.71	Pitted, numerous cracks
65-4 H-1 1.77 wt% H-2 1.77 H-3 1.80 H-4 1.80 H-5 1.85 avg 1.80	No cracks in fuel	151-4 H-1 1.75 wt% H-2 1.74 H-3 1.77 H-4 1.74 H-5 1.73 avg 1.75	No visible cracks	153-4 H-1 1.73 wt% H-2 1.70 H-3 1.71 H-4 1.71 H-5 1.73 avg 1.72	No visible cracks

TABLE XI

FISSION PRODUCT DISTRIBUTION
(EXPRESSED AS uc/gm AT T_o + 2.28 hrs.)

Sample No.	I-131	Ba-La-140	Ce-141	Zr-Nb-95	Cs-137	Sr-89
65-1	16	24	3.3	4.3	.026	4.7
65-2	23	47	5.9	9.1	.049	8.8
65-3	8	44	6.1	9.2	.057	8.4
65-4	23	23	1.3	4.2	.029	3.5
151-1	10	25	2.5	4.8	.025	4.6
151-2	22	39	3.6	7.8	.046	7.3
151-3	27	46	4.5	9.1	.057	8.1
151-4	15	23	2.4	4.4	.028	4.5
153-1	15	21	2.1	4.1	.024	3.8
153-2	17	34	3.4	6.7	.036	5.8
153-3	12	34	4.0	8.0	.026	6.6
153-4	----------Lost Sample----------					

The two cladding rings from fuel wafers 65-3 and 151-3 were analyzed for both total chromium and Cr-51 to determine the extent of chromium activation. The results corrected to T_o + 2.28 hrs are as follows:

Sample Identification	Total Chromium %	Cr-51 μc/gm
65-3	7.36	1.07
151-3	7.36	1.07

The Hastelloy-N cladding for both E-65 and E-151 fuel elements came from the same original tube prior to fabrication and would be expected to have the same total chromium analysis. The reason for identical chromium activation from two different areas of the core is covered later in this section.

It is possible that above approximately 1700°F a eutectic composition can be formed between the Hastelloy cladding and the Zr-U fuel. As a preliminary investigation of such a eutectic formation the dissolver solutions of the cladding rings of 65-3 and 151-3 were analyzed for both zirconium and uranium. The surfaces of both

1256132

Hastelloy-N cladding rings had been thoroughly cleaned prior to dissolution. The analytical results were as follows:

Sample	Uranium μgms/gm	Zirconium wt %
E-65-3	$< 9.15 \times 10^{-3}$	0.13
E-151-3	$< 2.31 \times 10^{-2}$	0.04

It must be pointed out that although the zirconium content of both samples appears rather low for a eutectic composition, the eutectic may have been formed in only one small section of the ring. In such a case, since the entire ring was dissolved, the eutectic concentration would be greatly diluted. The foregoing results represent approximately 40% of the planned post-test analyses.

NaK Analysis

The extent of the NaK-water reaction can be used to determine the overall mechanical and thermal energy release. An analysis of the environmental tank water gave a result of 15.4 ± 0.8 ppm Na which indicates that 6-1/2 pounds of NaK reacted with the 10,800 gallons of water initially available. Further sodium analyses on the water in a catch can at the top edge of the environmental tank and in a 5 section water catch tray located on the flatcar gave comparable sodium concentrations. Using these results, it can be concluded that all of the available NaK reacted with environmental tank water during and immediately following the reactor disassembly.

1256133

V. ANALYSIS OF RESULTS

Analysis has been performed on those phenomena which affect the general reactor behavior during the destructive test. A general discussion based on this analysis is presented to describe the phenomenological sequence following the initiation of the destructive test.

A. Phenomenological Time Sequence

Figure 26 represents the details of nuclear and non-nuclear phenomena that are salient in describing this test. The nuclear power, energy, and calculated fuel temperature are shown plotted in logarithmic form for easy comparison and identification of the time at which these traces deviate from the exponential rise. The reactivity trace shows deviation from the exponential rise at about 3 msec prior to peak power. The compensated reactivity is seen to vary inversely with energy until near to peak power when a significant increase in the reactivity compensation takes place. The rapid decline of the reactivity immediately following peak power is due to core disassembly. Since disassembly takes place after peak power, no contribution to the reactivity feedback up to peak power is seen to result from core expansion.

Once sufficient energy had been deposited in the various regions of the core to cause these regions to reach a temperature of about 1500°F, hydrogen gas commenced to pressurize the fuel elements. Until the load pressure exceeded the 1500 psi containment capability of the fuel cans, little reactivity was lost from the system due to hydrogen evolution phenomena. The onset of failure of the first vessel wall gauge at 100 μsec prior to peak power gives evidence that one or more fuel elements had either thermally expanded or ruptured due to hydrogen evolution. During the next 1.2 msec, the strain gauges, as discussed in Section IV-D, showed evidence that the vessel walls had exceeded an elongation of 0.2%. The generation of pressure in the water as shown in the pressure trace of Figure 26 indicates that core disassembly began at this time. This pressure trace has been moved back in time to account for the propagation time from the reactor to the location of

1256134

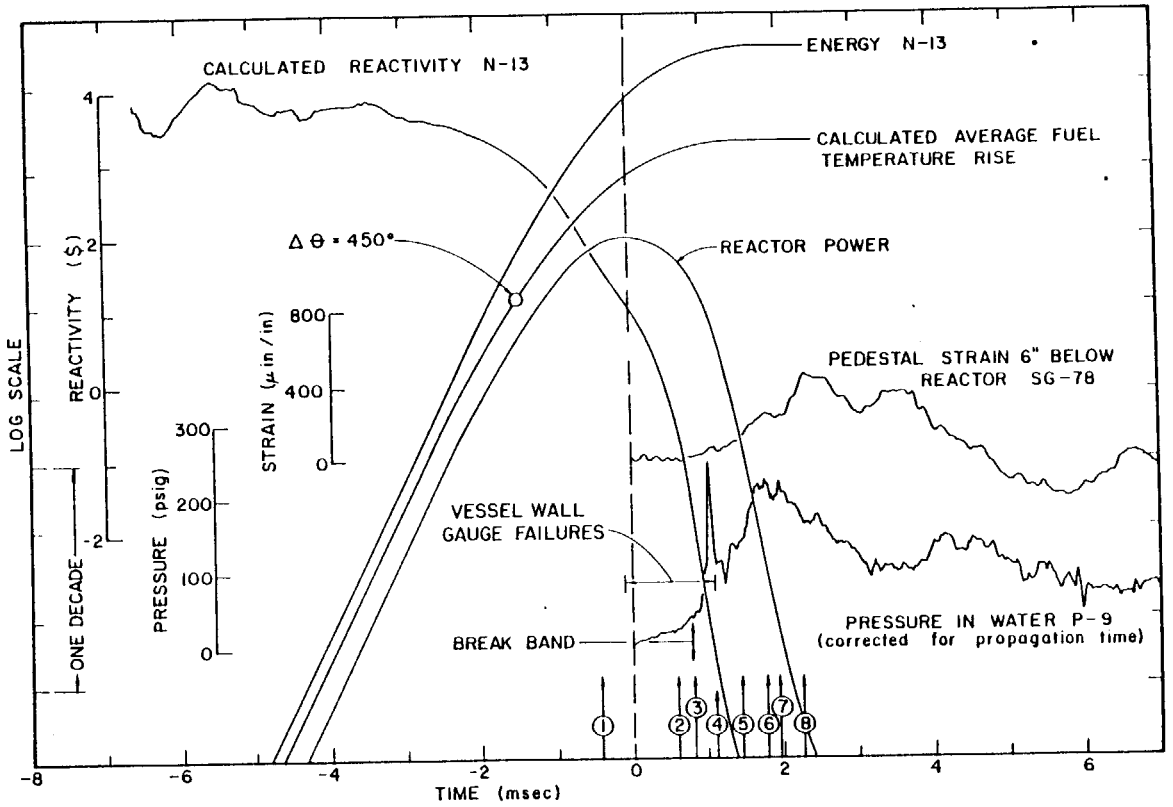

Fig. 26 Overall Data Summary Encompassing Power Excursion

1259135

the gauge. This trace shows the initiation of a disturbance at the reactor surface very near the time of peak power, with a rise to the pressure peak consuming the next 2 msec. Since the expansion of the fuel cans due to hydrogen release would be primarily in a radial direction during this time, the vessel walls would assume the greatest degree of displacement. Not until the vessel walls had reached the rupture point, would a reaction force appear on the pedestal. This reaction force is shown by the strain trace from the pedestal strain gauge located six inches below the reactor. This trace shows the forces generated by continued hydrogen expansion lasting approximately 3-1/2 msec. This would imply that the displacement forces from hydrogen release were probably terminated at about 2-1/2 msec after peak power after which the steam generation from hot core components and chemical reaction between water and NaK provided the continued expansion forces which maintained the environmental pressure at a significant level for approximately the next 20 msec.

The EG&G photographs as discussed in Section IV-D can be correlated with the above phenomena. The various frames of the EG&G pictures are indicated by the encircled numbers at the bottom of this plot. Pictures 1, 2, and 3 show very little evidence of vessel expansion indicating that very little reactivity loss resulted from displacement of the water reflector. Picture 4, however, shows the onset of rapid vessel expansion which continues to the near spherical shape of the vessel shown in picture 8. These pictures support the reactor disassembly evidence indicated by the vessel wall strain gauges, environmental pressure generation, EG&G breakband failure, and pedestal strain information. It can be concluded from this information that the contribution to negative reactivity from disassembly did not begin until 200-300 μsec after peak power and that the reactor power rise was terminated as the result of prompt reactivity effects due to intrinsic neutronic effects.

B. Feedback Analysis

A value of 0.19 cent/°F for the negative prompt temperature coefficient was determined from the destructive test data. A discussion of some of the important considerations follows.

1256136

In selecting a mathematical model which accurately defines the dynamic SNAP 2/10A reactor behavior, the major considerations are the ratio of prompt neutron lifetime (ℓ) to the effective delayed neutron fraction (β_{eff}) and the relation of reactivity feedback to various time dependent phenomena. While the value of ℓ/β_{eff} has been measured and is known to within 15%, the relationship which exists between the reactivity feedback and a time-space related reactor phenomenon is very difficult to define. In models which attempt to predict the SNAP-TRAN 2/10A-3 dynamic reactor behavior, two basic phenomena are considered as contributors to the non-destructive reactivity feedback coefficient, spectrum hardening as a function of temperature and geometric changes which may be either linearly or non-linearly dependent on core temperature.

The spectrum hardening as a function of temperature rise which occurs in zirconium-hydride fuel material has been described and experimentally examined by General Atomics[4]. In addition, Atomics International and Phillips Petroleum Company have made measurements concerning the neutron scattering phenomenon in zirconium-hydride[5,6]. Defining reactivity perturbations due to spectrum hardening is complex and requires careful treatment. Atomics International made such an assessment and determined the temperature feedback coefficient (α_T) to be approximately -0.1 cent/^{o}F. In Zr-H_x fuel the reactivity feedback due to spectrum hardening is manifested as a prompt effect.

In considering the various kinds of non-destructive geometry changes which are related to temperature changes (e.g., fuel expansion, grid plate growth, and fuel rod bowing), only those effects which are prompt in nature are of interest in defining the reactor dynamic behavior during the destructive excursion. In addition to spectrum hardening, the fuel growth as a function of temperature is thought to be the only other possible prompt contributor to the reactivity feedback coefficient. However, fuel growth affects the feedback coefficient only if it is accompanied by movement of the reflector-core interface. Axial and radial fuel growth have been examined separately as contributors to the prompt negative temperature coefficient.

The axial fuel growth affects the reactivity in three ways. The first, which is positive, results from coupling the fuel to the reflector. This effect is small due to the effective 1 to 2 inch void between the end of the fuel and the water reflector. The second, which is negative, results from reduction of the fuel density. This effect is larger and is essentially proportional to the density change. The third, which is also negative, is due to the transverse leakage. This effect is small in magnitude due to the low importance of the leakage in the corner region of the core. The axial fuel growth contribution to α_T was calculated to be small (i.e., ~ 0.01 cent/^{o}F), due primarily to the compensating effects.

The radial growth of the fuel has been found to result in very little reactivity change provided the core-reflector interface remains stationary. However, if this interface moves with the fuel growth, a reactivity coefficient of \$10/in. of vessel radius growth results in a fuel temperature coefficient of about -0.09 cent/^{o}F. However, if the interface is held fixed, the rearrangement of fuel within this boundary causes a very small amount of reactivity change. This is due primarily to a cancellation of the negative effects of reduction in fuel density and increase in neutron leakage by the positive effect of reflector to core coupling.

The movement of the fuel-reflector interface as a result of fuel growth depends on the following: (1) the radial clearance between fuel and clad, and (2) the ability of NaK between fuel elements to transmit clad motion to the vessel. The model chosen by Phillips Petroleum Company to predict the destructive transient reactor behavior of SNAPTRAN 2/10A-3 was based on spherical geometry in which the buckling was normalized to cylindrical buckling. The fuel to clad clearance was assumed to be the design clearance of 3 mils. Using a 3 mil clearance, the fuel expansion was predicted to affect the radial reflector boundary, and hence reactivity, when a fuel temperature of 900°F was reached. However, the average fuel-clad clearance in the SNAPTRAN 2/10A-3 fuel rods was 4.2 mils instead of 3 mils thus requiring a higher temperature for the onset of the negative feedback caused by vessel expansion. As a consequence a higher energy release resulted from the destructive test than would have been expected based on the 3 mil clearance.

1256138

The results of Phillips' "Reactivity" code treatment of N-13 power data are plotted in Figure 27. Compensated reactivity vs average core temperature is plotted in Figure 28. At a fuel temperature of about 1500°F, the reactivity deviates from a linear relationship with temperature indicating the introduction of a different mode of feedback which is attributed to core disassembly. Up to this point, the 0.3% radial growth (indicated by the vessel wall strain gauges) contributes only about 10 cents of reactivity compensation leaving approximately $2.70 having been compensated for by axial expansion and intrinsic neutronic effects such as spectrum hardening. Since the axial growth results in less reactivity compensation than does the radial growth, nearly all of the 0.19 cent/°F negative temperature coefficient may be attributed to intrinsic neutronic effects.

After peak power, core disassembly resulted in a rapid reduction of reactivity and hence power. The reactivity as a function of radial core growth was calculated from the EG&G pictures to be 10$/inch.

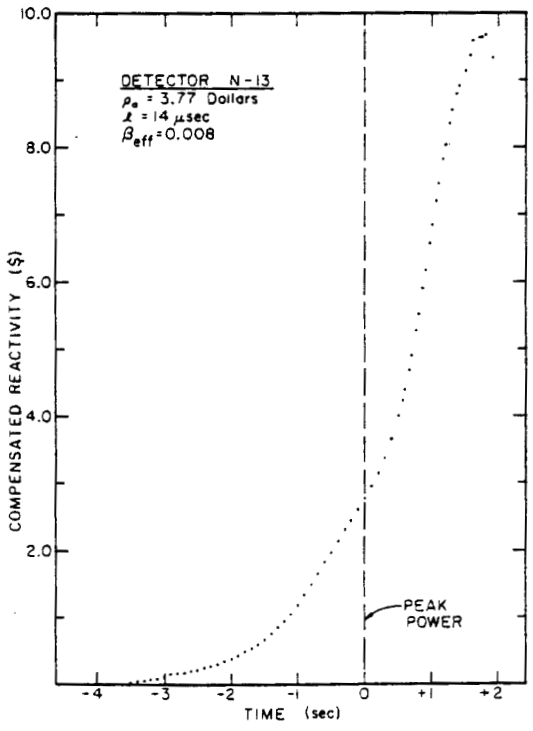

Fig. 27 Compensated Reactivity vs. Time During Destructive Test

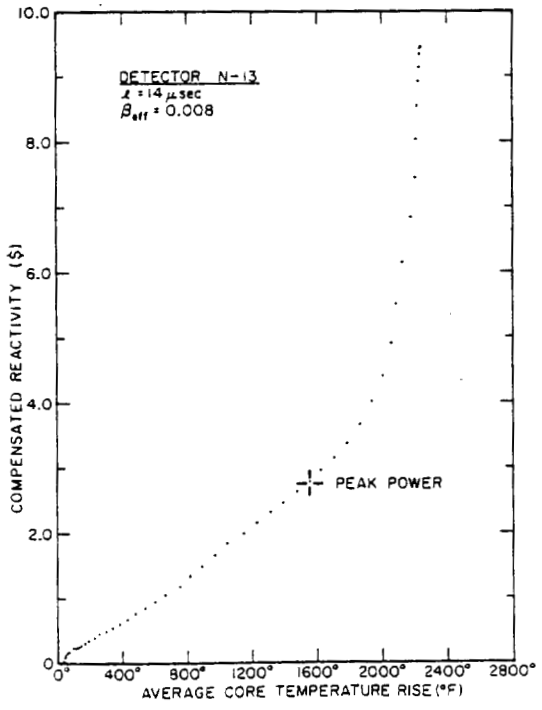

Fig. 28 Compensated Reactivity vs. Average Core Temperature During Destructive Test

C. Energy Probe Behavior

The temperature of the energy probes followed the integrated power burst shape indicated by nuclear detector N-13 with a linearly increasing departure over the temperature range from 300°F to 1500°F. For those probes which reached a temperature rise of 1500°F after peak power, the energy-temperature rise relationship at an individual probe is distorted by the onset of core derangement. It therefore appears that the specific heat of the fuel is linear with temperature up to approximately 1500°F. It would also appear that the energy deposited in an energy probe is proportional to that deposited in the fuel.

The ratio $\epsilon(t)/\Delta\theta(t)$, was computed for each probe where $\epsilon(t)$ is the time dependent integrated power indicated by N-13 and $\Delta\theta(t)$ is the time dependent temperature rise in degrees F of a given energy probe. The experimental determination of this ratio was found to be proportional to $(1.0 + 4.5 \times 10^{-4}\ \Delta\theta)$ with an average deviation in slope of less than 5% from 300°F to 1500°F. The above factor of linearity agrees well with the specific heat data for the fuel reported by Atomics International[5]. A value of 0.0097 Mw-sec/°F for the total fuel heat capacity at 68°F was derived from these reported data. The ratio $\epsilon(t)/\Delta\theta(t)$ for each energy probe was normalized to the averaged heat capacity, $\overline{C}_p$, where:

$$\overline{C}_p = \frac{\int_{68}^{68+\Delta\theta} m\, c_p(\theta)\, d\theta}{\Delta\theta} = C_o\,(1 + \beta\,\Delta\,\theta)$$

$$= 9.7 \times 10^{-3}\,(1 + 4.5 \times 10^{-4}\ \Delta\theta)$$

where

c_p = specific heat $\left(\frac{\text{Mw-sec}}{\text{g - °F}}\right)$

C_o = heat capacity $\left(\frac{\text{Mw-sec}}{\text{°F}}\right)$ @ 68°F

β = linearity constant °F^{-1}

m = core fuel mass (grams)

The plots of the comparison of the energy probe data with the theoretical curve are shown in Figures 29 and 30. Previously reported data[6] indicate a heat capacity of 1.1×10^{-2} Mw-sec/°F for the SNAPTRAN 2/10A-3 core (for temperatures up to 1400°F). A high degree of linearity for the

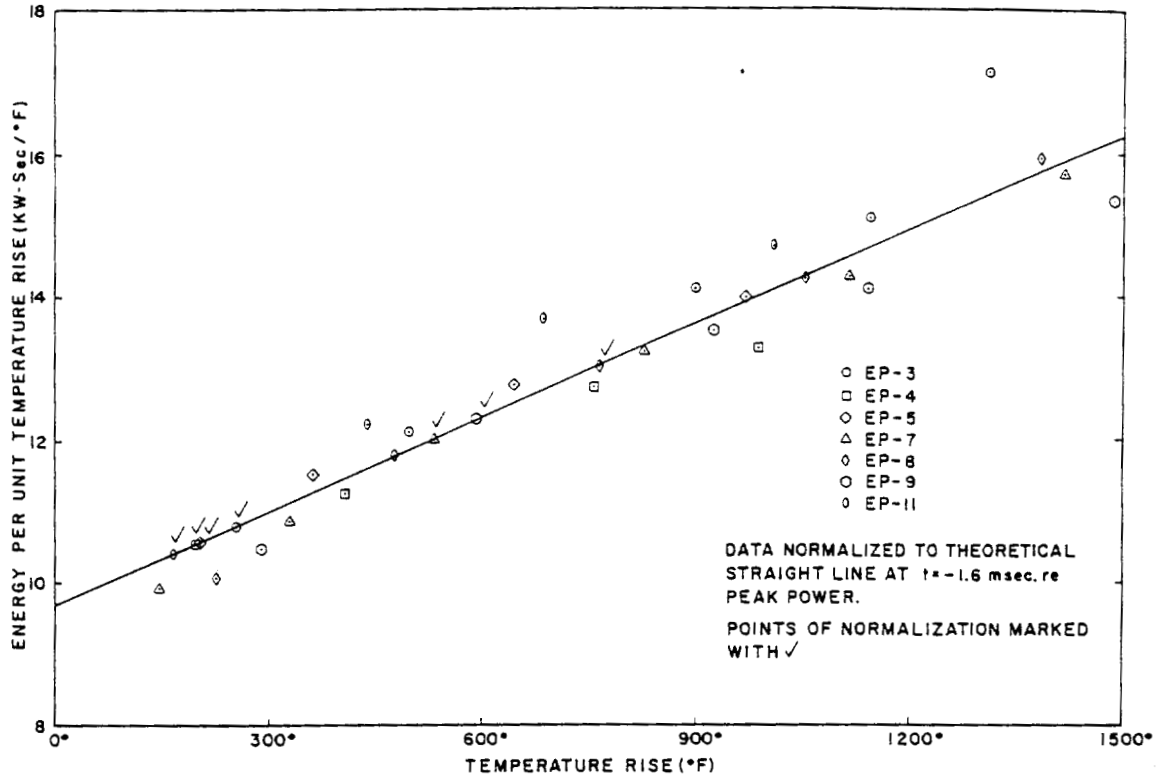

Fig. 29 Nuclear Energy per Unit Temperature Rise of 5 wt% Energy Probe vs. Temperature Rise of 5 wt% Energy Probe

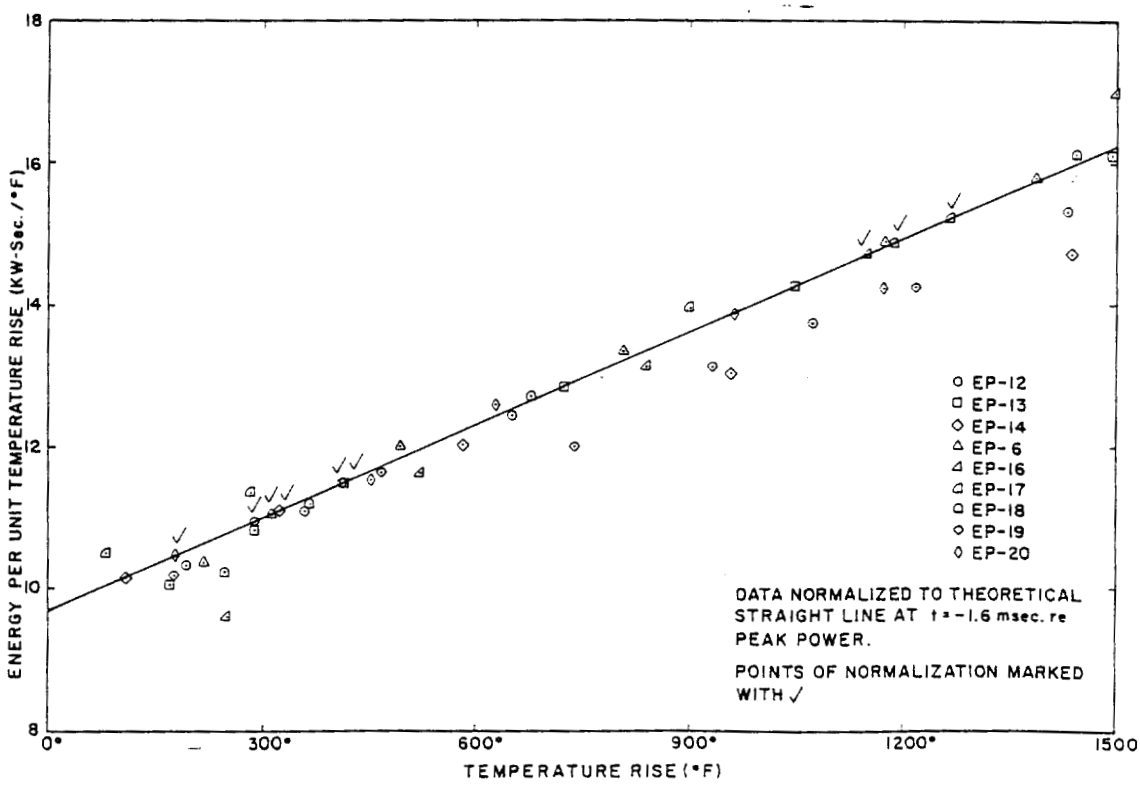

Fig. 30 Nuclear Energy per Unit Temperature Rise of 10 wt% Energy Probe vs. Temperature Rise of 10 wt% Energy Probe

1256141

experimentally determined averaged heat capacity is observed from the energy probe data; however, there is considerable uncertainty about the magnitude of the heat capacity at 68°F.

If a linear heat capacitv is assumed, then

$$E_f/\Delta\theta_n = \frac{1}{f_n} C_o (1 + \beta\Delta\theta_n)$$

where E_f is the average prompt nuclear energy release deposited in the fuel, $\Delta\theta_n$ is the temperature rise of the n-th probe, C_o is the heat capacity of the fuel at 68°F ($\Delta\theta_n = 0$), f_n is the point to average source factor for the n-th probe, and $\beta = 4.5 \times 10^{-4}/^{o}F$, the linearity factor described above. If the integrated detector output is designated as $\epsilon(t)$, then $E_f = g\,\epsilon(t)$ where g is a proportionality factor.

Therefore,

$$\frac{C_o}{f_n g} = \frac{\epsilon(t)}{\Delta\theta_n(1 + \beta\Delta\theta_n)}$$

The quantity on the right was computed for each energy probe at t = 1.6 msec prior to peak power, with the 5 wt% probes normalized to the 10 wt% probes by a factor of 2. An integration over the core volume was performed on the quantities of $f_n g/C_o$ to determine a core averaged value of g/C_o. The experimentally determined radial and axial relative source distributions are shown in Figures 31 and 32. The value of g determined was then applied to the integrated nuclear detector output and the results corrected to provide a value for the total nuclear energy release. The resulting energy release as determined from detector N-13 was 37 Mw-sec, using $C_o = 9.7 \times 10^{-3}$ Mw-sec/°F. The principal uncertainty of this method, in addition to the lack of definitive heat capacity data, is the difficulty in determining an appropriate average of the quantities $f_n g/C_o$ over the core volume or, alternatively, chosing a computer-generated power shape to which the quantities $f_n g/C_o$ may be fitted.

The time variations in the temperature profile (see Figures 33 and 34) could arise from slight differences in hydrogen content (and therefore specific heat) and from spatially dependent spectral changes.

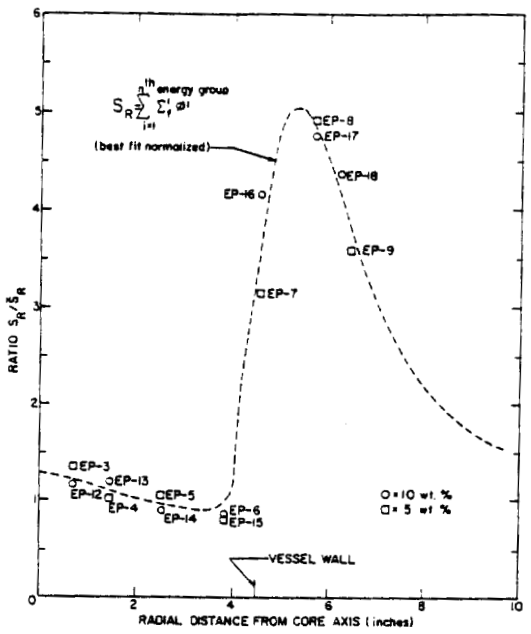

Fig. 31 Radial Fission Source Distribution as Defined by Energy Probes

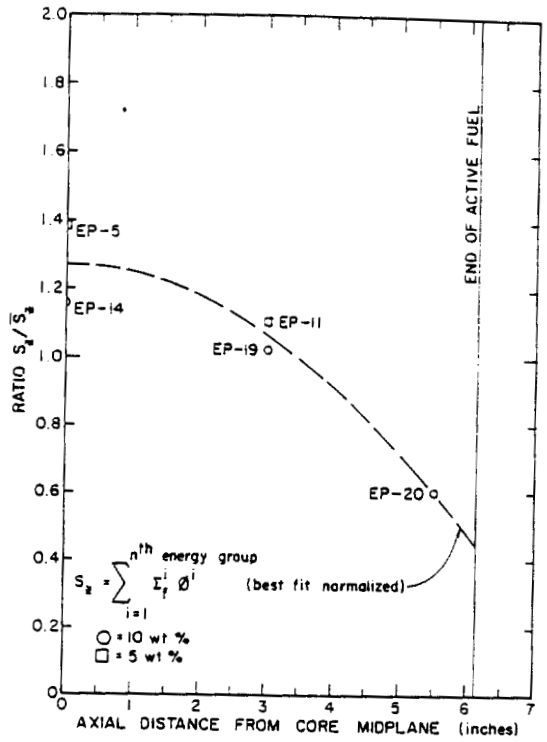

Fig. 32 Axial Fission Source Distribution as Defined by Energy Probes

Because of the unknown flux shape within an interstice, uncertainty exists in interpreting the source shape of the core from energy probes. This consideration is important since it permits a misinterpretation of the energy release from energy probe data by introducing a bias to the data.

The two unfueled energy probes included to study the effect of gamma heating on zirconium hydride showed a temperature rise of approximately 8% of the temperature rise of an equivalently positioned 10 wt% U-235 probe or about 16% of that of a 5 wt% probe. In order to use data from the 5 wt% probes to interpret fuel temperature of 10 wt% fuel, the gamma heating contribution was accounted for in determining the 5 wt% to 10 wt% correlation factor.

D. Energy Determination

Several methods were used in the determination of the nuclear energy release and are listed in Table XII with the mean energy as determined by each technique. A discussion of each method follows the table.

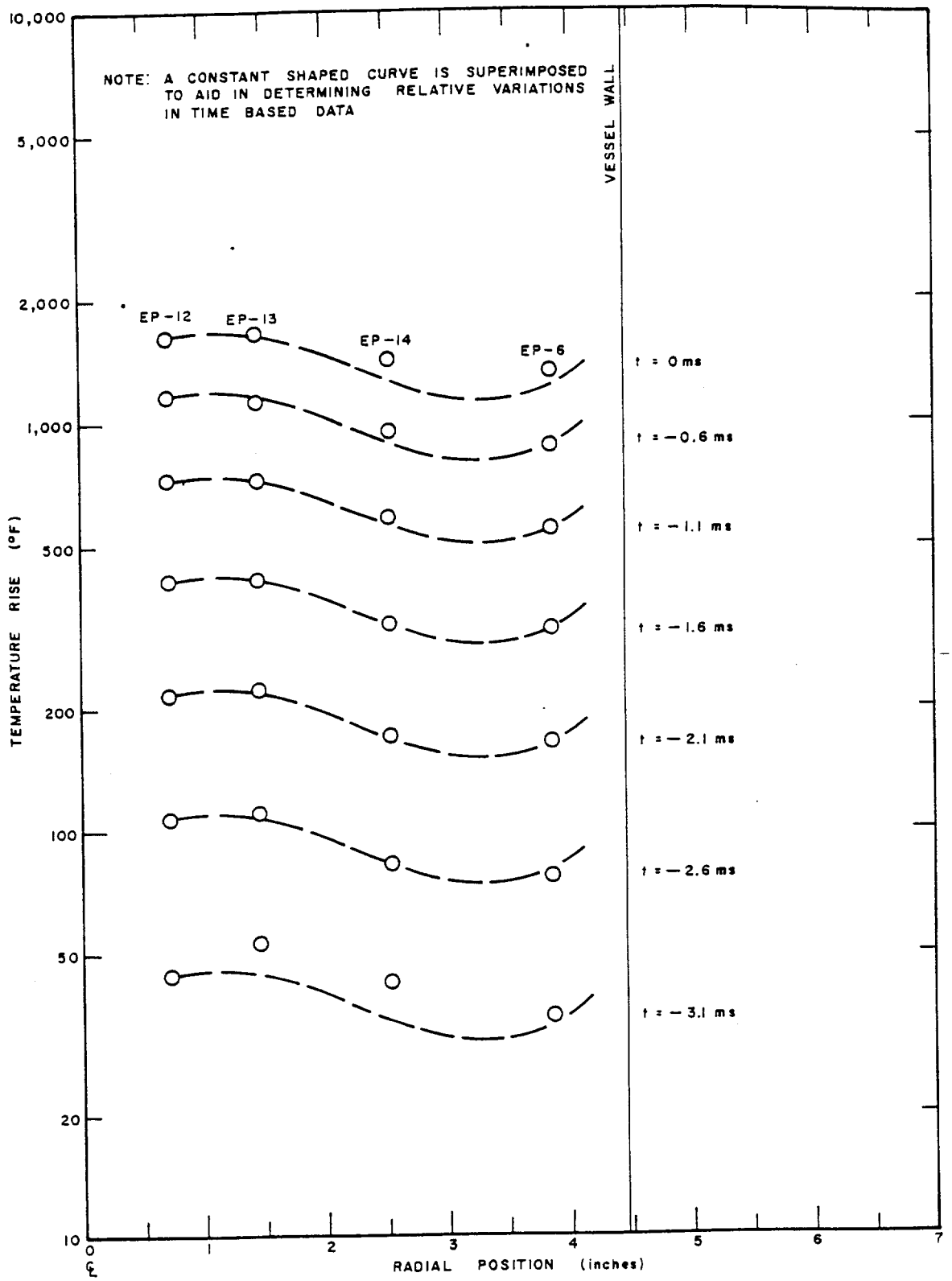

Fig. 33 Time Variation in Radial Temperature Distribution

1256144

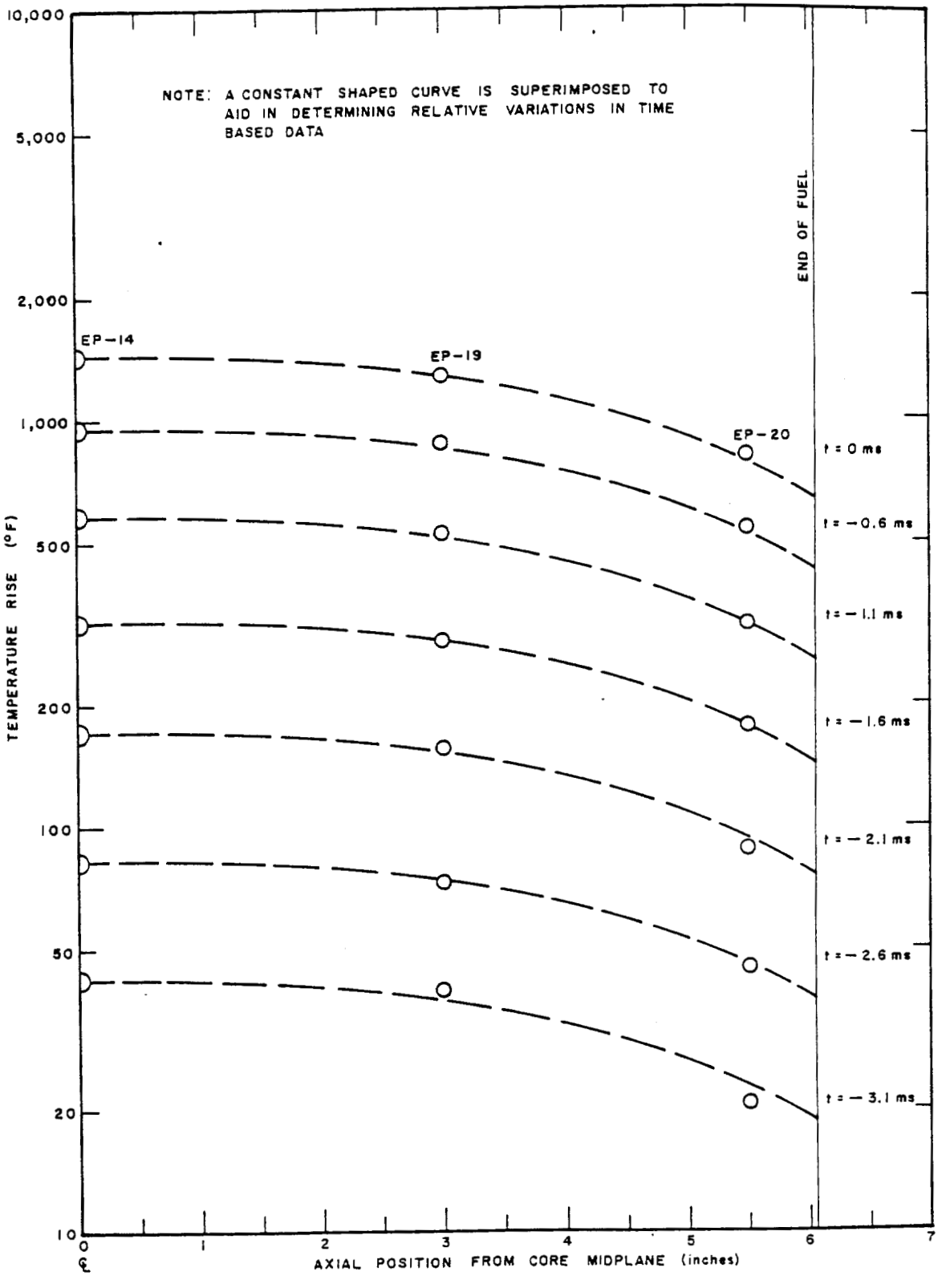

Fig. 34 Time Variation in Axial Temperature Distribution

1256145

TABLE XII

DESTRUCTIVE TEST ENERGY DETERMINATION BY VARIOUS METHODS

(j)	Method	Energy Release	Uncertainty* ($2\sigma_j$)
(1)	Nuclear Detector Calibration Against Known Static Power Level	46.0 Mw-sec	± 13.2 Mw-sec
(2)	Flux Wire (in-core)	61.3 Mw-sec	± 14.5 Mw-sec
(3)	Flux Wire (out-of-core)	55.2 Mw-sec	± 15.0 Mw-sec
(4)	Fission Product Radio-chemical Analysis	53.4 Mw-sec	± 7.0 Mw-sec
(5)	LASL Capsule Irradiation	56.6 Mw-sec	± 10.6 Mw-sec
(6)	Environmental Tank Water Temperature Rise	43.2 Mw-sec	± 15.7 Mw-sec
(7)	Energy Probe	36.8 Mw-sec	± 4.1 Mw-sec
	Most Probable Value	45.3 Mw-sec	± 3.6 Mw-sec

* The value of uncertainty for each method represents a 95% confidence interval for those uncertainties which are known to influence the energy computation for each method and are treated as a standard deviation. While all contributing uncertainties for each method are not precisely known an attempt was made to evaluate each to the extent possible.

Normally, with the performance of a steady state, calorimetrically recorded power run followed by several high level, fast transient power excursions, the nuclear detectors can be calibrated against power level to within 5% accuracy. However, in the power calibration run performed on the SNAPTRAN 2/10A-3 reactor, the coolant mixing was insufficient to allow high reliance in calorimetric power determination. Instead, a transient heat flux balance on the energy probes was done to determine a value of 1.94 kw for the power level during the run. Compared to this value is the flux wire calibration data which yielded 2.08 kw. A value of 2.0 ± 0.1 kw was used for all subsequent power calibration correlations. Since chambers N-9 and N-11 indicated during the power calibration and destructive test, an intercalibration was made between these chambers and those linear chambers which followed peak power. The output signals from N-9 and N-11 were recorded in logarithmic form which normally

1256146

reduces the accuracy of indicated output. However, with 20 point/decade log-linear calibration, the error is less than 5%. In addition, although the raw data from these chambers (N-9 and N-11) had slightly different periods, the log-linear calibration resulted in somewhat better period agreement and both indicated the same power level at 117.5 msec after test initiation. The energy release as determined from N-10, N-13, N-17, and N-19 were respectively 45.4, 42.5, 52.7 and 43.4 MW-seconds.

Gold, cobalt, and uranium-235 flux wires, contained in the core during the destructive transient, were analyzed to determine total nuclear energy. The integrated flux for the power calibration was accounted for in determining the integrated flux for the destructive test. Source weighting factors were used to relate the localized activation to the average core energy. While the gold activation analysis is questionable due to spectrum or fast fission corrections which are not well understood, the cobalt and uranium activations are considered to be relatively accurate. The results are: gold - 39 MW-sec, cobalt - 67 MW-sec, and U-235 - 55 MW-seconds. Fifteen samples were analyzed from each wire to determine statistical variance.

The out-of-core flux samples which were located 1-1/2 in. from the vessel wall consisted of gold, copper, U-235 aluminum alloy, zinc, and nickel wires. A fast neutron activation analysis was made on the nickel and zinc, and a thermal neutron activation analysis was performed on the copper and gold wires. (The U-235 Al alloy exceeded the melting point and was not usable). Wires of these types were positioned 1-1/2 in. away from the vessel wall during the power calibration, located radially opposite the middle of a beryllium filler piece and axially 4 in. from the bottom of the fuel. During the destructive test the wires were located radially opposite the gap between two beryllium filler pieces and axially 6 in. above the lower end of the fuel. Calculations were performed in which the power calibration power level and the different geometries were taken into account. Values for the nuclear energy release were determined to be 34 and 57 MW-sec for the thermal and fast neutron analyses respectively, with a much higher confidence level being imposed on the fast flux analysis.

The Cs-137 content from several fuel elements has been analyzed. Examination of these results has been related through source factor corrections to the average number of fissions which occurred in the core during the destructive test. Corrections for the fission product accumulation during the power calibration have been made. The samples which were closest to the average core source were weighted most heavily and resulted in an average energy release of 53.4 Mw-seconds. The amount of noble gas release is normally important in this determination. However, since a very low percentage (< 5%) of noble gas release was detected, these values have not been corrected for this effect.

A capsule containing LASL fuel was positioned relative to the core in the same positions for power calibration and destructive test as those described above for the external flux monitors. The relationship of the measured fissions in the LASL fuel samples to the fissions taking place in the core yielded an energy release of 56.6 Mw-seconds. The change in geometry and attenuation medium was accounted for; however, the capsule fuel self-shielding factor was not known for the SNAPTRAN spectrum but is believed to constitute less than 5% reduction and was therefore not included.

The temperature rise in the environmental tank water resulting from the destructive test was 0.60 ± 0.15°F. Relating this to the heat capacity of 70°F water, the total amount of thermal energy required to yield this temperature rise is 58.4 ± 15 Mw-seconds. Since the result of the NaK water analysis yielded a non-nuclear thermal energy generation of 15.2 Mw-sec, the nuclear energy contribution is about 43.2 Mw-seconds. This value assumes a thermal energy release which is adiabatic with respect to the water. Any heat which is given to the environmental structure and the air will raise the calculated value of nuclear energy. Since there is photographic evidence that a NaK water reaction probably took place in the northeast corner above the tank and temperature rise above the tank is noted after the excursion, the value of 43.2 Mw-sec is thought to be a lower limit to the nuclear energy release.

The energy probe data have been analyzed. By relating the prompt temperature rise to the fitted heat capacity relationship, values of 37 and 42 Mw-sec were obtained depending on the initial value of heat

1256148

capacity chosen. This technique is very inter-consistent from probe to probe but some uncertainty exists in relating to probe behavior to the core fuel behavior.

Using the uncertainty associated with each method as two standard deviations, a systematic statistical approach was used to arrive at a most probable value for the energy release. In general, the statistical technique considered the propagation of errors throughout the various methods and accounted for the co-variance of systematic uncertainties. This technique is felt to represent the best possible approach to statistically treating systems in which some uncertainties are independent while other uncertainties are interdependent from one system to another. This treatment of the data listed in Table XII yields a most probable value of 45.3 with a 95% confidence interval of 3.0 Mw-sec for the destructive test nuclear energy release.

The energy value of 37 Mw-sec determined from the energy probe treatment agrees very well with the Atomics International determination from the energy probes. This value is approximately 20% lower than the value obtained when all measurements are included.

Mechanical Energy

The mechanical energy generated during the destructive test is the result of: (1) hydrogen release from the $Zr\text{-}H_x$ fuel matrix, (2) hydrogen release from the NaK-water reaction, and (3) steam generation caused by hot core components coming into contact with water. This mechanical energy was manifested as a series of pressure disturbances which lasted until the hydrogen burned or combined chemically with some other element or until the steam vapor pressure was reduced to the point of bubble collapse. All mechanical energy was ultimately returned as heat to the environment or was deposited in mechanical displacement or deformation (e.g., ejection of environmental tank water).

Using the relationship given by Cole[7] for the energy contained in a spherically propagating acoustic wave (including the "afterflow" term), 1.8 Mw-sec of mechanical energy was calculated to have been released.

1256149

The flatcar absorbed about 0.9 Mw-sec from the initial pulse and later returned all but 0.2 Mw-sec (dissipated in permanent deformation of the flatcar) to the environmental tank system. Air pressure measurements indicated that 0.1 Mw-sec was absorbed in the air while an additional 0.4 Mw-sec was dissipated in ejecting water from the environmental tank. The remaining 1.1 Mw-sec is assumed to have been dissipated as cavitation at the free surface of the environmental tank water.

The chemical reaction of 6-1/2 pounds of NaK with water theoretically yields about 3.2 Mw-sec of mechanical energy. While this amount of mechanical energy was not measured, the series of long term "red glows" which can be seen in the color motion pictures indicates that much of the NaK reacted in the vapor cloud. This appears to be the result of a sizeable quantity of the NaK having been trapped inside the vessel head as it was blown free of the environmental tank water.

While the various manifestations of mechanical energy were not well defined, the value of 1.8 Mw-sec is throught to represent a good assessment of the total energy release. This amount of mechanical energy is equivalent to that which is released from one pound of TNT. The SNAPTRAN 2/10A-3 destructive test mechanical-to-nuclear energy release (determined to be 4%) is in the same range (0.3 to 3.0%) as that resulting from the SPERT I, SL-I, and Borax I destructive excursions.

VI. CONCLUSIONS

The objectives of the SNAPTRAN 2/10A-3 destructive test are fundamentally related to reactor safety. Major emphasis was given to the determination of (1) the radiological hazards and (2) the dynamic reator behavior. The general conclusions which can be drawn from the destructive test analysis are:

(1) The radiological hazards as determined from this test were considerably less than were calculated. First, an indescernable amount of fuel was thrown from the tank which implies that in such an accident confinement of reactor components can be expected. Secondly, even with this close confinement of fuel components, the radiation levels were very low and radioactive iodine release to the atmosphere was negligible. It was also shown that less than 5% of the fission products were released from the fuel. Complete reactor disassembly precluded further buildup of fission product inventory which could have resulted from continued operation.

(2) The dynamic reactor behavior is better understood. The temperature dependent reactivity feedback coefficient has been determined to be 0.19 ¢/°F. Since this coefficient is between 2 and 3 times the previously estimated value, the SNAP 10A/2 type reactors can be expected to be more self-limiting than previously anticipated.

The maximum core temperature threshold for the onset of reactor disassembly was determined to be about 1900°F. While this threshold is dependent on the rate of energy deposition, the threshold for this test is thought to represent the value which could be expected for most accidents involving the SNAP 10A/2 type reactors.

When the SNAPTRAN 2/10A-3 reactor reached the 1900°F threshold it disassembled at a slower rate than predicted. However, with higher energy deposition rates and hence higher temperature thresholds for disassembly, reactor disassembly can be expected to occur more rapidly and more violently. This would

serve to disperse fission products to a greater extent than exhibited in the SNAPTRAN 2/10A-3 test.

It is felt that this type of test is valuable in determining and confirming the existence of disassembly thresholds. In addition, considerable information with respect to reactor kinetics can be gained for application in the Reactor Safety Field.

REFERENCES

1. Sandia Corporation Aerospace Safety Biweekly Status Report (September 23, 1962).

2. L. I. Moss, "Experiments with Water-Reflected, Undermoderated, Zirconium Hydride Critical Assemblies", NAA-SR-8490 (September 1963).

3. A. W. Castleman, Jr. and F. J. Salzamo, "Current Studies of Fission Product Behavior at BNL", BNL-7423 (September 1963).

4. J. C. Young, J. A. Young, G. K. Houghton, G. D. Trimble, and J. R. Beyster, "Neutron Thermalization in Zirconium-Hydride", Nuclear Science and Engineering, Vol. 19, No. 2 (June 1964).

5. J. Miller, R. L. Brehm, and W. J. Roberts, "Temperature Coefficients", NAA-SR-7140 (1962).

6. Dr. H. L. McMurry, Phillips Petroleum Company, Personal Communication.

7. Atomics International Aerospace Safety Biweekly Progress Report (May 22, 1964).

8. R. E. Taylor, "Pulse Heating of Modified Zirconium-Uranium Hydrides", NAA-SR-7736 (February 1963).

9. R. H. Cole, "Underwater Explosions" (1948).

APPENDIX A

EXPERIMENTAL MEASUREMENTS

I. Reactor Behavior Measurements

A. Experimental Measurements Criteria

The SNAPTRAN 2/10A-3 program differed from normal operational and transient test programs in that the SNAPTRAN 2/10A-3 test series was primarily concerned with a single-event nonrepetitive destructive test with limited statics testing being performed only for the purpose of checkout and instrument calibration. The destructive test rquired an extensive measurement process not only because of the importance of the test but also because of the uncertainty in predicting the reactor behavior under the conditions in which it was to be tested. The measurement process necessarily included: primary measurements for providing a basic understanding of the destructive event; protective, redundant, and backup measurements for providing coverage of the upper and lower limits of the expected phenomena range, and for providing several independent sources of data; and redundant and academic measurements supplementing the more important measurements.

A discussion of the experimental measurements must include the measurement requirements, instrument capabilities, and other factors governing the choice of the measuring unit.

The measurement criteria of primary importance adhered to for the destructive test were: (1) amplitude accuracy, (2) rise time, (3) dynamic range coverage, (4) time history and event time coverage, (5) spatial coverage, and (6) supplementary coverage.

Amplitude Accuracy - The most important aspect of the nuclear and physical events occurring during the destructive test was the amplitude variation in time; therefore, the majority of measurements were concerned with obtaining information describing the magnitude of the phenomena. This was especially true of nuclear and pressure measurements because of their importance in satisfying the technical objectives.

1256154

Rise Time - Another measurement requirement to satisfy was that of rise time. Accomodations were made to measure phenomena expected to vary rapidly in time exhibiting rise times of the order of μseconds - requiring broad bandwidth instrumentation having a frequency response capability of 20 kcps - 100 kcps or better.

Dynamic Range - Much of the destructive test phenomena was expected to extend over several decades of dynamic range. For example, nuclear phenomena was expected to vary from background source level to 10^{18} nv, while pressure phenomena were expected to reach a maximum of 6×10^4 psi. Signal conditioning equipment limits the dynamic range coverage to 6-7 decades for logarithmic current amplifiers, to 3 decades for logarithmic voltage amplifiers, and to 2-1/2 decades for linear amplifiers. The measuring unit is further limited to 1-1/2 decades per recorder channel. The limitations of the conditioning and recording equipment necessitated the use of a large number of amplifiers and recording channels to cover the dynamic range of a single parameter. Several techniques were used to reduce the amount of equipment necessary for a given measurement:

(1) Range compression - Logarithmic current and voltage amplifiers were used to compress several decades of detector output current or voltage into the 1-1/2 decade range coverage of the recorder channels.

(2) Signal mixing - The outputs from several transducer elements were recorded by the same recorder channel. By this means several events separated in time were observed on the same analog trace - thus conserving recorder channels.

(3) Amplifier "stacking" - Where more than 2-1/2 decades of linear range coverage was required, two amplifiers were used. The ranges of 2-1/2 decades per amplifier were overlapped to give a total range coverage of 4-1/2 decades of coverage using one transducer, two linear amplifiers, and four recorder channels.

(4) Range staggering - Since a total of 4-1/2 decades of coverage was the maximum range coverage obtainable from a single measuring unit, several units were used to provide a complete measurement of the nuclear power. By slightly overlapping the lower portion of the range coverage from one measuring unit with the upper portion of the coverage from a second measuring unit, the dynamic range coverage was extended to cover the total range.

Time History Accuracy - A knowledge of the time-dependent behavior of a parameter is essential for interpretation of a specific measurement and for correlating parameters to acquire an understanding of the entire destructive event.

A system was used by which a timing signal was placed on one channel of each recorder transport. The signal began several seconds before test initiation and continued through the test. All events were referenced to this signal, thus providing a means of correlating data on different transports and channels. All data channels on the oscillographic recorders were printed in analog form on a single photographic chart giving a visual event-time correlation.

Spatial Coverage - A knowledge of the spatial distribution of all phenomena is essential in analyzing the disassembly behavior of the reactor. Information concerning flux peaking in the core and reflector, vessel strain, and pressure generation and propagation were obtained from nuclear energy and flux measurements at various locations in the core and in the water, from strain gauges on the vessel bottom and sides, and from pressure transducers along several radii and above the environmental tank. The information obtained from these measurements was necessary for determining the nuclear and mechanical energy release and energy partition. Time-of-arrival type data was acquired from detectors positioned a known distance apart.

Supplemental Coverage - Since neither phenomena nor electronic systems are completely predictable, protective and redundant measurements were made for the purpose of providing coverage in the event of loss or malfunction of the primary measuring units and in the event the excursion

was not of the predicted magnitude.

B. Detector Selection

Transducer selections for the destructive test were dependent on the type of information desired and on the availability of suitable commercial detectors. Other factors which determined the choice of the transducers were:

(1) transducer capability,

(2) transducer sensitivity to environmental effects,

(3) transducer sensitivity to directional effects,

(4) stability and reliability of transducer, and

(5) compatability of transducer with facility and other systems.

Since most transducers were not capable of satisfying all measurement requirements simultaneously, several different transducers were used - one type of instrument for rise time coverage, another for accuracy, and a third for protective coverage.

Most transducers were installed several weeks before the test was conducted; therefore, in order to reduce or prevent detector failure NaK resistant materialswere used in the fabrication of in-core detectors or the detector was covered with a protective coating. The detectors in the environmental tank were sealed against the effects of moisture and those detectors in the atmosphere were removed between calibrations and checkouts.

To reduce gamma and neutron contributions to non-nuclear measurements, detectors were tested in radiation fields and only those transducers having comparatively low sensitivity to radiation were chosen. To further reduce spurious outputs caused by radiation, inactive transducers were used for cancelling radiation effects.

Nuclear Detectors - Thermal and fast neutron detectors and gamma detectors were used at various locations in the core, in the environmental tank, and under the flatcar. The locations of these

detectors are summarized in Figure A-1 and their intended range coverage is shown in Figure A-2.

Four miniature ion chambers were sealed in the reactor vessel and three identical chambers were located 1-1/2, 2-1/2, and 3-1/3 inches from the Binal sleeve. These chambers were to have provided information concerning the in-core and reflector flux distribution; however, three of the four in-core chambers were found defective before the destructive test was conducted. As a backup and protective measure, three neutron and two gamma detectors were installed in protective canisters in the environmental tank. A 20th Century neutron chamber, located 2 feet from the vessel provided protective coverage over the low power levels if the nuclear excursion failed to reach the expected magnitude. Two semi-rad neutron detectors at 9 inches and 2-1/2 feet from the vessel provided peak power, period, and flux distribution coverage. Two gamma chambers, one approximately 3 feet from the vessel and one near the environmental tank floor were used to provide data concerning burst shape, period, and peak gamma flux. The chamber at 3 feet from the vessel monitored the lower portion of the burst. Its range coverage overlapped the range coverage of the chamber near the tank floor.

Because of problems caused by environmental effects, attenuation, thermalization, etc., a flight tube (Figure A-3) was designed and installed in the reactor pedestal. The flight tube was a steel tube 84-3/4 inches long with a 3 inch O.D. and a 2.6 inch I.D. having a water tight aluminum cap nominally 2 inch thick at the vessel end. The flight tube was located off center below the core parallel to the pedestal. Neutrons leaving the core passed through 1 inch of water and entered the aluminum cap. The neutrons traveled down the tube and through a lead plug at the bottom end. By attenuating gammas more than neutrons, the lead plug increased the neutron-gamma ratio; thereby giving better neutron measurements. The tube was devoid of water thus eliminating thermalization of fast neutrons, and since the detectors were more than 7 feet from the vessel, minimizing the possibility of the chambers being destroyed before termination of the power burst. The following detectors were stacked beneath the flight tube: one semi-rad neutron detector, three fast neutron scintillators, and a 20th Century neutron chamber.

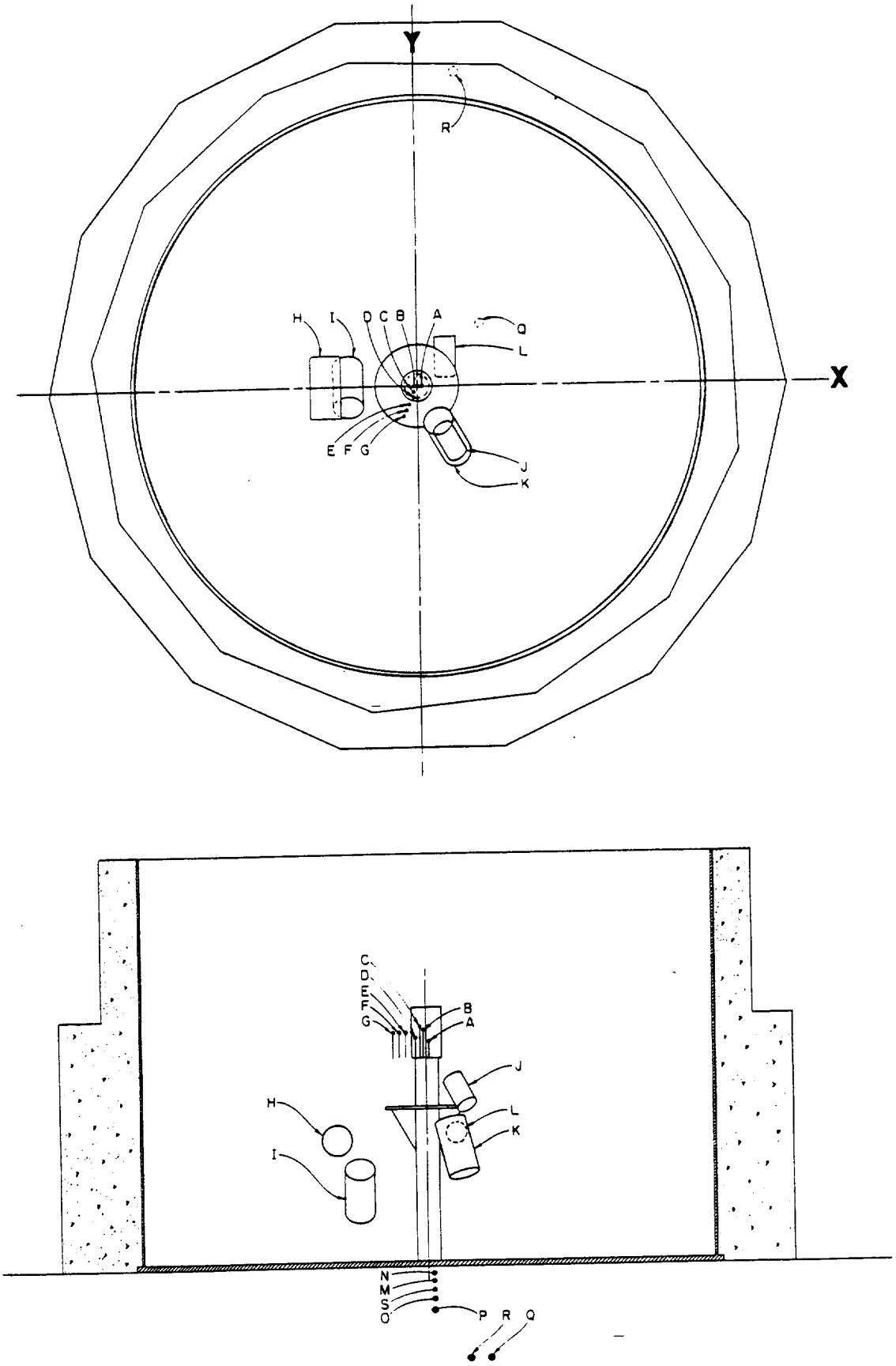

Fig. A-1a SNAPTRAN 2/10A-3 Nuclear Detector Layout

CODE	DETECTOR	LOCATION
N-1 A	GENERAL ELECTRIC NEUTRON MINI-CHAMBER, S/N 5452640	(DAMAGED) IN-CORE (1)(3)(4) Z = -3"
N-2 B	GENERAL ELECTRIC NEUTRON MINI-CHAMBER, S/N 5452641	IN-CORE (1)(4)(5) Z = +2"
N-3 C	GENERAL ELECTRIC NEUTRON MINI-CHAMBER, S/N 5452642	(DAMAGED) IN-CORE (4)(12)(13) Z = +2¼"
N-4 D	GENERAL ELECTRIC NEUTRON MINI-CHAMBER, S/N 5452639	(DAMAGED) IN-CORE (12)(26)(27) Z = -1½"
N-5 E	GENERAL ELECTRIC NEUTRON MINI-CHAMBER, S/N 5452251	1½" FROM BINAL SLEEVE Z = +2¾", θ ~ 200°
N-6 F	GENERAL ELECTRIC NEUTRON MINI-CHAMBER, S/N 5452262	2½" FROM BINAL SLEEVE Z = +2¾", θ ~ 200°
N-7 G	GENERAL ELECTRIC NEUTRON MINI-CHAMBER, S/N 5452249	3½" FROM BINAL SLEEVE Z = +2¾", θ ~ 200°
N-8 H	20th CENTURY NEUTRON CHAMBER, S/N TE 845	-X AXIS, X = -26½", r = 41" Z = -31½", R = 33"
N-9 I	GENERAL ELECTRIC GAMMA CHAMBER, S/N 4131132	-X AXIS, X = -20", r = 50" Z = -46", R = 43"
N-10 J	REUTER STOKES SEMI-RAD NEUTRON CHAMBER, S/N E-531	X = 9½", Y = -16", r = 26" Z = -18", R = 20"
N-11 K	REUTER STOKES GAMMA CHAMBER, S/N E-643	X = 8½", Y = -15", r = 38" Z = -34", R = 31"
N-12 L	REUTER STOKES SEMI-RAD NEUTRON CHAMBER, S/N D-1542	X = 8½", Y = 8½", r = 38" Z = -30", R = 30"
N-13 M	ITT PHOTOTUBE WITH PILOT SCINTILLATOR B, S/N 1462	FLIGHT TUBE POSITION 2
N-14 N	ITT PHOTOTUBE WITH PILOT SCINTILLATOR B, S/N 1421	FLIGHT TUBE POSITION 1
N-15 O	20th CENTURY NEUTRON CHAMBER, S/N UH-164	FLIGHT TUBE POSITION 5
N-16 P	REUTER STOKES SEMI-RAD NEUTRON CHAMBER, S/N E-530	FLIGHT TUBE POSITION 4
N-17 Q	REUTER STOKES GAMMA CHAMBER, S/N E-498	UNDER FLAT-CAR X ~ 1½', Y ~ 1½', Z ~ -9½'
N-18 R	GENERAL ELECTRIC GAMMA CHAMBER, S/N 5451839	UNDER FLAT-CAR X ~ 1', Y ~ 7½', Z ~ -9½'
N-19 S	ITT PHOTOTUBE WITH PILOT SCINTILLATOR B, S/N 1478	FLIGHT TUBE POSITION 3

r = CENTER OF CORE TO CENTER OF CHAMBER
R = CENTER OF CHAMBER TO SURFACE OF VESSEL

Fig. A-1b SNAPTRAN 2/10A-3 Nuclear Detector Summary

1256160

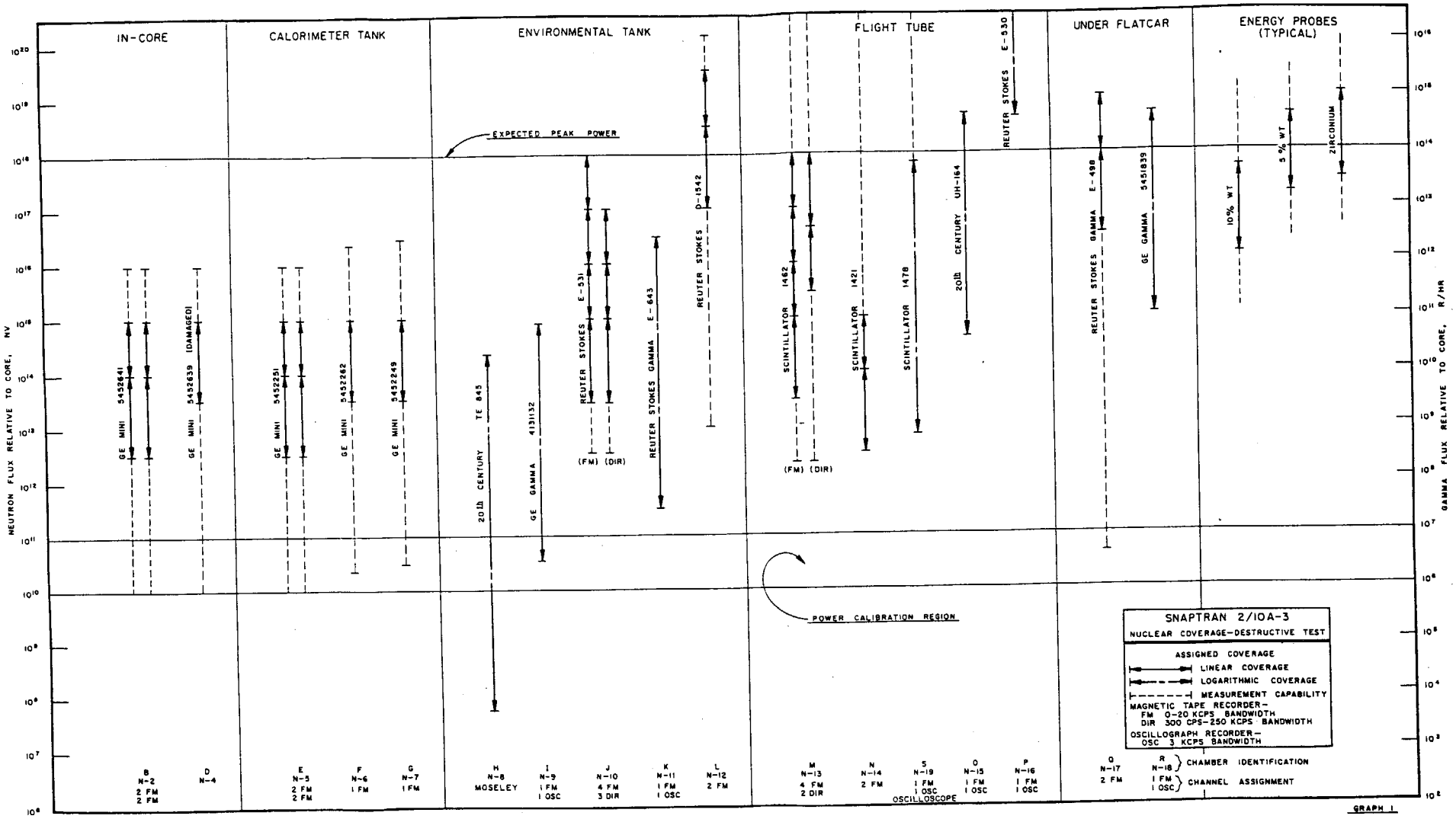

Fig. A-2 SNAPTRAN 2/10A-3 Nuclear Detector Range Coverage

1256161

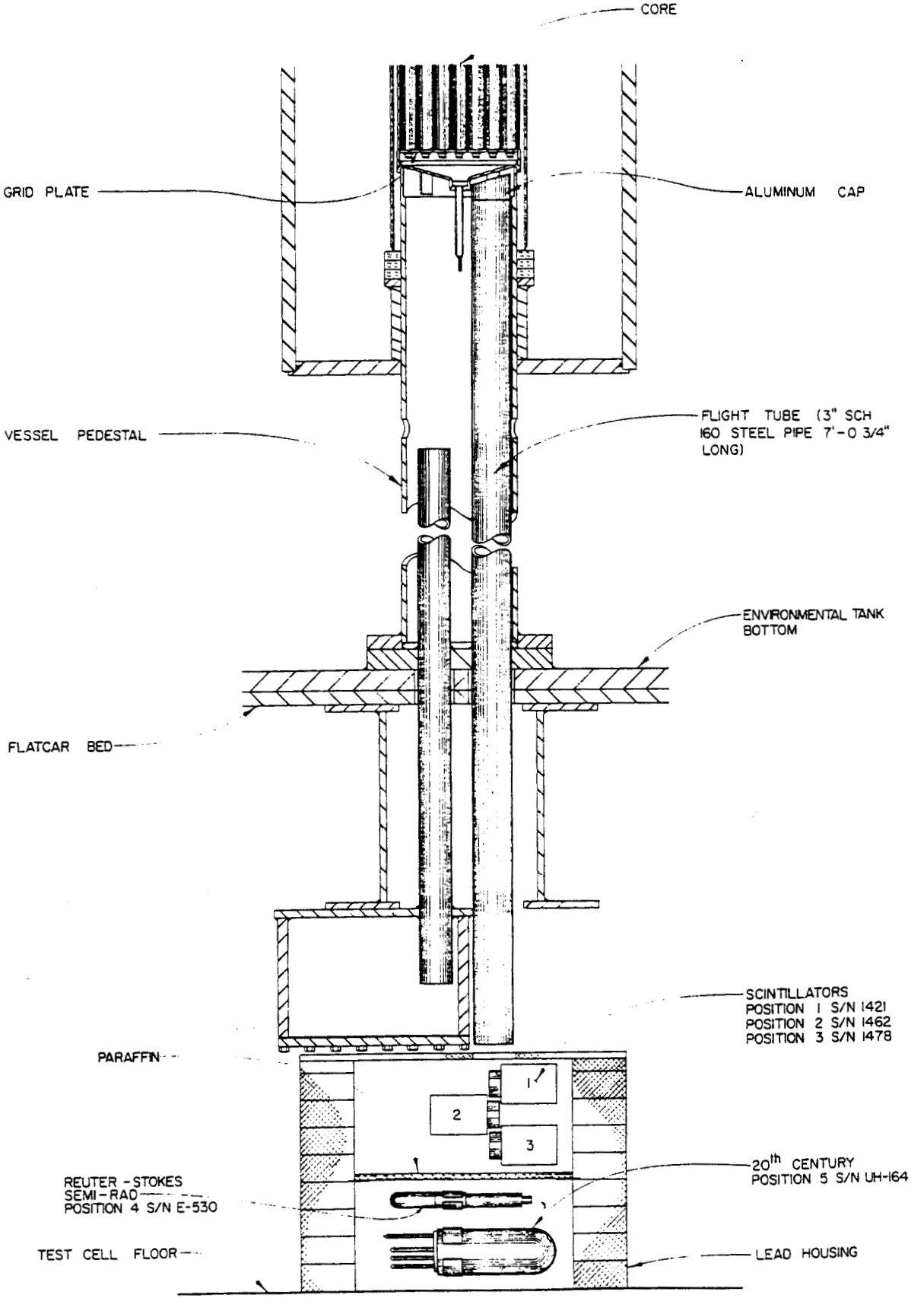

Fig. A-3 SNAPTRAN 2/10A-3 Flight Tube Arrangement

1256162

Two gamma chambers were located under the flatcar to provide information regarding peak power, burst shape, period, and total nuclear energy release. These chambers were chiefly for backup and protective purposes.

Energy probes fabricated from two 0.5 mil chromel-alumel wires embedded in a small fuel sample were used to obtain information concerning the space-time history of nuclear energy deposition in the fuel, power, period, flux distribution and hydrogen release. Three types of probes were used: (1) 10% enriched fuel sample, (2) 5% enriched fuel sample, and (3) zirconium-hydride sample. Fourteen probes were sealed in the core in the following distribution: six 10% enriched probes, six 5% enriched probes and two zirconium-hydride probes. Six probes (three 5% and three 10%) were located outside the vessel. The probes on the outside of the core were aligned in a radial array with those on the inside of the core (Figure A-4) to provide a measurement of the flux profile in the core and reflector.

Non-nuclear Detectors - Pressure transducers were positioned along the negative X and Y axes in the environmental tank (Figure A-5). The detectors along the negative X axis were considered primary sources of data, while those along the negative Y axis were considered slightly less important because of reflection effects caused by the photographic periscopes. Three sets of two transducers each were located in the tank at 0°, 45°, and 90° to determine the extent of disassembly symmetry. Several transducers were located beneath the calorimeter support flange, near the tank floor and walls, and near the water surface. The transducers beneath the support flange were expected to be important for giving a time history coverage of the excursion, and the transducers at the tank walls and bottom and at the water surface were located to provide information concerning pressure reinforcement and reflection at the boundaries.

Strain gauges (Figure A-6) were installed on the reactor sides and bottom for the purpose of investigating pressure buildup in the core and expansion and disassembly of the vessel. Each of the gauges on the

1256163

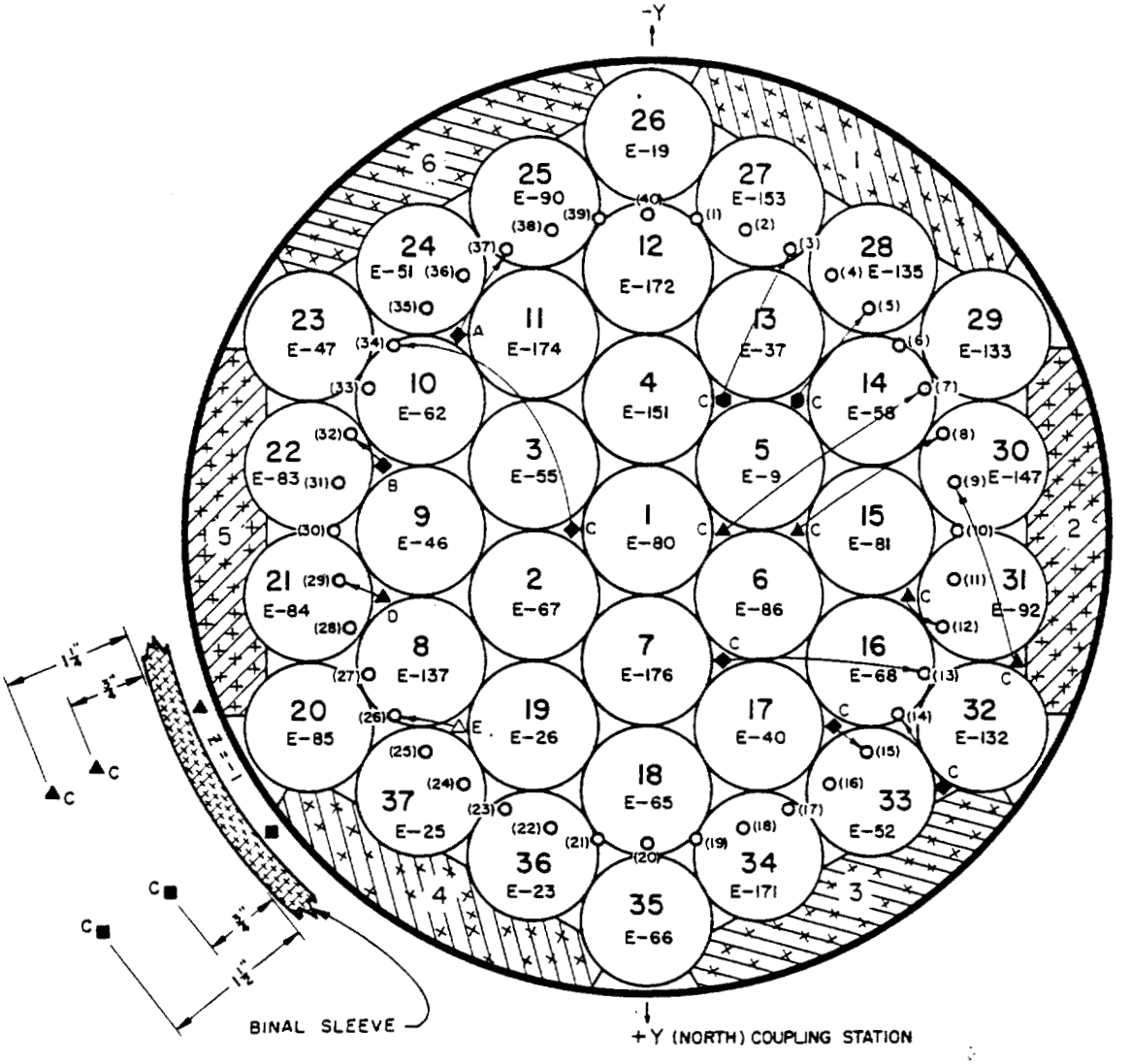

IN-CORE ENERGY PROBE LOCATION

- ▲ 5 % ENRICHED
- ● 10 % ENRICHED
- ● ZIRCONIUM
- △ DAMAGED

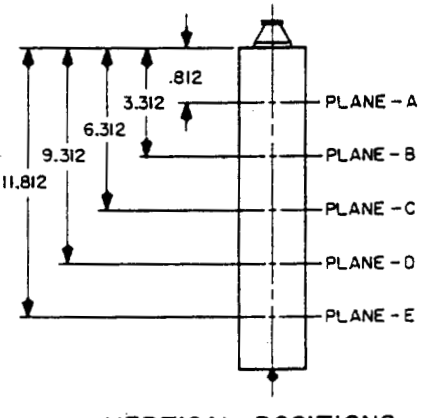

VERTICAL POSITIONS

NOTES

1. TOP VIEW OF CORE BEFORE INVERTING FOR INSTALLATION ON PEDESTAL.
2. ALPHABETICAL LETTER BEFORE ENERGY PROBE SYMBOL INDICATES VERTICAL POSITION.

Fig. A-4 SNAPTRAN 2/10A-3 In-Core Energy Probe Locations

1256164

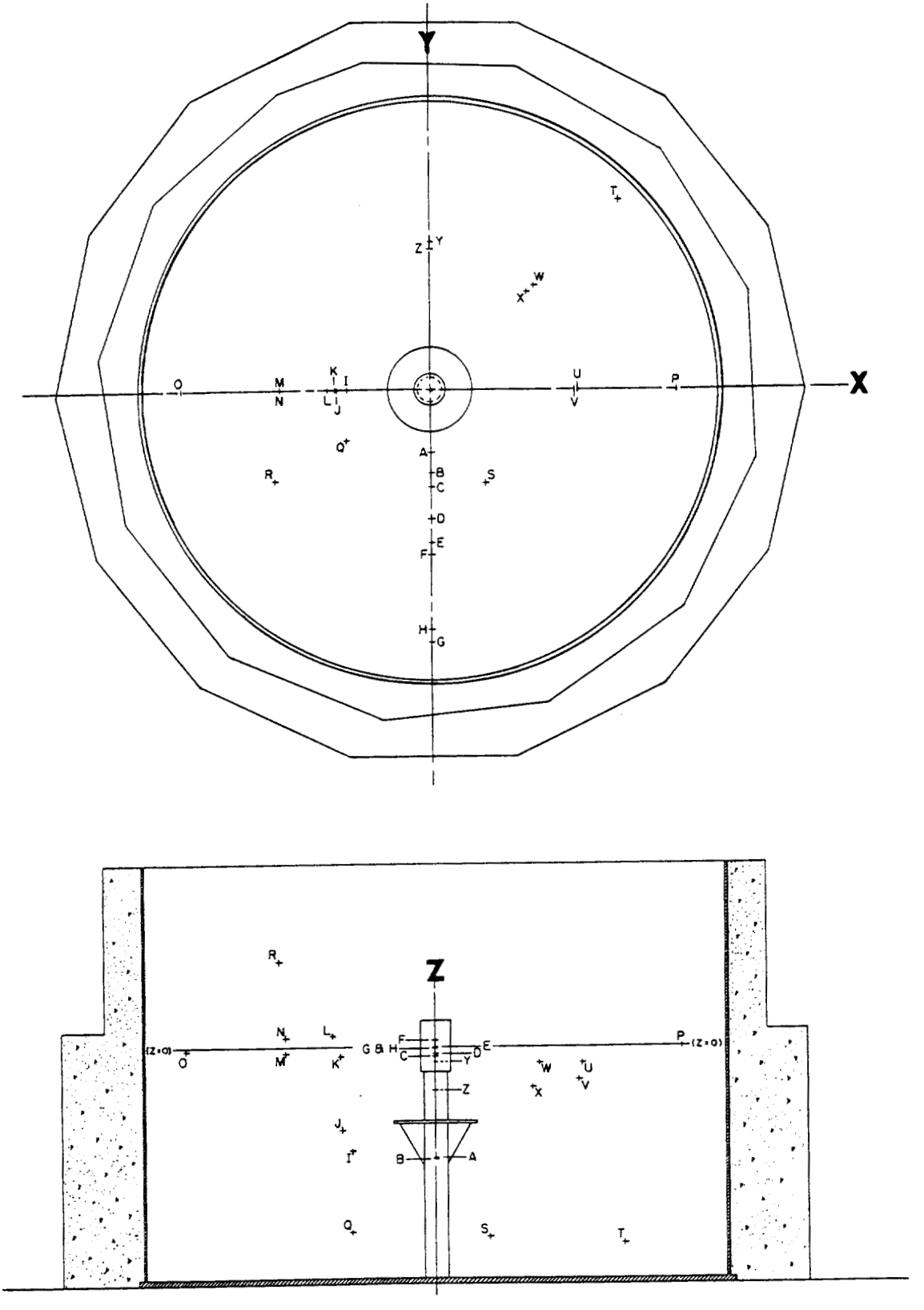

Fig. A-5a SNAPTRAN 2/10A-3 Pressure Transducer Locations

1256165

CODE	DETECTOR	LOCATION
P-1 A	KAMAN NUCLEAR MODEL K-1200-3, S/N 47	Y ~ -18" IN TANK Z ~ -32"
P-2 B	CRYSTAL RESEARCH MODEL R-63, S/N 431	Y = -24" IN TANK Z = -32¼"
P-3 C	NORWOOD MODEL 114, S/N 6514	Y = -28" IN TANK Z = -2¾"
P-4 D	CRYSTAL RESEARCH MODEL R-63, S/N 432	Y = -37" IN TANK Z = -2⅛"
P-5 E	KAMAN NUCLEAR MODEL K-1200-3, S/N 49	Y = -44" IN TANK Z = 0"
P-6 F	CRYSTAL RESEARCH MODEL R-63, S/N 441	Y = -47½" IN TANK Z = 2¼"
P-7 G	KISTLER MODEL 617 A, S/N 4387	Y = -72½" IN TANK Z = -½"
P-8 H	CRYSTAL RESEARCH MODEL R-63, S/N 442	Y = -69" IN TANK Z = -½"
P-9 I	CONSOLIDATED ELECTRODYNAMICS CORP. MODEL 4-317, S/N 2156	X = -24" IN TANK Z = -30"
P-10 J	CRYSTAL RESEARCH MODEL R-63, S/N 433	X = -27" IN TANK Z = -23¾"
P-11 K	NORWOOD MODEL 114, S/N 6477	X = -27½" IN TANK Z = -2½"
P-12 L	CRYSTAL RESEARCH MODEL R-63, S/N 434	X = -29½" IN TANK Z = 3"
P-13 M	NORWOOD MODEL 114, S/N 6479	X = -43½" IN TANK Z = -1¾"
P-14 N	CRYSTAL RESEARCH MODEL R-63, S/N 435	X = -43½" IN TANK Z = 2¾"
P-15 O	NORWOOD MODEL 114, S/N 6484	X = -71¾" IN TANK Z = -¾"
P-16 P	CRYSTAL RESEARCH MODEL R-63, S/N 437	X = -71¼" IN TANK Z = 0"
P-17 Q	CONSOLIDATED ELECTRODYNAMICS CORP. MODEL 4-317, S/N 2293	X = -24¼" IN TANK Y = -14¼" Z = -53½"
P-18 R	KISTLER MODEL 617 A, S/N 4388	X = -45" IN TANK Y = -26" Z = 25"
P-19 S	CRYSTAL RESEARCH MODEL R-63, S/N 438	X = 15½" IN TANK Y = -26⅜" Z = -55"
P-20 T	CRYSTAL RESEARCH MODEL R-63, S/N 439	X = 54½" IN TANK Y = 54½" Z = -57"
P-21 U	NORWOOD MODEL 114, S/N 6649	X = 42½" IN TANK Z = -4½"
P-22 V	CRYSTAL RESEARCH MODEL R-63, S/N 440	X = 41½" IN TANK Z = -9½"
P-23 W	NORWOOD MODEL 114, S/N 6485	X = 30" IN TANK Y = 30" Z = -4½"
P-24 X	CRYSTAL RESEARCH MODEL R-63, S/N 444	X = 28" IN TANK Y = 28" Z = -11¾"
P-25 Y	NORWOOD MODEL 114, S/N 6486	Y = 42½" IN TANK Z = -4½"
P-26 Z	CRYSTAL RESEARCH MODEL R-63, S/N 443	Y = 40½" IN TANK Z = -12½"

Fig. A-5b SNAPTRAN 2/10A-3 Pressure Transducer Summary

1256166

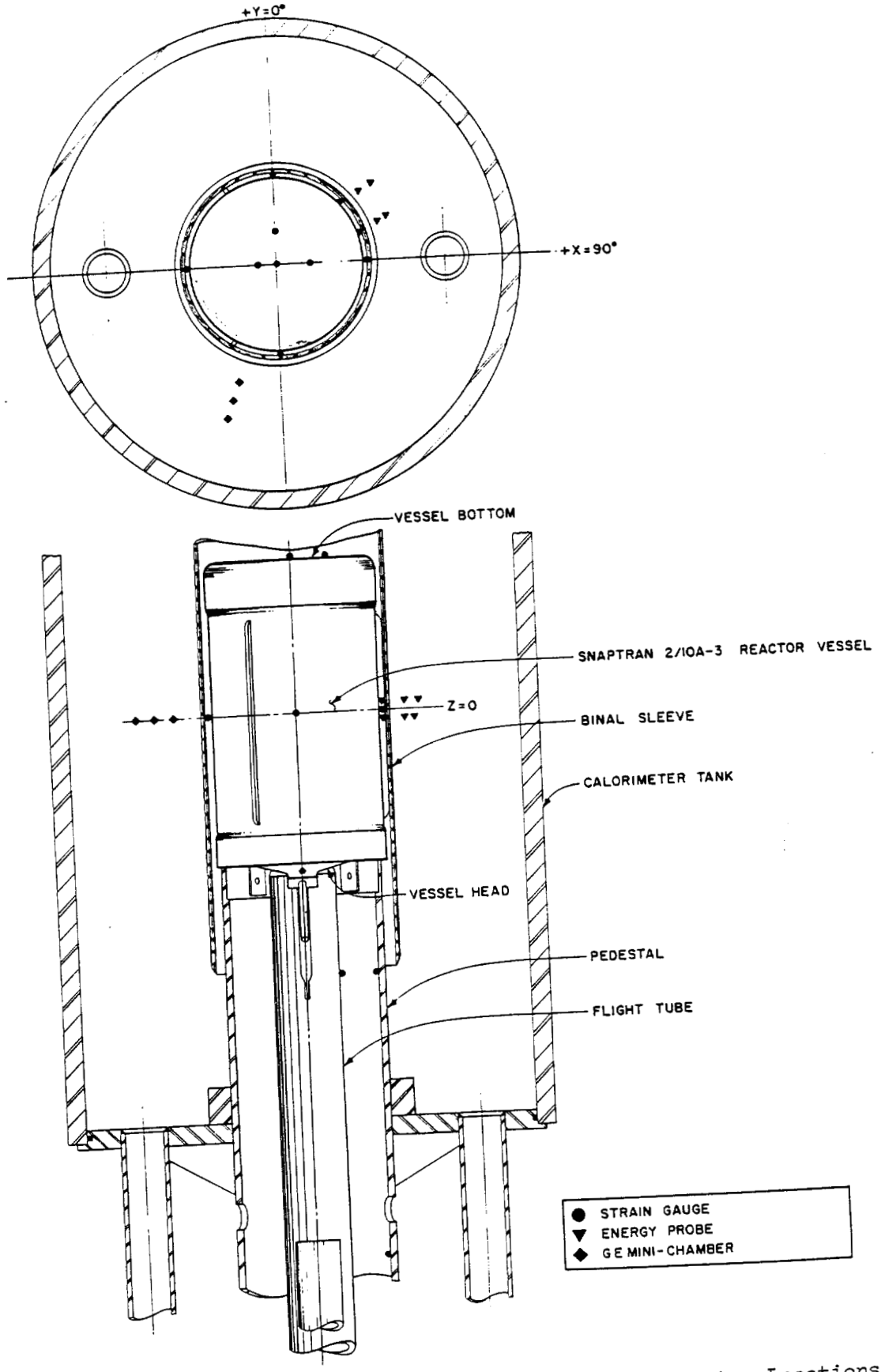

Fig. A-6 SNAPTRAN 2/10A-3 Strain and Nuclear Detector Locations Proximate to Core

1256167

reactor walls were installed 90° apart to provide information describing the disassembly process - indicating whether the excursion was symmetric about the core centerline or whether perferential rupture occurred.

Strain gauges were installed at various locations on the reactor pedestal, flight tube, inside and outside the environmental tank walls and in the concrete backing surrounding the tank. Two hoop gauges were placed around the outside of the concrete. Several strain measurements were made at positions near the ends and center of the flatcar to determine the mechcanical energy converted to stress and deformation of the flatcar.

A number of special measurements were made during the destructive test for the purpose of obtaining information which would supplement other measurements and which would aid in interpreting data from other sources. The chief purpose of most of the miscellaneous measurements was to tie together information from the primary measurements such as nuclear and pressure with information from strain, acceleration, and temperature measurements to obtain a complete interpretation of the test.

Due to the relatively short period of time required for hydrogen release and vessel rupture as compared with the time necessary for heat transfer from the fuel to the cladding, no observable temperature changes were expected to occur outside the fuel material until after disassembly and non-nuclear sources of thermal effects came into existence. For this reason, temperature measurements by standard thermometry techniques were not made in the reactor vessel.

Several temperature measurements were made at positions above the environmental tank and on the photographic tower to provide information concerning the mechanical energy appearing as thermal energy, to provide information concerning the magnitude of steam, NaK-water and zirconium-air interactions and to show the energy release of each interaction, and to determine the thermal contributions to other measurements - particularly pressure measurements.

Miscellaneous Detectors - Two types of acceleration measurements were made during the destructive tests: (1) water

acceleration measurements, and (2) flatcar acceleration measurements. Small floats, free to travel along a slidewire, were used for determining the displacement and accelerometers were installed beneath the flatcar to measure vertical and horizontal acceleration.

Other miscellaneous measurements included: measurements to show that the maximum amount of reactivity was inserted, measurements to show that the photographic lights and cameras were operating at the critical moment of vessel expansion and disassembly, measurements to show the profile and velocity of water expulsion from the tank, and finally measurements to give velocity of pressure propagation in water and air.

Two types of passive measurements were conducted during the test: (1) neutron flux measurements, and (2) peak pressure measurements. The purpose of making flux measurements was to determine the total energy release, and to determine the peak power and flux level achieved during the excursion. Flux wires were placed in the following locations: (1) below the flight tube, (2) inside the core, (3) inside the environmental tank, and (4) above the environmental tank.

C. Signal Conditioning and Recording Equipment

In order to satisfy the measurements criteria, a variety of fast-response, wide-dynamic range, high-performance signal conditioning and recording equipment was used. Figure A-7 shows a schematic representation of typical channel arrangements for the various types of signal conditioning and recording equipment used.

Configurations A and B are indicative of channels used for low-impedance detectors such as displacement potentiometers, thermocouples and bridge-balance strain gauges, pressure transducers, and accelerometers. The signal conditioning is accomplished with low-level, high-common mode rejection dc amplifiers with frequency response capability to 150 kcps. Two outputs, at 100% and 10% of the amplifier full scale (10 volts), are provided to permit recording the full dynamic range available from the amplifier. The uncertainties of gain stability, linearity, drift, noise for each type of channel is no greater than ± 2% of full scale.

1256169

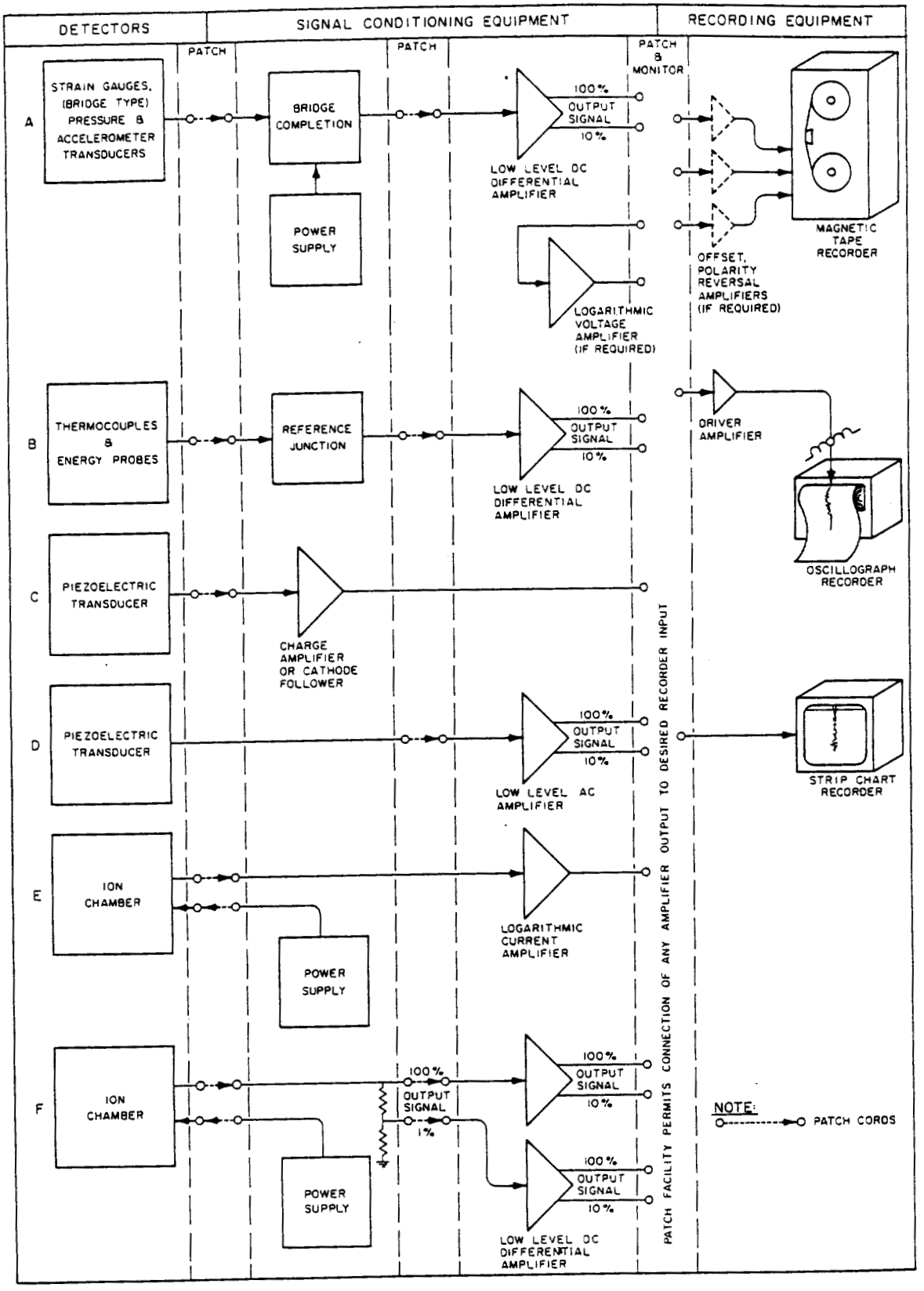

Fig. A-7 SNAPTRAN 2/10A-3 Signal Conditioning and Recording Equipment Block Diagram

1256170

Configuration C represents a channel used for crystal accelerometers and pressure transducers where impedance conversion is required near the detector to prevent loss of frequency response by cable loading. For this configuration, the detectors have sufficient output so no additional gain is required prior to the recorder amplifiers. The impedance conversion cathode follower and charge amplifiers are generally capable of 20 cps to 200 kcps with overall uncertainties no greater than ± 5% of full scale.

Configuration D, also used for crystal type detectors, represents a channel where impedance conversion is not necessary but additional gain is required. The signal conditioning equipment for these channels is capable of 200 cps to 200 kcps in frequency response and is provided with two outputs similar to configuration A and B for recording the amplifier entire dynamic range. This type of channel is intended primarily for sensing ultra-fast changing phenomena, e.g., impact loading, shock generation, etc.

Configuration E is used primarily for low-level current generating neutron and gamma detectors. The signal conditioning is accomplished with "micro-microammeters" where the output is a voltage proportional to the logarithm of the input current signal. The frequency response of this type amplifier is 10 kcps for greater than 10^{-7} amps and is directly proportional to the input current below 10^{-7} amps. This frequency response is that associated with the linear amplifier in conjunction with the logarithmic converter and input cable capacity. It can be shown however, that as a result of the logarithmic conversion, a 10 kcps frequency response is equivalent to 150 kc at the detector. The uncertainties for this type of channel when referred to a twenty point per decade linearity calibration are less than ± 5% per decade.

Configuration F is used for current source detectors similar to those described in configuration E. However, the conversion from current to voltage is linear. The signal conditioning is accomplished with dc low-level amplifiers with an upper frequency response of 40 kcps. In order to acquire the maximum dynamic range from the detector, the source signal is tapped for 100% and 1% of the detector full scale and is conditioned by an amplifier channel at each tap and recorded on four

1256171

magnetic tape channels, permitting a usable dynamic range at the detector of nearly five decades. The uncertainties for this configuration are no greater than ± 2% of full scale.

The signals from all detectors are amplified such that the required normal full scale output at the particular detector is equivalent to 1 volt at the 10% output tap of the signal conditioning equipment. Recording of the 100% tap, in addition to the 10% tap, permits acquiring the full three decade dynamic range capability of the signal conditioning equipment. Where accuracy is not important, a voltage logarithmic amplifier is available for compressing 3-1/2 decades of amplifier capability output onto a single recording channel. The accuracy of these units is within about ± 10% per decade and was used for protective range coverage.

The outputs of the signal conditioning equipment are terminated at a patch and monitoring facility using patch boards. This provides flexibility in utilizing a variety of recording channel arrangements for selected types of measurements as well as permitting isolation of signal conditioning and recording equipment for troubleshooting and calibration. The patch approach used also permits oscillographic reproduction of information acquired on magnetic tapes without disturbing the calibrated state of the signal conditioning equipment.

The recording equipment used consisted of analog magnetic recording, oscillograph recording, and strip chart potentiometric recording. The magnetic tape recording, using "FM" and "direct" modes, was capable of dc to 20 kcps on FM and 250 to 250 kcps on direct. These are high performance recorders with record, store, and reproduce uncertainties less than ± 1% of full scale (± 1.4 volt) for FM and ± 10% of full scale for the direct mode. Table A-I lists the recording channel requirements. The oscillographic recorders are capable of dc to 3500 cps with uncertainties less than 3% of full scale. The potentiometric recorders, although capable of only 3 cps, have accuracies to within ± 0.2% of full scale and are used primarily for slow changing phenomena during static testing.

The system calibration techniques used to place the entire signal conditioning and recording equipment in a calibrated state consists of

1256172

TABLE A-I

SUMMARY OF SNAPTRAN 2/10A-3 RECORDING CHANNEL REQUIREMENTS

Measurement Location or Type	Detectors Monitored	Recorder Channels
Nuclear		
a. In-core	1	4
b. Reflector	3	6
c. Environmental tank	5	13
d. Flight tube	5	14
e. Under flatcar	2	4
	16	41
Temperature (Energy Probe)		
a. In-core	13	21
b. Reflector	6	7
	19	28
Pressure		
a. Environmental tank	46	46
b. Air	7	9
	53	55
Strain		
a. Vessel	6	11
b. Environmental tank	4	4
c. Flight tube	2	2
d. Pedestal	2	2
e. Flatcar	4	6
f. Concrete outside	2	2
	20	27
Temperature (thermocouple)		
a. In-core	1	
b. Above environmental tank	4	5
c. Photographic tower	2	3
	7	8
Acceleration		
a. Under flatcar	5	7
	5	7
Miscellaneous		
a. Time-of-arrival	3	3
b. Sleeve velocity	1	2
c. Sleeve displacement	1	2
d. Flatcar displacement	1	2
e. Water surface velocity	5	5
f. EG&G lights	1	2
g. NaK reservoir pressure	1	1
h. Water surface displacement	3	6
i. EG&G electronic signal	1	1
	17	24
Timing		16
	136	206

1256173

inserting bipolar, ramp, and step signals of known amplitude into the detector cable termination points and recording the programmed calibration signal. The magnetic tape information is then reproduced on recording oscillographs to verify overall system performance of gain setting, polarity, frequency response, linearity, noise threshold, zero offset, overload recovery time, etc. For highly accurate calibration reduction, as well as test information reduction of magnetic tape signals, real-time analog-to-digital conversion with a bandwidth of 10 kc was used where the information was digitally recorded on magnetic tape and later plotted on high accuracy potentiometric digital recorders. The ac channels were calibrated by inserting a monopolar one kilocycle square wave into the signal conditioning equipment at 1/2 decade increasing steps. This technique permitted a check on frequency response, gain setting, and linearity. Calibration information was reduced in a manner similar to that for the ramp signals discussed above.

II. Radiological Measurements

Details of the sampling devices and grid sampling equipment used to instrument the grid are given below along with measurements which were expected to be made with each instrument. The radiological grid layout is shown in Figures A-8 and A-9.

Radiological Tower and Stack-Cloud-Height Samplers - In order to measure the height of the radioactive cloud as it left the reactor area, sampling equipment was located at various heights on the downwind side of the reactor. Part of the elevated samplers were fastened to a 150 foot metal monitoring tower which was installed at approximately 20 meters northeast of the reactor. The remaining samples were placed on a rope elevator which was fastened to the top of the 150 foot IET stack located approximately seventy five meters north of the reactor.

Water Samplers - Three types of water samplers were set up to obtain data concerning fission and neutron activation products retained in the water. These samplers included long compartmented trays, water catch cans with three inch diameter tops and environmental tank drain sample bombs.

1256174

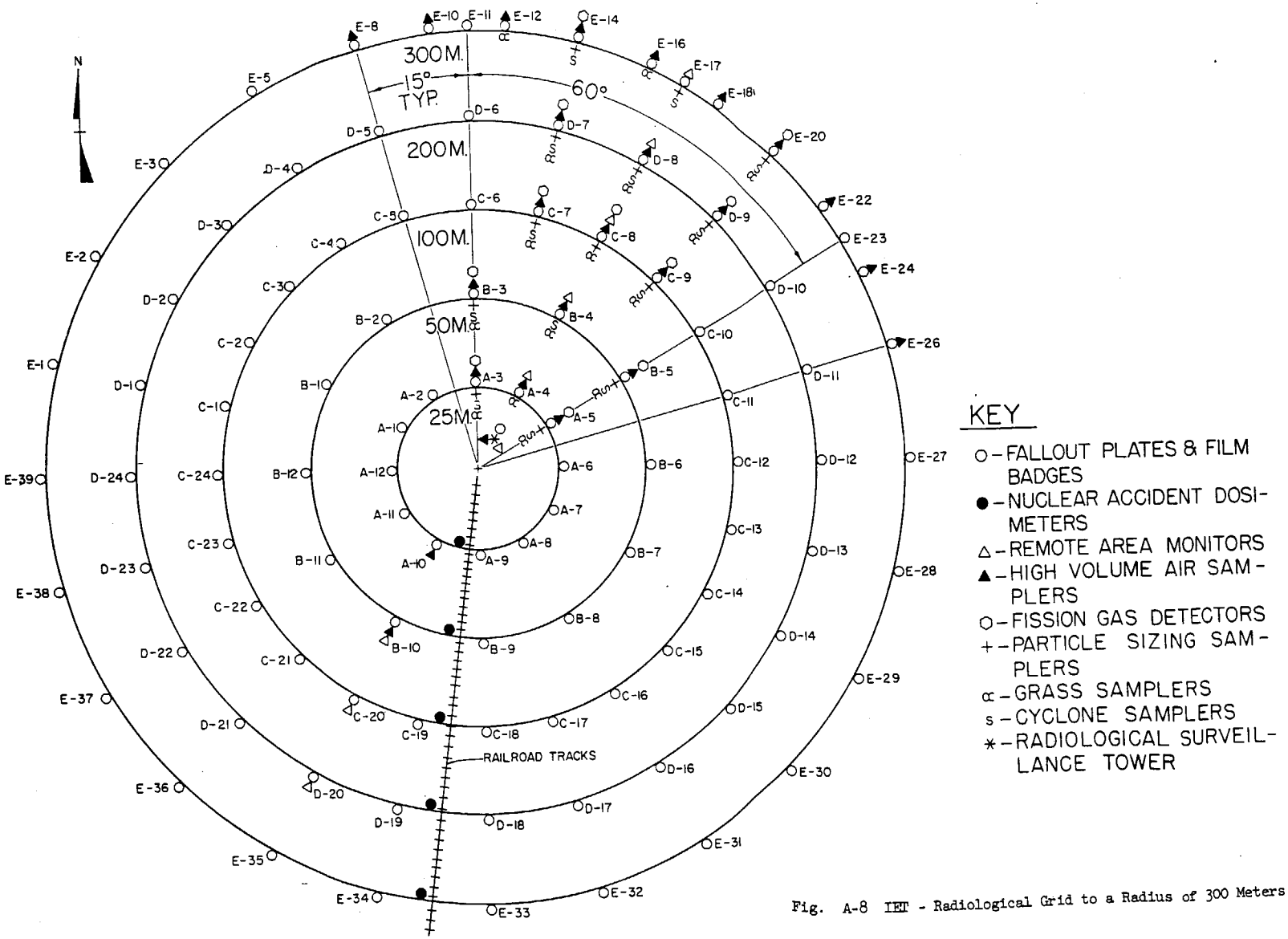

Fig. A-8 IET - Radiological Grid to a Radius of 300 Meters

125b115

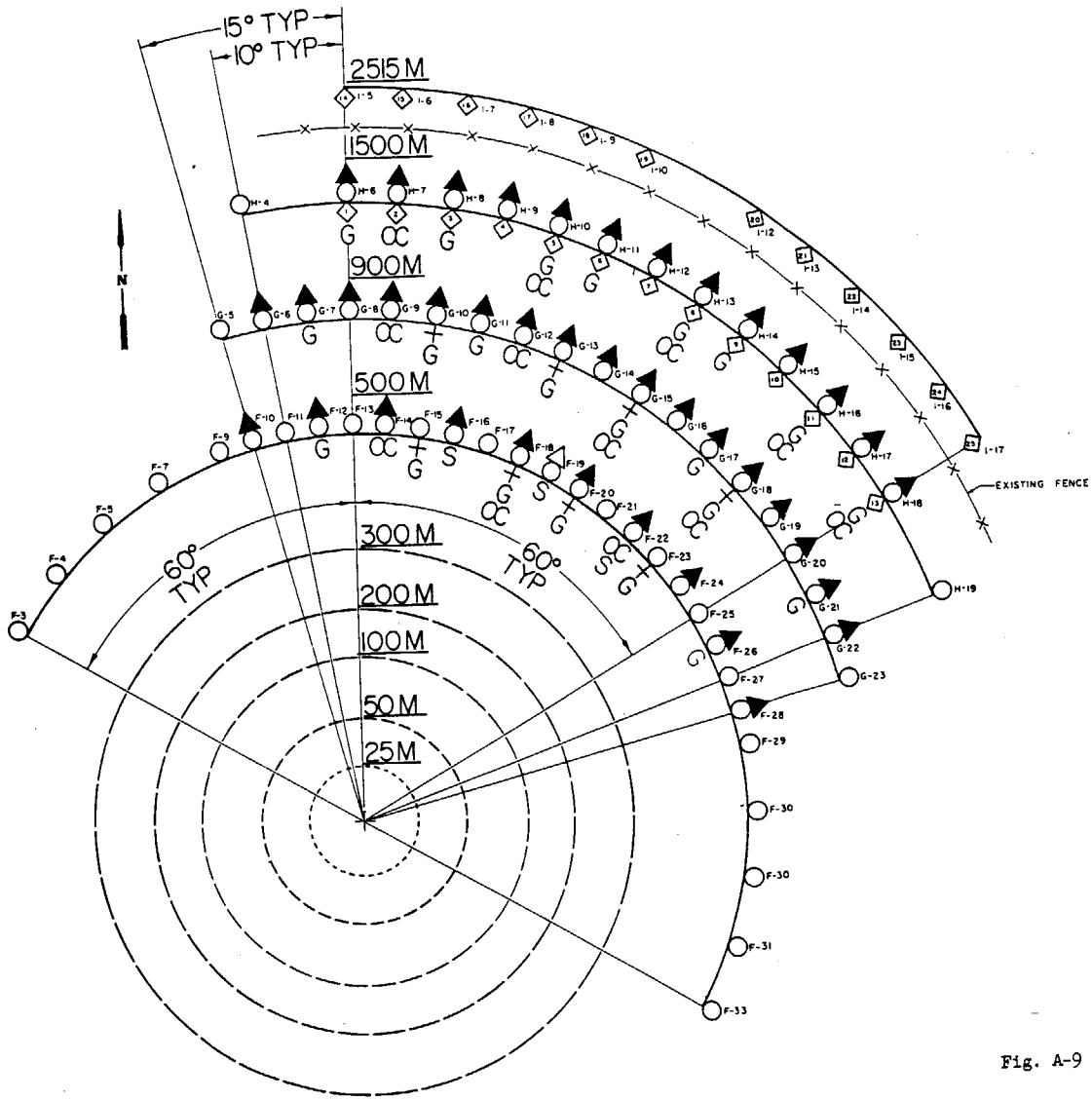

KEY

- ○ - FALLOUT PLATES & FILM BADGES
- G - GENERATORS
- ▲ - HIGH VOLUME AIR SAMPLERS
- ◇ - TELEMETERING STATIONS
- + - PARTICLE SIZING SAMPLERS
- ∝ - GRASS SAMPLERS
- S - CYCLONE SAMPLERS
- △ REMOTE AREA MONITORS

Fig. A-9 IET - Radiological Grid Beyond a Radius of 300 Meters

125b176

Compartmented trays (Figure A-10) were set on each corner of the railroad dolly to catch water and debris that might be expelled from the environmental tank immediately following the reactor excursion.

Supplementing the trays, a series of water-catch-cans (Figure A-11) were located on the edge of the environmental tank, the 10, 20, 25, 50, and 100 meter arcs. Catch-cans on the edge of the environmental tank and on the 10 meter arc completely surrounded the reactor while those on the outer arcs were limited to the 60° downwind sector. Each can contained a filter which screened the water sample before it was collected in a reservoir at the bottom of the can.

Sample bombs were set up to draw off water samples from the water remaining in the environmental tank following the test and prior to emptying the water to the liquid waste tank.

Film Badge Drops - Two sources of radiation exposure occur in this type of reactor experiment, that which accompanies the excursion and that which occurs as a result of the fission products produced during the excursion. To separate the contribution of each of these sources, nine film badge drop stations were located on an approximate ten meter arc surrounding the reactor.

The film badge drop station consisted of two identical film badge dosimeters, one was permanently attached to the station while the other badge was held in place by an energized solenoid which released the badge immediately following the power burst. The released badge dropped into a shielded receptacle buried in the ground, measuring only the excursion dose, while the duplicate badge at that station was exposed to obtain the total integrated dose. The contribution from fission product radiation was then obtained by subtracting the "burst" dose from the integrated dose.

Air Support - Air support for the destruct test was provided by the ID Health and Safety Division. An airplane equipped with radiological monitoring instruments was used prior to the test to check conditions in the immediate area and to confirm that downwind restricted areas were cleared of vehicles and personnel.

Following the excursion, the aircraft was used to locate and follow

1256177

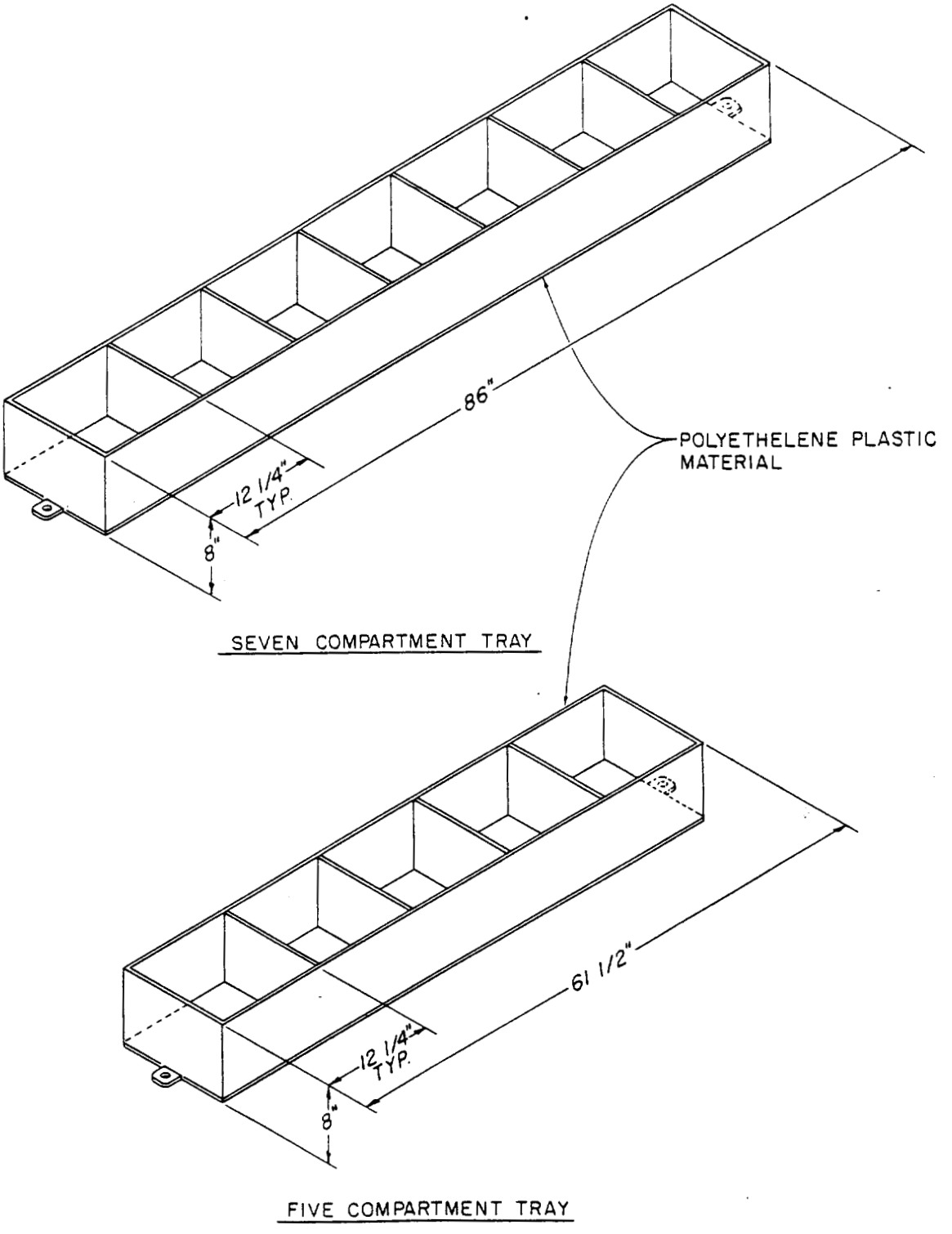

Fig. A-10 SNAPTRAN 2/10A-3 Compartmental Catch Trays for Destructive Test Debris

1256178

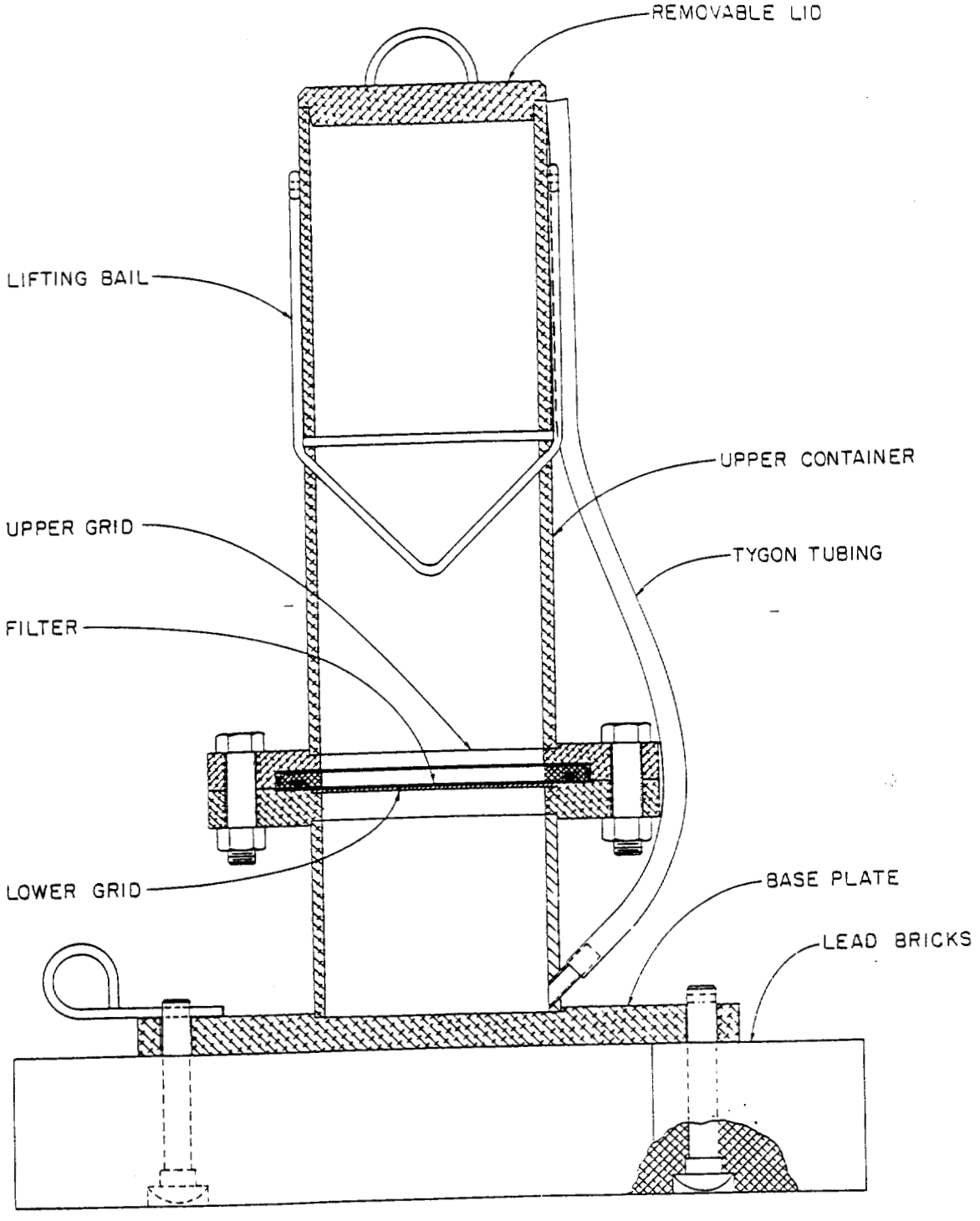

Fig. A-11 SNAPTRAN 2/10A-3 Catch Cans for Destructive Test Debris

1256179

the radioactive cloud as it passed beyond the monitoring grid and the boundaries of the testing station.

"Clothes-Line" - To avoid excessive exposure during the early recovery of the priority samples located near the reactor a "clothes-line" type device with pulleys was utilized. With this arrangement, the priority samples could be positioned and recovered by a recovery team at the end of the 200 foot clothes-line. This system was used to position two Nuclear Accident Dosimeters (Hurst Threshold Detectors)[A1], two film badges (ID-NRTS type), a section of copper wire, an activation foil box, a sample of human hair, and a high range gamma dosimeter.

High Volume Air Samplers and Filters - Because very low concentration of some of the fission produced isotopes are biologically significant, the classical technique to obtain measurable samples for analytical work has been to draw large volumes of air through a high efficiency aerosol filter assuming isokinetic sampling. Since a high flow rate is necessary, the Staplex model high volume air sampler was used. The average flow rate of these samplers was approximately 22 CFM. The high volume air samplers placed on the outer arcs were modified to increase the air flow to approximately 40 CFM by enlarging the inlet side.

Particle Size Distribution Samplers - Selective samplers were placed on the grid in an attempt to distinguish between particle sizes. The three types of particle sizing samplers used were the cyclone sampler[A2], the Unico cascade impactor[A3], and the Anderson sampler[A4].

These particle-sizing samplers were positioned in the 60° downwind sector of the grid.

Noble Fission Gas Sampler - The radioactive noble gas concentration in the cloud near ground level was measured by drawing a sample of the cloud through a high efficiency filter and then into an air tight balloon. The entrapped noble gases were then allowed to decay until recovery teams made re-entry and deflated the balloons through a second high efficiency filter. The radioactive daughters from the gases were trapped on the second filter and on the inside of the balloon. The balloon and filters were analyzed on a multichannel analyzer to determine

1256180

the quantitative amounts of the daughters deposited.

Eleven of these samplers were used on the 60° grid sector out to, and including, the E arc.

Beryllium Sampling Equipment - Beryllium sampling was performed by utilizing beryllium free filtering media on air samples taken for radioactive analysis. The majority of the radioactive analysis were made by gamma ray spectrometry after which the samples were analyzed on a mass spectrometer for beryllium. In addition, two sequential samplers (Figure A-12) with 12 sampling stages and four stationary air monitoring samplers were used specifically for beryllium monitoring.

Remote Radiation Monitors - Twelve direct radiation monitors, commonly known as remote area monitors, were utilized for the test. These remote units consisted of detector units, housed in weather proof containers, which were connected by cable to a central recording and control panel located in the IET building. The gamma ray dose rates from the remote stations were indicated on the rate meters at the central control panel and also on continuous strip chart recorders. These detectors recorded primarily gamma rays since beta particles are for the most part shielded out by the detector housing assembly.

Film Packet Dosimeters - Two types of film dosimeters were used for passive radiation monitoring during the test. The majority of these dosimeters were made up of a beta and gamma sensitive film packet hermetically sealed in a special plastic film holder[A5]. The remaining film type dosimeters were identical to the film badge monitors worn by nearly all personnel at the NRTS.

The hermetically sealed packets included a single lead insert to provide independent measurement of the beta and gamma doses by comparing the density of the film under the lead filter to that of the unshielded portion. The film packet was the Dupont packet which contains both sensitive and insensitive film for measuring high and low range exposure. A special red plastic convering was selected to reduce the effects of exposure to the sun's rays since many of the film packets were positioned on the grid several days prior to the actual test.

1256181

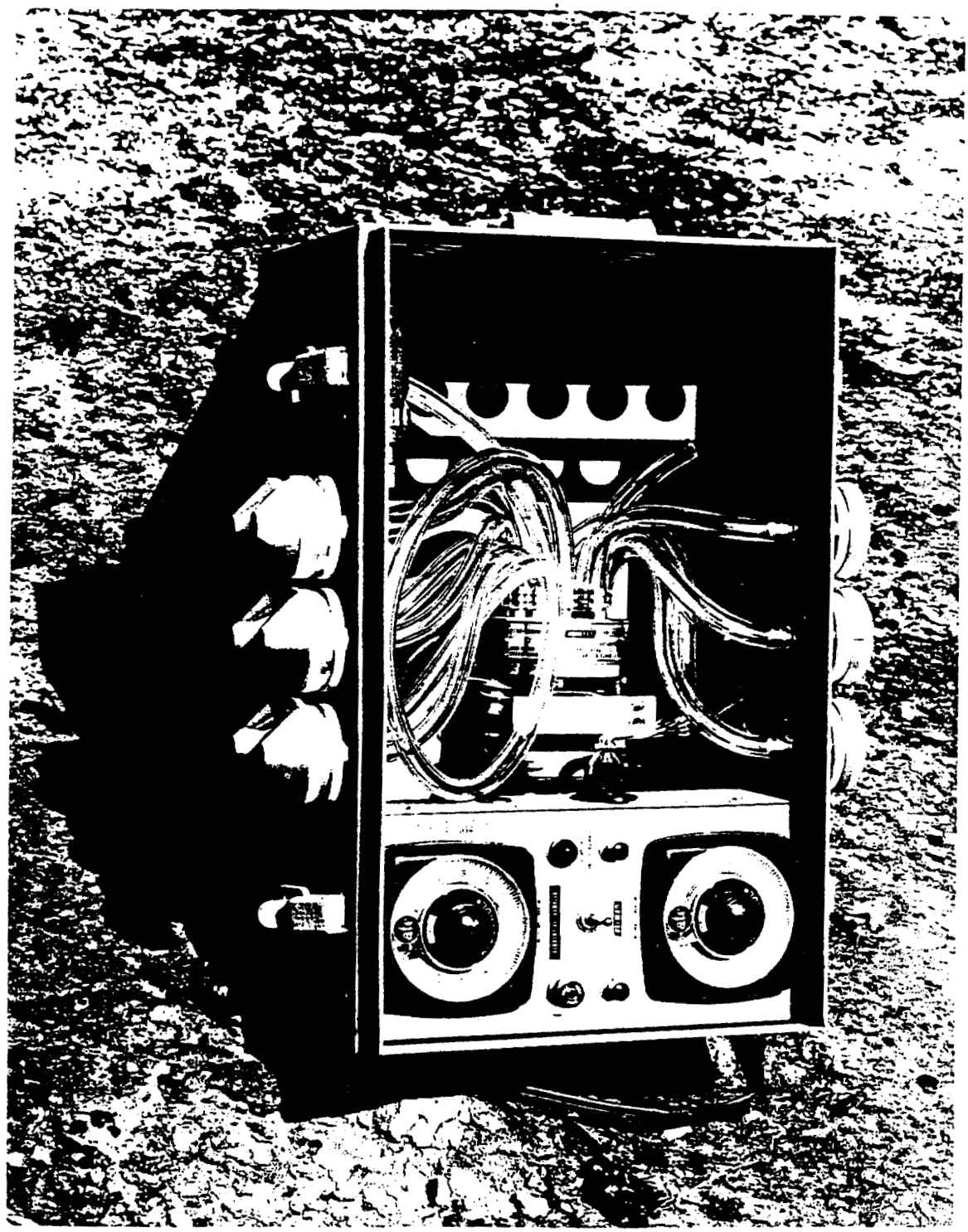

Fig. A-12 Radiological Sequential Air and Particle Sampler

1256182

Telemetering Network - A telemetering radiation monitoring network consisting of 25 remote stations (Figure A-13) and a master read-out control panel was used during the destructive test. The network was designed to measure and immediately report the cloud gamma integrated dose and the relative amount of gross airborne particulate beta and gamma activity near ground level due to the passage of a radioactive cloud. Each station unit contained both a high level and low level ion chamber for measuring cloud gamma dose and an air particulate monitor for measuring airborne activity. Each station also contained a motor generator set and a voltage converter which converted the voltage induced on the memory unit due to radiation exposure to an audible tone which was broadcast to the central unit. The central unit printed out this information on an IBM typewriter and a punched tape.

Mobile HP Field Office - A 35 foot trailer was modified for use as a mobile central control facility for the dispatching, installation and recovery of the sampling media on the exterior arcs immediately preceeding and subsequent to the destructive test. Equipment in the trailer included a radio, partable survey instruments, scalers, air monitor, clothing, hot and cold change areas, shower and lavatory facilities.

The trailer was located between the 1500 and 2500 meter arcs near the obstruction fence 1000 feet west of the 60° arc. Samples recovered were brought to the trailer by recovery teams. The samples were monitored, placed in containers and given to sample transfer taxis for delivery to the Health and Safety Building, TAN-606, for analysis.

High Range Dosimeters - Since high dose rates from the reactor transient were expected in the immediate vicinity to the test cell, several types of high range dosimeters were installed. The commercially available chemical and glass dosimeters were supplied by the Edgerton, Germeshausen, and Grier Company. Two thermo-luminescent dosimeters were acquired from the Control for Radiation Incorporated.

These high range dosimeters were positioned around the top of the environmental tank, on the reactor dolly, on the EG&G dolly, on the clothes-line, and on the ten meter arc to provide additional monitoring on the reactor transient.

1256183

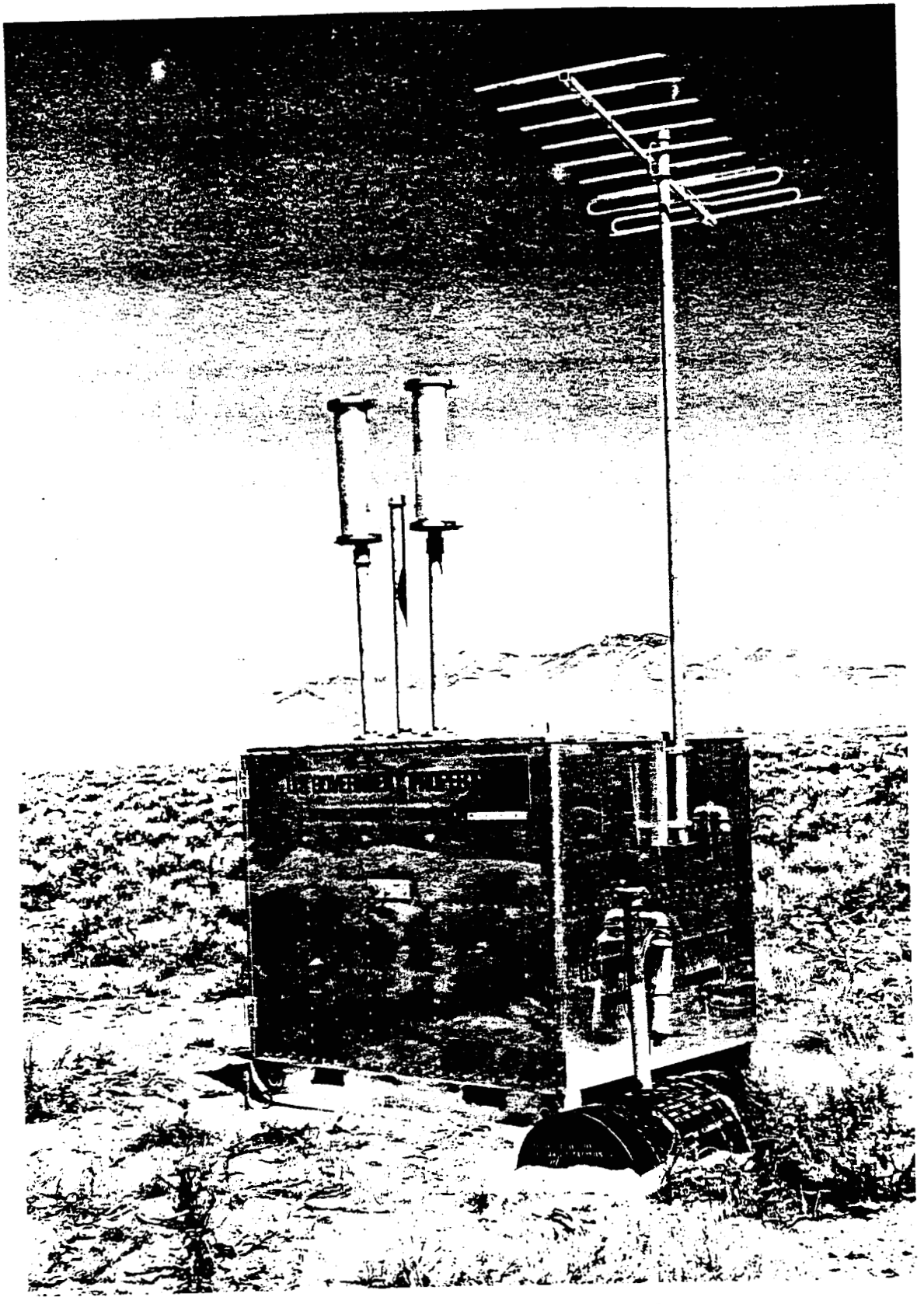

Fig. A-13 Telemetering Radiological Monitoring Station

1256184

Nuclear Accident Dosimeter - The Nuclear Accident Dosimeters (NADs) were of the ORNL Hurst type which utilizes bare gold, cadmium-covered gold, three fission foils and sulfur contained in a fireproofed can. This combination allows an approximate measurement of the neutron spectrum.

Six of these NADs were placed around the reactor where they could be recovered as soon as possible after the test.

Fallout Plates - Fallout plates (Figure A-14) were utilized for obtaining the fallout distribution, concentration and isotopic identification of the fission products deposited on the grid from the radioactive cloud. Sticky type fallout paper similar to transparent office-tape was employed to retain the fallout particles.

Sticky paper was mounted on metal frames which were in turn mounted on a stand located at each grid position four feet above ground level. In addition, fallout plates were installed on the radiological tower, IET stack and at several locations in the proximity of the reactor.

Mobile Surveillance Vehicles - Recovery of test samples from distant points on the radiological grid was accomplished with several four wheel drive vehicles equipped with radios and radiological monitoring equipment including scintillation type dose rate meters and conventional type air monitors.

1256185

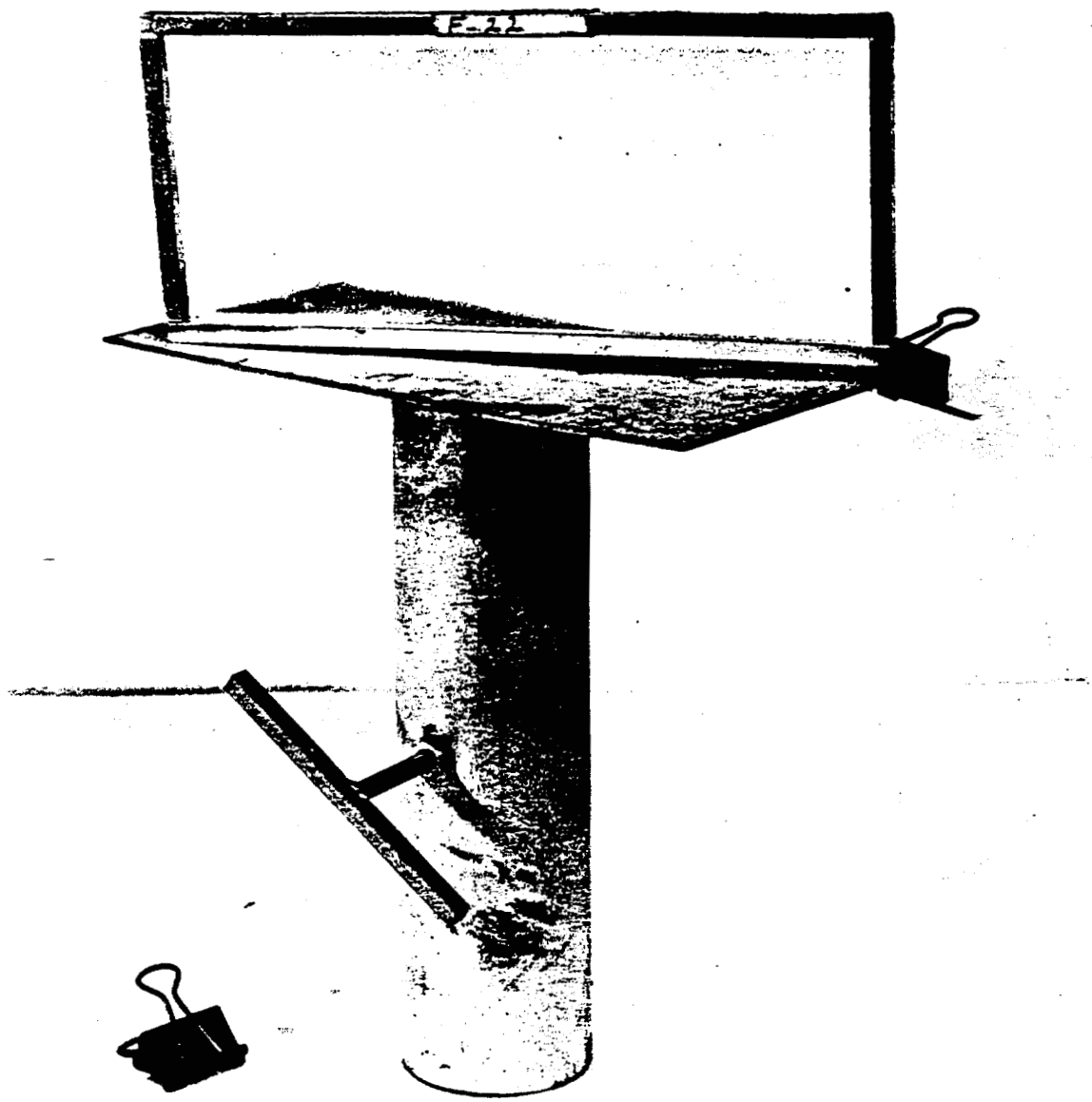

Fig. A-14 Radiological Fallout Plate

1256186

REFERENCES

A1. G. S. Hurst and R. H. Ritchie, "Radiation Accidents: Part A", ORNL-2748.

A2. M. Lippman and W. B. Harris, "Size -Selective Samplers for Estimating Respirable Dust Concentrations", Health Physics, Vol. 8, p-155 (1962).

A3. Unico - Manufacturers - Union Industrial Equipment Corporation, Port Chester, New York.

A4. Dougway Proving Grounds Research Report No. 108.

A5. F. V. Cipperley, Private Communication.

1256187

APPENDIX B

DETAILS CONCERNING CONDUCT OF TEST

I. Static Physics Measurements

A program of static physics measurements was conducted to obtain standards of reference for analysis of the data obtained during the destructive test. The following is a summary of the results of this program.

A. Sleeve and Water Height Critical Configurations

Investigation of the reactor's static characteristics was begun by determination of sleeve and water height critical configurations. Results of these determinations were compared with results of similar experiments performed by Atomics International on the SCA-4B reactor. This comparison was made to determine what reactivity effect, if any, resulted from the use of NaK and in-core instrumentation.

Results showed that the SNAPTRAN 2/10A-3 reactor, using the Binal sleeve (10.5 wt % Boron) and the calorimeter water volume, had critical configurations similar to those of the SCA-4B reactor (see Table B-I). These results indicated that the introduction of NaK and in-core instrumentation had negligible reactivity effects.

An attempt was made to measure the excess reactivity available by means of adding boric acid to the water reflector. However, the pump used to mix the solution was too small, and, consequently, the data obtained had excessive statistical scatter. Therefore the method used to determine the excess reactivity was integration of a calculated differential sleeve-worth curve normalized to the measured critical value. This resulted in a value of 3.80 ± 0.20 dollars for the excess reactivity.

1256188

TABLE B-I

MEASURED CRITICAL CONFIGURATIONS

	Critical Positions	
	SCA-4B[1]	SNAPTRAN 2/10A-3
Critical Water Height (inches)	9.02 ± 0.05	8.96 ± 0.05
Critical Sleeve Height (inches)	7.32 ± 0.125	7.27 ± 0.05
Mean Change in Critical Water Height (inches)	0.0	-0.06 (within measurement error)
Mean Change in Critical Sleeve Height (inches)	0.0	-0.05 (within measurement error)

NOTE: The critical configurations were measured from the base of the fuel. Critical sleeve height is the length of fuel not covered by the Binal sleeve. Critical water height is the length of fuel exposed to the water reflector with the Binal sleeve removed.

B. Power Calibration

The initial attempt at obtaining a thermodynamic power calibration by the use of a water-filled calorimeter tank, as a heat sink, was not successful due to insufficient water circulation within the tank. Poor circulation created temperature gradients and random convection currents throughout the water volume and between the sleeve-water interface. Thus the resulting data were insufficient for a calorimetric power determination.

However, during the power calibration experiment the outputs of all the in-core energy probes and thermocouples were recorded on magnetic tape, and these outputs indicated the heating and cooling rate for specific points within the reactor. A heating and cooling curve for a typical energy probe, along with the current generated by a typical ion chamber during this experiment, is depicted in Figure B-1. The output of these probes was appropriately normalized to the volume-weighted average core temperature during the period immediately after scram. The product of the maximum rate of change of temperature

1256189

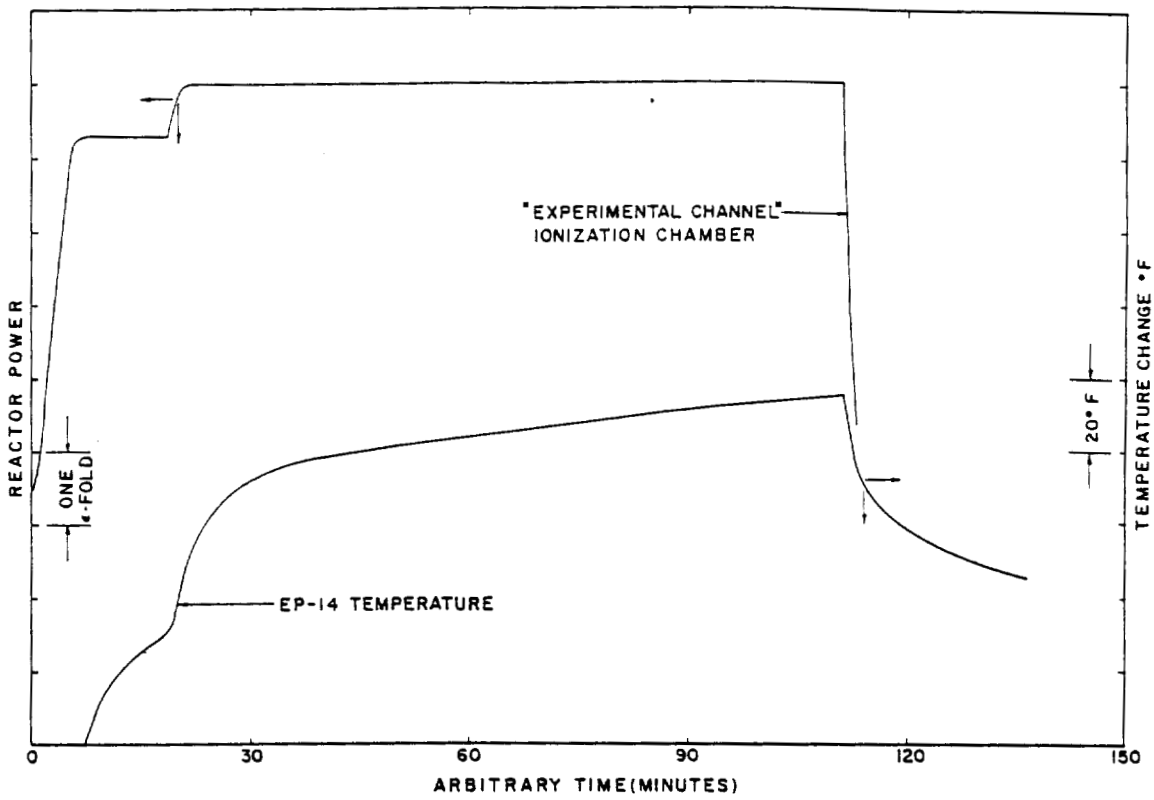

Fig. B-1 Time History of Typical Energy Probe and Nuclear Detector During Power Calibration

(as a function of time along the cooling curve) and an appropriately averaged fuel heat capacity permitted an energy rate determination.

The first step in reaching this determination was to make a thermal energy balance for a particular volume element as represented by the location of the energy probe within the cylindrical core. The generalized partial differential equation representing thermal balance of the heat conduction with a source term added is:

$$\frac{\partial}{\partial t} [C (T,r) T (r,t)] = \nabla \cdot K (T,r) \nabla T (r,t) + S (r,t)$$

STORED TRANSFERRED GENERATED

WHERE: T is temperature

r is a space variable

t is time

C is volume heat capacity

1256190

K is thermal conductivity

S is the source term per unit volume, i.e., volumetric heat generation rate

If it is assumed that:

1. The field considered extends over a single homogeneous body (the fuel),
2. The body is isotropic,
3. The thermal conductivity, density, and specific heat, (in other words, the physical properties which appear as coefficients in the differential equation) are independent of position and time,
4. No phase change takes place within the field,

then the heat balance equation can be written for a cylindrical geometry:

$$\frac{\partial}{\partial t} T(r,t) = \frac{K(T)}{C(T)} \nabla^2 T(r,t) + \frac{S(r,t)}{C(t)}$$

These assumptions are valid if the fuel is a uniform material and the temperature peak and differences are not orders of magnitude above ambient, i.e., 265 °F and 152 °F, respectively.

For the low peak temperatures involved and the small temperature changes, the thermal conductivity K(T) is essentially independent of temperature and can be written as a constant. The specific heat capacity of the fuel can be represented by the empirical equation $C_p = 0.0898 + 8.44 \times 10^{-5}\ T$ cal/gm-°C between the temperatures of 25 °C and 850 °C. The specific heat capacity used in these calculations was an average heat capacity - C_{ave} - defined over the temperature range involved as follows:

$$C_{ave} = \frac{\int_{T_1}^{T_2} (0.0898 + 8.44 \times 10^{-5} T)\, dT}{T_2 - T_1} = 0.0898 + 8.44 \times 10^{-5} \frac{(T_2 + T_1)}{2}$$

Thus, for a cylindrical geometry, the heat balance equation now takes the form:

$$\frac{\partial T(r,t)}{\partial t} = \frac{K}{C_{ave}} \left[\frac{1}{r} \frac{\partial T(r,t)}{\partial r} + \frac{\partial^2 T(r,t)}{\partial r^2} \right] + \frac{S(r,t)}{C_{ave}}$$

1256191

Again, if it be assumed there is no heat loss from the fuel other than that removed by the coolant, then for large reactivity removals, the period of the removal transient is so short that there is insufficient time for significant heat transfer from the fuel during the time immediately following the transient. Therefore, the heat transfer term can be eliminated from the balance equation without significant error in the calculation, and

$$\frac{\partial}{\partial t} T(r,t) \approx \frac{S(r,t)}{C_{ave}}$$

Thus, the maximum change in the slope of the temperature vs. time curve corresponds to the maximum change in the source term, that is

$$S(r,t) \approx C_{ave} \left. \frac{\partial T(r,t)}{\partial t} \right|_{max}$$

Each value of the source term thus obtained, representing the volumetric heat generation rate at a particular probe location, must be normalized to an average core generation rate. This normalization factor was obtained from the point-to-average source edit of a R-Z diffusion theory computer program which was written to satisfy the critical configuration criteria achieved during the power calibration experiment. As a point of interest, the two NaK thermocouples and all energy proves, with the exception of EP-3, EP-6, EP-15 and those probes located in the water, were evaluated to obtain a power level using the C_p of the fuel and the appropriate point-to-average source factor. Temperature data and results of calculations are shown in Table B-II. Probes Ep-3, Ep-6 and Ep-15 produced inconclusive data in that they were highly insensitive to the temperature changes encountered during the test.

Since the average heat capacity used in the calculation represented that of the 10 wt % probes, only the cooling curves (Figure B-2) represented by the 10 wt % probes were used to calculate reactor power. Of the five 10 wt % probes thus available for calculation, only four of these produced consistent values. These four probes produced values that were averaged to obtain 1.94 Kw at the power level at which the ion chamber currents were read for calibration.

1256192

TABLE B-II

POWER CALIBRATION RESULTS

CODE	TRANSDUCER	RADIAL DIST. FROM C (cm)	AXIAL DIST. FROM C (cm)	^{o}F/sec max	C_p $\frac{kw\text{-}sec}{^{o}F}$	Pt-to-ave FACTOR	POWER
TC-1	NaK PPCo	3.71	0	0.268	11.73	0.629	1.97
TC-2	NaK PPCo	6.50	0	0.223		0.766	1.72
EP-1	AI 73-6.5-0	3.71	0	0.278		0.629	2.05
EP-2	AI 74-6.5-5	3.71	0	0.234		0.629	1.73
EP-4	AI 96-6.5-5	3.71	0	0.260		0.629	1.92
EP-5	AI 97-6.6-5	3.71	0	0.260		0.766	2.13
EP-11	AI 95-6.5-5	6.50	-7.62	0.168		1.04	2.05
EP-12	AI 90-6.5-10	1.85	0	2.75		0.592	1.91
EP-13	AI 79-6.5-10	3.71	0	0.266		0.629	1.96
EP-14	AI 88-6.5-10	6.50	0	0.248		0.766	2.23
EP-19	AI 76-6.5-10	6.50	+7.62	0.207		0.782	1.90
EP-20	AI 91-6.5-10	6.50	+14.0	0.116		1.42	1.93

1256193

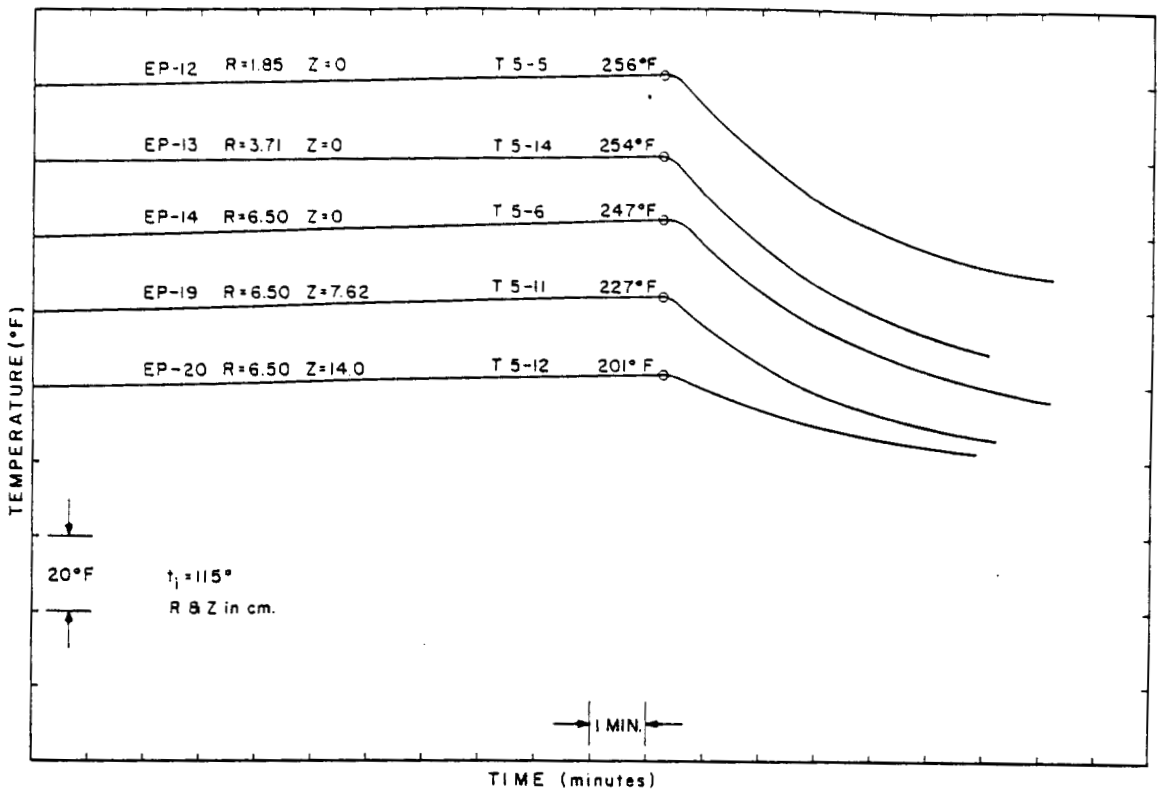

Fig. B-2 Time History of 10 wt% Energy Probes During Power Calibration

The accuracy of this power calibration calculation depends primarily on three things: a knowledge of the precise location of the active portion of the energy probe within the core, the value of the fuel heat capacity over the temperature range involved, and the rate at which power termination occurs. Because of the size of the SNAPTRAN 2/10A-3 core, the location of the active portion of the energy probe within the core must be known to be within plus or minus 0.5 cm in order to obtain accurate point-to-average source factors. Flux gradients near the reflectors and possible intersticial flux disadvantage factors can introduce 10% errors.

One problem that arises in determining the power level is the choice of the initial value of heat capacity to be used at ambient temperatures. A more accurate value of heat capacity would reduce much of the uncertainty in this technique.

1256194

If the reactor had been scrammed instead of driving the sleeve electrically, a much better defined transition would have resulted. This rate of power reduction appears to be adequate to reduce the uncertainty to ± 5%.

II. Destructive Test

A. Preparation

Upon completion of the static physics measurements, preparations for the destructive test were begun. Prior to an attempt to perform a destructive test, a rigid set of requirements had to be completely satisfied. A summary of the preparations made and requirements to be satisfied are enumerated in the following paragraphs.

Test Package Changes - During the static physics measurements, several of the analog strain gauges and Edgerton Germeshausen and Grier (EG&G) break bands located on the side of the reactor vessel were destroyed. These strain gauges were replaced and the break bands were put back in service.

Initially, the control drive rod attached to the Binal sleeve was free to fall upon loss of power to the control rod drive magnet. However, it was believed that, during the destructive test, the sleeve might drop over the reactor after the explosive charge had removed the sleeve. Therefore, a mechanism was installed to retain the ejected sleeve in its uppermost position.

In the event the reactor was not disassembled during the destructive test but chugged along at some power level depending on its heat dissipation rate, it would have been necessary to shut the reactor down by removing the water from around the reactor before a large fission product inventory was built-up. Therefore a large pump was provided to quickly remove the water from around the reactor.

Observation and Measurement - During the preparation period Phillips cameras were positioned at various stations. It was necessary to align all cameras on the test package with the test building removed and run film through the camera to insure proper operations.

1256195

EG&G cameras mounted in shielded "doghouses" on a removal railroad dolly required alignment and frame exposure staggering in order to record the disassembly profile of the reactor vessel. In addition, the mirrors attached to the three periscopes mounted on the environmental tank required alignment. Timing signals from the break bands on the reactor and gamma scintillation detector had to be coordinated with the flash lamps, and they, in turn had to be coordinated with the shutter openings on the cameras.

The nuclear, pressure, temperature, strain and acoustical detectors underwent a rigid continuity, polarity and sensitivity check. The data acquisition and conditioning equipment was thoroughly analyzed for noise on data channels, calibrated, and placed in a state of readiness.

An extensive radiological grid extending from the test pad had to be placed into operation. The TAN Health and Safety organization, responsible for the grid extending out 2500 meters, required the systematic placement of telemetering stations and various radiation detector and sampling equipment.

AEC site survey personnel, responsible for the radiological grid network extending from 2500 meters to beyond 8000 meters required placement of the various sampling equipment for biological studies was also placed on and next to the test pad.

The Weather Bureau, responsible for predicting and providing up-to-the-minute atmospheric conditions during the test, required the placement of telemetering weather stations, a radar station for tracking tetroons, digital acquisition equipment for meteorological parameters studies and the placing of existing IET weather data equipment operational.

Communication equipment was prepared or checked out for operational service. Four separate radio networks were employed to tie together site "C" network, mobile radiological sampling stations, radar, camera stations, two aircraft, locomotive, radiological grid network security, etc. Three separate intercom systems at IET were required. A telephone was supplied for emergency purposes, direct telephone lines

1256196

were used for weather control between CF, control trailer, and the weather room at IET.

Dry Runs Requirements - Upon completion of the preparations for the destructive test, three all inclusive dry runs were performed. The purpose of these dry runs was to insure that all equipment and participating personnel were prepared for the destructive test, to insure that all the necessary steps and assignments could be carried out efficiently and accurately in the time alloted in the countdown schedule, to determine reliability of the equipment, to establish confidence in the test personnel, and to establish where "holds" could judiciously be performed with respect to the countdown progress, if required.

Weather Conditions Required - Because in a test of this type significant amounts of radioactive fission products could be released to the atmosphere, certain weather conditions had to be met before the destructive test could be initiated. These conditions were as follows:

(1) Wind velocity 10 - 30 mph

(2) Wind direction between 180° to 240° - 0° being south

(3) Wind persistency - 2 hr minimum

(4) Precipitation - none in immediate area

(5) Light conditions - greater than 2000 lumens

The minimum wind velocity was established for persistency, and the maximum velocity was based on aircraft safety. The wind direction requirements corresponded to the downwind radiological grid network. Percipitation one hour prior to the destructive test could not be tolerated because it might spot the mirrors of the EG&G periscopes and might seriously affect fallout plates, etc. on the grid. Lighting conditions had to be sufficient for data aquisition on high-speed movie film.

Sequence of Events Prior to the Reactor Destruction - Once a sufficient number of dry runs had been successfully completed and it

1256197

was determined that the destructive test could be efficiently and successfully performed, all equipment and personnel were placed in a state of readiness, and the execution of the test was dependent upon meteorological conditions. The weather bureau provided the test personnel with two weather reports daily. Upon issuance of a 50-50 probability that the weather conditions would be suitable for performance of the test, all participating personnel were notified and the countdown which required $4\frac{1}{2}$ hours of count time before time zero (T-0) was scheduled. Three attempts were made to perform the destructive test. Two of these times, the test had to be aborted because of unsuitable weather conditions. On the third attempt, the destructive test was performed

B. Test Sequence

The test was initiated when the Binal sleeve was removed by the explosive charge in the actuator. The reactor was allowed to undergo an uncontrolled power excursion which resulted in disassembly. The sequence of events is outlined below.

Steps Taken After Reactor Destructive Test - Immediately following the nuclear excursion, the environmental tank drain systems were actuated, the winch to remove the EG&G dolly from the test area was started, and the cameras were turned off and camera shield doors allowed to drop. The TV cameras were extended from their missile shield houses for a close-up inspection of the inside of the environmental tank.

When the water had been removed from the environmental tank, TV observations revealed that the reactor had indeed completely disassembled itself and posed no criticality problem.

Soon after the test was completed, site survey personnel entered the area with an aircraft instrumented to track any radioactive cloud evolved from the test. After the aircraft completed the tracking of the radioactive cloud and left the grid area, a second aircraft entered the test area and obtained aerial photographs.

1256198

Re-entry - When it was resolved that the reactor was in a safe shutdown condition, and the remote area radiological monitoring equipment indicated that radiation levels in the reactor area were not prohibitive and that there was no significant airborne contamination, approval was given for personnel to enter the test cell area.

Two health Physicists entered the coupling station to collect a sample from the environmental water sample bomb. The direct radiation level in the coupling station was 5 mrem/hr. The first re-entry team entered the test cell area at approximately 40 minutes after the test. Direct radiation levels were as follows: 0.2 mrem/hr in the change room, 50 mrem/hr at the corridor shielding door, 150 mrem/hr at the test cell entrance and 400 mrem/hr on the test pad adjacent to the environmental tank.

At approximately 1 hour after the test, recovery teams began retrieving samples and sampling equipment from both the inner and outer radiological grids. Upon notification of re-entry authorization, the camera recovery teams removed the film from the various stations.

The following day, detailed contamination and radiation surveys of the test area were made. This survey indicated that a very insignificant amount of fuel had escaped from the environmental tank. A smear reading 800 dpm taken from the concrete pad 30 feet downwind from the reactor was the maximum contamination found outside the test cell. Most smears taken on the test cell floor showed less than 500 dpm/smear. A direct radiation survey showed readings of 5 to 8 mrem/hr at the west entrance of the test cell and 3 rem/hr at the edge of the environmental tank.

Reactor Dolly Removal to Hot Shop - Once the dolly surfaces external to the environmental tank were decontaminated, the dolly was prepared for removal to the Hot Shop for post-test examination. Removal to the hot shop took place seven days after the test.

Test Pad Decontamination - After all samples were removed and a detailed radiation survey had been completed, the test pad area decontamination was undertaken. All fuel particles and debris from

1256199

the reactor dolly and test pad floor was placed in plastic bags and removed from the area. After the reactor dolly was removed to the TSF area, decontamination of the test area was performed.

1256200

RECEIVED
PHILLIPS PETROLEUM CO.
JAN 28 1965
NRTS
TECHNICAL LIBRARY

This report belongs to the INEL Technical Library. It has been loaned to you, and you are accountable for it. The library may recall it after two weeks for use by another employee. Please return this report to the library when it is recalled or when you are no longer using it.

INEL Technical Library-IF
Report Section

PHILLIPS PETROLEUM COMPANY

PHILLIPS 66

ATOMIC ENERGY DIVISION

1256201